The Air Quality Impact of Aviation in Future-Year Emissions Scenarios

by

Akshay Ashok

B.S. Aeronautical and Astronautical Engineering
Purdue University, 2009

SUBMITTED TO THE DEPARTMENT OF AERONAUTICS AND ASTRONAUTICS
IN PARTIAL FULFILLMENT OF THE REQUIREMENTS FOR THE DEGREE OF

MASTER OF SCIENCE IN AERONAUTICS AND ASTRONAUTICS
AT THE
MASSACHUSETTS INSTITUTE OF TECHNOLOGY

SEPTEMBER 2011

© 2011 Massachusetts Institute of Technology. All rights reserved.

Signature of Author……..……..
Department of Aeronautics and Astronautics
September 2011

Certified by……..……..
Ian A. Waitz
Dean of Engineering
Jerome C. Hunsaker Professor of Aeronautics and Astronautics
Thesis Supervisor

Accepted by……..……..
Eytan H. Modiano
Professor of Aeronautics and Astronautics
Chair, Committee on Graduate Students

The Air Quality Impact of Aviation in Future-Year Emissions Scenarios

by

Akshay Ashok

Submitted to the Department of Aeronautics and Astronautics
on August 18, 2011 in Partial Fulfillment of the
Requirements for the Degree of Master of Science in
Aeronautics and Astronautics
At the Massachusetts Institute of Technology

ABSTRACT

The rapid growth of aviation is critical to the world and US economy, and it faces several important challenges among which lie the environmental impacts of aviation on noise, climate and air quality. The first objective of this thesis addresses the requirements of section 753 of the US Energy Policy Act, and entails the quantification of present and future-year regional air quality impacts of US Landing and Take-Off (LTO) aviation emissions. In addition, this thesis characterizes the sensitivity of these impacts to variations in the projection of non-aviation anthropogenic emissions (referred to as background emissions). Finally, the implication of a future-year background emissions scenario on the current policy analysis tool, the response surface model (RSMv2), is discussed.

Aviation emissions for 2006 are generated using the Aviation Environmental Design Tool (AEDT), while future-year aviation emissions are developed for 2020 and 2030 using the Federal Aviation Administration (FAA) Terminal Area Forecast (TAF) and the International Civil Aviation Organization (ICAO) Committee on Aviation Environmental Protection (CAEP/8) NO_x Stringency scenario #6. Background emissions for the year 2005 and 2025 are generated from the US Environmental Protection Agency (EPA) National Emissions Inventory (NEI), and two additional sensitivity scenarios are derived from the emissions forecasts. Uncertainties in present and forecast aviation and background emissions are also characterized.

The Community Multiscale Air Quality (CMAQ) model is evaluated to quantify its performance in predicting ambient $PM_{2.5}$ and ozone concentrations, and it is used to estimate aviation air quality impacts of aviation. Future-year aviation particulate matter ($PM_{2.5}$) concentrations are found to increase by a factor of 2 and 2.4 by 2020 and 2030, and are dominated by nitrate and ammonium PM. Aviation 8-hour daily maximum ozone is seen to grow by a factor of 1.9 and 2.2 by 2020 and 2030, with non-homogeneous spatial impacts. Aviation $PM_{2.5}$ varies by ±25% with a ±50% variation of the forecast change in background emissions, while changes in ozone impacts are less symmetric at +34%/-21%. The RSMv2 is shown to under-predict future-year aviation nitrate and ammonium $PM_{2.5}$. Finally, the implications of these results on the aviation industry and on aviation policy are discussed.

Thesis Supervisor: Ian A. Waitz
Title: Dean of Engineering, Jerome C. Hunsaker Professor of Aeronautics and Astronautics

Acknowledgements

I would first and foremost like to express my sincere gratitude for the guidance and support that my advisor Ian Waitz has provided in several capacities: as an academic advisor, thesis supervisor and research mentor. His words of encouragement, direction and support have always served to renew the motivation and passion for my work.

I acknowledge and greatly appreciate the mentorship of Prof. Steven Barrett. I thank Steven for the many enjoyable and informative discussions we have had thus far, and look forward to continued collaboration in the future.

I thank Christopher Sequeira at the FAA for managing research projects in a fair and effective manner, and Dr. Sarav Arunachalam at UNC for assistance with the CMAQ model setup.

The PARTNER lab is one of the most interesting and unique places I have had the pleasure of working in, largely due to the people in it. Special thanks to Dr. Steve Yim for discussions scientific and otherwise, and to Dr. Aleksandra Mozdzanowska for sound advice when it was much-needed. To my friends: Jamin, who joined me in the joys and pains of classes, research and thesis writing alike; Christoph, with whom I share the joy of flight; Sergio, with his unrelenting motivation to work; and to Jim, Philip, Fabio, Chris, Rhea, amongst others: I thank you all for making the lab environment vibrant, even if it was by simply being around for a chat.

Finally, I am deeply indebted to my family for all the moral support, helpful suggestions and understanding that they have provided. Indeed, I would not have reached this point without them.

The aviation emissions inventories used for this work were provided by US DOT Volpe Center and are based on data provided by the US Federal Aviation Administration and EUROCONTROL in support of the objectives of the International Civil Aviation Organization Committee on Aviation Environmental Protection CO2 Task Group. Any opinions, findings, and conclusions or recommendations expressed in this thesis are those of the author and do not necessarily reflect the views of the US DOT Volpe Center, the US FAA, EUROCONTROL or ICAO.

Contents

List of Figures

List of Tables

List of Acronyms

CAA	Clean Air Act
CAEP	Committee on Aviation Environmental Protection
EPA	Environmental Protection Agency
EPAct	Energy Policy Act
FAA	Federal Aviation Administration
ICAO	International Civil Aviation Organization
NAAQS	National Ambient Air Quality Standards
NEI	National Emissions Inventory
SCC	Source Classification Code
AEDT	Aviation Environmental Design Tool
APMT	Aviation environmental Portfolio Management Tool
CMAQ	Community Multiscale Air Quality
CTM	Chemical Transport Module
RSM	Response Surface Model
AMET	Atmospheric Model Evaluation Tool
AQS	Air Quality System
CASTnet	Clean Air Status and Trends Network
DV	Design Value
FRM	Federal Reference Method
IMPROVE	Interagency Monitoring of Protected Visual Environments
MATS	Modeled Attainment Test Software
NMB (NMdnB)	Normalized Mean (Median) Bias
NME (NMdnE)	Normalized Mean (Median) Error
RRF	Relative Response Factor
SMAT	Speciated Modeled Attainment Test
STN	Speciation Trends Network
AFE	Above Field Elevation
AGL	Above Ground Level
AMSL	Above Mean Sea Level
CONUS	Contiguous United States
LTO	Landing and Take-Off
PBL	Planetary Boundary Layer

BFFM2	Boeing Fuel Flow Method 2
ETFMS	Enhanced Tactical Flow Management System
ETMS	Enhanced Traffic Management System
FOA	First Order Approximation
OAG	Official Airline Guide
TAF	Terminal Area Forecast

BC	Black Carbon
CBIV/CB05	Carbon Bond IV/05
CDA	Continuous Descent Approach
EC	Elemental Carbon
EI	Emissions Index
FA	Free Ammonia
FSC	Fuel Sulfur Content
HC	Hydrocarbon
NO_x	Oxides of Nitrogen
OC	Organic Carbon
$PM_{2.5}$	Particulate matter < 2.5 µm in diameter
SOA	Secondary Organic Aerosol
SO_x	Oxides of Sulfur
TIM	Time In Mode
TOG	Total Organic Gases
ULS	Ultra-Low Sulfur
VOC	Volatile Organic Compounds

Chapter 1 Introduction

The aviation industry has experienced an average annual growth rate of approximately 4.4% over the past three decades [1], and demand for air travel is expected to expand in the future [2]. This growth in aviation activity is critical for the economic welfare of both the global as well as the domestic US markets ([3], [4]). The rapid growth in air transportation, however, faces several challenges such as air traffic management in over-crowded airspaces, airport capacity constraints and those related to advancements in airframe and engine technology. The environmental impacts of aviation present some of the most important challenges and are paramount in many policy decisions undertaken to manage the anticipated expansion of aviation [5].

1.1 The Air Quality Impacts of Aviation

Aviation impacts the environment through noise, climate and air quality, giving rise to environmental and societal damages on different spatial and temporal scales. Aircraft noise typically affects the local community, while climate impacts are expected to be felt tens to hundreds of years into the future and occur on a global scale. Air quality impacts occur not only in near-airport locales but also on regional and global scales. The work presented in this thesis focuses on the regional air quality impacts of aviation on an annual time-scale.

The primary air quality concern is the contribution of aviation emissions to ambient particulate matter smaller than 2.5 μm in aerodynamic diameter ($PM_{2.5}$) and ambient ozone levels, owing to the adverse health effects that arise as a result of exposure to elevated concentrations [6]. Aircraft emissions consist of several chemical compounds that form as a result of the fuels and combustion process in aircraft engines; while a proportion of these emissions comprise $PM_{2.5}$ (known as primary $PM_{2.5}$), the majority of PM is formed through the physical and chemical processes that gaseous precursor emissions of NO_x, SO_x and unburnt hydrocarbons (UHC) are subject to in the atmosphere. Aviation contribution to ozone may be positive or negative (as noted in Ratliff et al. [7]), due to the chemistry between NO_x emissions, volatile organic compounds (VOCs) and ozone.

Chemical Transport Models (CTMs) such as the Community Multiscale Air Quality (CMAQ) and GEOS-Chem models are often employed to capture the aforementioned natural processes in

the atmosphere, and take as inputs emissions and meteorology and output concentrations of various species in the atmosphere. There have been several prior studies that have used CMAQ to quantify the regional air quality impacts of aviation within the US. Ratliff et al. [7] used CMAQ to calculate regional impacts of aviation Landing and Take-Off cycle (LTO, defined as operations at or below 3000ft) emissions within the US, and estimated an increase in national annual-average aviation-attributable hydrated $PM_{2.5}$ of 0.01 $\mu g/m^3$ in the year 2001. A more recent study by Woody et al. [8] estimated US aviation contributions to current (2005) and future (2025) dry PM to be 0.0032 $\mu g/m^3$ and 0.011 $\mu g/m^3$, respectively. Kuhn [9] employed CMAQ in a regulatory context to assess the air quality impacts from aviation LTO emissions of implementing Ultra-Low Sulfur (ULS) jet fuel, reporting that a ULS policy leads to a 28% decrease in ambient $PM_{2.5}$ concentrations within the US.

Masek [10] used statistical regression methods to construct a Response Surface Model (RSM) for LTO aviation-attributable annual $PM_{2.5}$ within the US, based on CMAQ outputs. The RSM was further updated by Brunelle-Yeung [11] to the RSMv2, which output speciated $PM_{2.5}$. The RSMv2 was used by Brunelle-Yeung to quantify the impact of LTO aviation in 2005, yielding an increase in domain-averaged annual $PM_{2.5}$ of 0.00105 $\mu g/m^3$ due to aviation. Mahashabde et al. [12] used the RSMv2 in a regulatory framework to quantify the current and future-year air quality and health benefits of implementing several NO_x stringency policies in a full cost-benefit analysis (CBA) of the International Civil Aviation Organization Committee on Aviation Environmental Protection (ICAO CAEP/8) NO_x Stringency.

This thesis builds on these methods in the assessment of aviation air quality impacts. However, regulatory modeling of these impacts in future years has yet to be conducted, as will be discussed in the following section, and this forms the basis for the research conducted in this thesis.

1.2 Motivation for Thesis – Future-year Impacts Assessment

The motivation for this thesis stems from section 753 of the US Energy Policy Act (EPAct) of 2005, which requires the Environmental Protection Agency (EPA) and the Federal Aviation Administration (FAA) to perform an analysis to identify the impacts of aviation emissions on air quality in nonattainment areas. The analysis is restricted to aviation activity within the LTO regime, as emissions from the LTO cycle are regulated by ICAO [13] and considered in air quality assessments by the EPA and FAA [14]. The growing importance of aviation activity in

the future warrants the quantification of the air quality impacts in the future years in addition to the present-day conditions. Aviation policies typically span 20-30 years into the future [15], and therefore aviation impacts must be evaluated over this time period. The Energy Policy Act study by Ratliff et al. [7] was aimed at addressing the aviation air quality issues set forth by the Energy Policy Act, and although they quantified aviation air quality impacts for the present-day (2001) conditions they did not consider future-year impacts. Of the previous air quality studies presented in Section 1.1, Mahashabde et al. and Woody et al. have estimated the future air quality impacts of aviation, though these studies have limitations as well.

The study by Woody et al. utilized emission forecasts for 2025 aviation emissions as well as those from other anthropogenic sectors, in addition to base year 2005 scenarios. However, the flight activity information used in the study was limited to data from 99 major airports in the US and employed scaling factors to convert a seed day of activity into an annual inventory [8]. This could potentially lead to an under-representation of aviation air quality impacts in certain areas. The study also considered aviation activity up to 10,000ft, thereby including aviation emissions outside of the currently-regulated LTO regime. Therefore, these results might not appropriately represent the air quality impact of aviation on non-attainment areas from a regulatory perspective.

The study by Woody et al. did, however, highlight a significant parameter that influences aviation's air quality impacts – non-aviation anthropogenic emissions, which are termed as "background emissions". Background emissions are responsible for establishing the majority of the atmospheric species concentrations with which aviation emissions react to form PM and ozone. It is therefore necessary to take into account not only the anticipated growth in aviation emissions but also the anticipated changes in future-year background emissions when assessing the future aviation impacts on air quality.

The work by Mahashabde et al. considered future growth in aviation in the assessment of ICAO CAEP/8 NO_x Stringency; however, the policy analysis tool (the RSMv2) that was employed in the CBA does not account for changing future-year background emissions scenarios, and therefore the study may not adequately represent the aviation air quality impacts in the future years as well.

1.3 Focus and Outline of Analysis

In light of the requirements of the US Energy Policy Act, and the limitations of prior studies in estimating future-year air quality impacts of aviation, this thesis aims to address the following three key issues:

A Quantify the future-year impacts of LTO aviation emissions on regional air quality in the US – this is done through the base-year implementation and future-year projection of aviation activity and emissions, and the simulation of the atmospheric response to these emissions amid a present-day and future-year background emissions scenario

B Estimate the sensitivity of the air quality impacts of LTO aviation emissions to the background emissions forecasts – a sensitivity study is performed, perturbing the background emissions to ascertain their influence on the resulting aviation-attributable $PM_{2.5}$ and ozone concentrations

C Identify the implications of a changing background emissions scenario on the current policy analysis methodology – the current aviation air quality policy analysis tool, the RSMv2, is used to calculate future-year aviation $PM_{2.5}$ concentrations, and subsequently compared against the outputs from the CMAQ model

The set up of the modeling platforms and performance evaluation that was conducted to validate the model are outlined in Chapter 2. Chapter 3 discusses the present and future year aviation scenarios, and Chapter 4 provides more detail on the background emissions and its forecasts. The future-year air quality impacts of aviation are illustrated in Chapter 5, including their sensitivity to background emissions. Chapter 6 discusses the results and their implications for the aviation industry and aviation policy. The final chapter concludes the thesis with a summary and suggests future avenues of research.

Chapter 2 Model Setup and Configuration

Air quality models are used to study the fate of pollutants within the atmosphere by simulating the natural processes that occur in the atmosphere. The spatial extent of coverage varies: global CTMs such as GEOS-Chem model most of the Earth's atmosphere, incorporating long-range mixing and chemistry. Models such as AERMOD and CALPUFF simulate plume-scale dispersion (with limited chemistry) over tens of kilometers. The aim of the present work is to study air quality over the Contiguous United States (CONUS), and therefore a regional-scale model is used in this thesis. The Community Multiscale Air Quality (CMAQ) modeling system is chosen for the study, given its applicability and widespread usage in modeling regional air quality. CMAQ is employed to address issues (A), (B), and (C) that were posed in Section 1.3.

The RSMv2, originally built by Masek (2008) and later updated by Brunelle-Yeung (2009), is a reduced-order response surface model that estimates annual surface-level particulate matter concentrations due to aviation LTO emissions. The model exists as part of the FAA's Aviation environmental Portfolio Management Tool (APMT) [12], and is used to perform cost-benefit analyses of aviation policy scenarios. The current RSM does not account for changes in background emissions; its performance in calculating the future-year impacts of aviation is therefore compared with the results from the CMAQ application, in order to identify the effects that a changing background emissions scenario has on the tool.

Both modeling systems comprise multiple components including meteorology, initial and boundary conditions, and emissions. Details of these components as well as the model configuration and simulation scenarios are presented in the sections below. Section 2.5 of this chapter describes the performance evaluation of the CMAQ model.

2.1 Modeling Scenarios

Modeling scenarios are chosen in order to address the research questions set forth in Chapter 1. Table 1 outlines the simulations that were conducted, and identifies their objectives pertinent to this thesis. Simulations for objectives (A) and (B) will be performed using the CMAQ model, while scenario (C) will involve an RSM simulation.

Table 1: CMAQ aviation/anthropogenic emission combinations and RSM input inventory

Sim. #	Description	Year of Non-aviation Emissions	Aviation LTO Emission Year	Objective of Simulation(s)
1	2005 Control	2005	--	(A)
2	2005 Base year scenario	2005	2006	
3	2025 Control	2025	--	
4	Future year (2020) scenario	2025	2020	
5	Future year (2030) scenario	2025	2030	
6	0.5xDelta Control	0.5xDelta	--	(B)
7	0.5xDelta (2020) scenario	0.5xDelta	2020	
8	0.5xDelta (2030) scenario	0.5xDelta	2030	
9	1.5xDelta Control	1.5xDelta	--	
10	1.5xDelta (2020) scenario	1.5xDelta	2020	
11	1.5xDelta (2030) scenario	1.5xDelta	2030	
12	RSMv2	--	2006-2020-2030	(C)

*Note: "Delta" refers to the change in background emissions from 2005 to 2025.

A control simulation without aviation emissions is conducted for each unique background emissions dataset (as seen in Simulations #1, 3, 6 and 9), and the aviation impact on air quality is estimated by taking the difference between the CMAQ model outputs of each of the modeling scenario and their appropriate control cases; that is, 2006 aviation impacts are estimated by taking the difference between Simulation #2 and Simulation #1, 2020 impacts between Simulation #4 and Simulation #3 and 2030 impacts between Simulations #5 and #3.

Objective (A) is achieved by simulating the base year 2006 and future years 2020 and 2030 aviation scenarios. These simulations were conducted as part of the EPAct Follow-On study, aimed at addressing one of the main requirements of the Energy Policy Act to identify the impact of aviation emissions in air quality nonattainment areas in the USA. The aviation emissions are considered only within the LTO cycle, and will be elaborated upon in Chapter 3. Ideally, the non-aviation emission inventory would be derived to match these modeling years. For the base year simulation, the year 2005 emissions dataset is used since it is the closest to the analysis year. For the future years, only the 2025 dataset was available in a CMAQ-ready format at the time of the study, and as such it was used as a proxy for both 2020 and 2030 anthropogenic emissions. This is not expected to introduce additional uncertainty as projections of future aviation and background emissions are already uncertain by at least an amount equivalent to 5

years (see Section 3.6). The source and methodologies of the background emissions data are described in greater detail in Chapter 4.

To understand the sensitivity of aviation-attributable PM to background emissions variations, each future aviation case (2020 and 2030) is paired with two additional background emissions scenarios: one representing a less-than-predicted change in background emissions (50% of the change) between 2005 and 2025, and second describing a greater-than-predicted change in background emissions (150% of the change). The methodology behind these modified background emissions scenarios is given in Chapter 4.

Finally, the implication of changing background emissions scenario on the current policy analysis tool, the RSMv2, is identified with the aid of simulation #12. There is no background emissions input to the RSMv2, since the model approximates PM due to aviation through a regression model which is a function of aviation LTO emissions assuming a fixed background emissions level. Aviation emissions for the three forecast years are input to the model, and a comparison between the resulting RSM outputs and those of the CMAQ simulations is performed in Section 6.3.

2.2 Modeling Domain

The CMAQ modeling domain is centered about the CONUS, with parts of Canada and Mexico included within the domain, as shown in Figure 2-1. The grid boundaries are located away from the CONUS region of interest, to reduce the influence of boundary conditions on species concentrations over the region of interest.

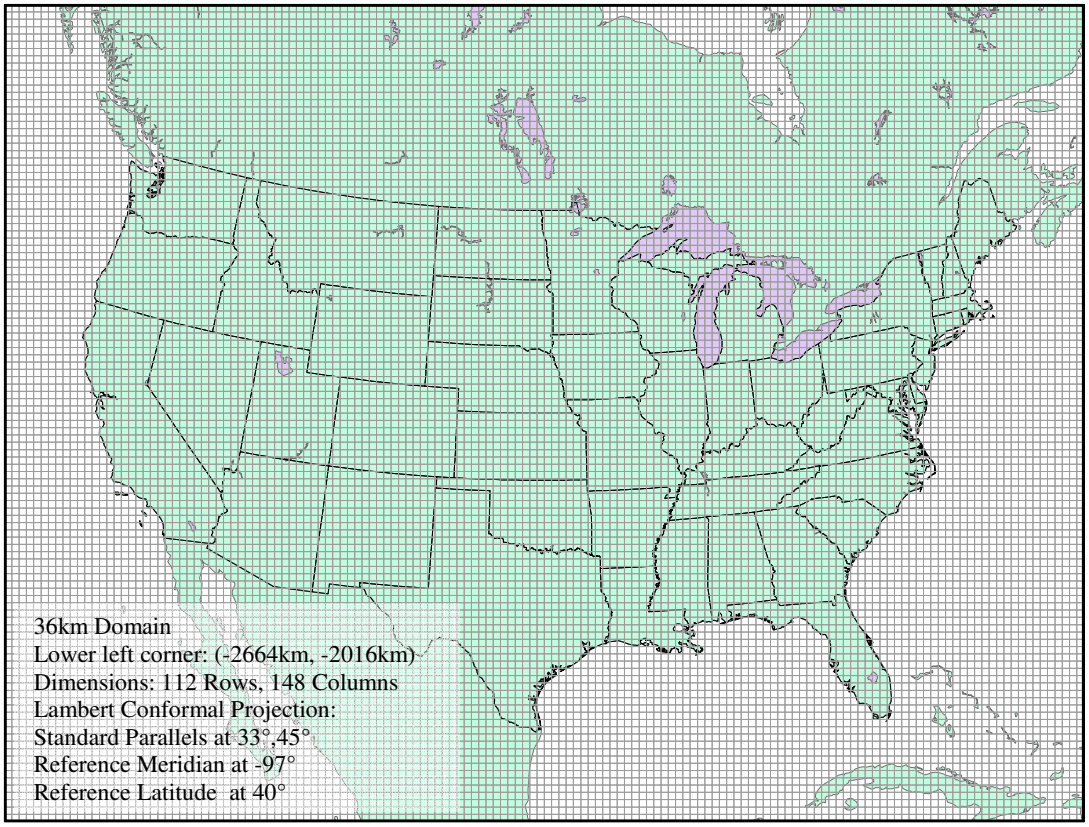

Figure 2-1: The CMAQ 36 km modeling domain

The regular horizontal grid comprises 112 rows by 148 columns, the size of each grid cell being 36 km square. The domain lies in a plane defined by a Lambert Conformal Conic Projection of the Earth; the projection is centered at (40°N , 97°W) with reference parallels at 33°N and 45°N. The origin of the grid (specified as the lower left-hand corner) is located <-2664km, -2016km> from the center of the domain.

The vertical domain is discretized into 34 layers up to an altitude of approximately 52,000ft (16km) above mean sea level (AMSL). The layers are defined by a sigma-pressure coordinate system which conforms to changes in terrain elevation. Sigma coordinates are defined relative to the ambient pressure at the surface of the Earth (denoted p_0), as per Equation (2.1).

$$\sigma(p) = 1 - \frac{p - p_0}{p_{top} - p_0} \qquad \textbf{(2.1)}$$

where p_{top} is the pressure at the top of the domain of 100 millibars (~52,000ft AMSL).

The coordinate begins at 1 on the surface of the Earth (where $p=p_0$), and decreases to 0 as the pressure p drops to 100 millibars at the top of the domain. The pressures at the bottom face of the grid cells within the first model layer (also known as the ground-layer) may not be uniform, owing to the fact that the vertical grid is terrain-following. Both the grid box heights as well as their altitude above ground are therefore not uniform between neighboring vertical columns. It is important to note also that the vertical grid is not fixed in space temporally, since the surface pressure levels on which it is based fluctuates as a function of meteorological phenomena.

The sigma coordinates are defined in order to provide high resolution near the surface of the Earth. Figure 2-2 shows a typical vertical grid structure, while the sigma coordinates and corresponding pressure and altitudes are tabulated in Appendix A. The first few layers are 30-60 meters in height, with the first 14 layers under 1 km. The requirement for higher resolution in this region is two-fold: first, the objective of the modeling is to calculate surface-level $PM_{2.5}$ and ozone concentrations, since population exposure to PM and ozone leads to adverse health effects. A finer vertical grid improves the estimate of pollutant concentration in the ground-layer cells, leading to more accurate air quality impacts. Second, the atmosphere near the surface of the Earth is turbulent and forms the planetary boundary layer (PBL). Although the thickness of the layer is dependent on the stability of the atmosphere as well as the land use and related surface roughness, an average PBL height of 1km exists over the CONUS [16]. A fine grid is required to resolve the vertical mixing processes occurring within the PBL, necessitating that more than a third of the vertical layers are located within 1km.

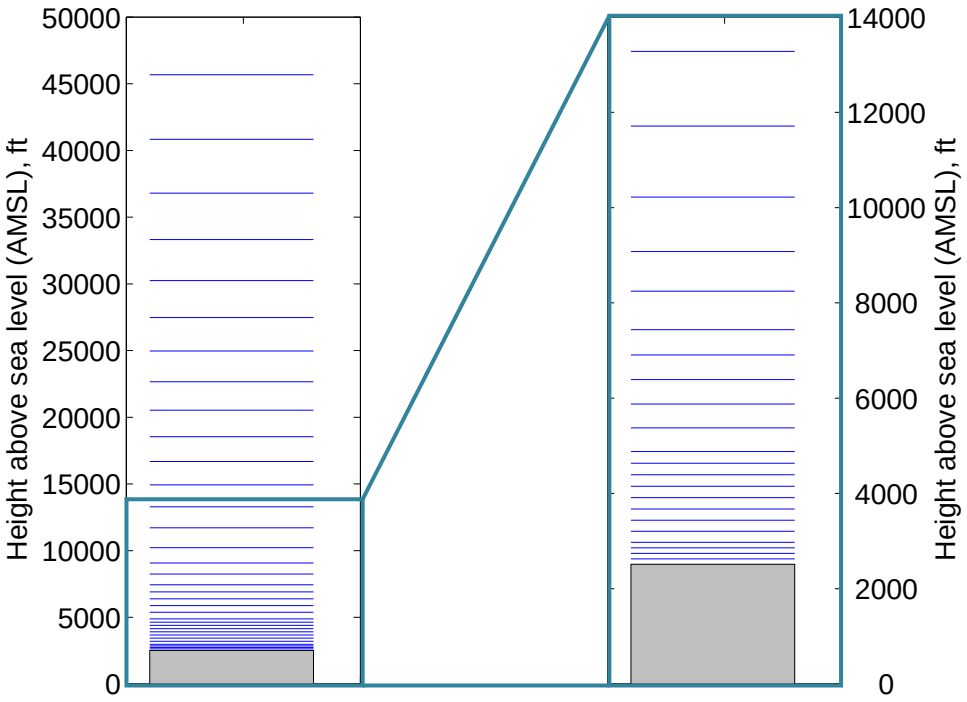

Figure 2-2: Vertical layers in the CMAQ domain over a typical grid-cell

The temporal domain of modeling is one calendar year, from January 1 to December 31. This is done in order to capture both seasonal exposure to ozone during the ozone season of May through September as well as long-term (annual) exposure to $PM_{2.5}$. Prior studies ([10], [17]) have attempted to capture the annual variability in ambient PM and ozone concentrations by performing simulations for four months, one during each season: January (winter), April (spring), June (summer) and August (fall). However, in order to better capture the annual mean in the species concentrations a full year of simulations is preformed in this thesis. The CMAQ simulations include a spin-up period of 11 days, to mitigate the effects of the initial conditions used to start the calculations and reach a quasi-steady state, a duration that is consistent with prior studies ([18], [19]).

The RSM domain is similar to the one presented in Figure 2-1, with the exception of a shift of the origin of the grid by two grid-cells in each horizontal direction to <-2736km,-2088km>. Since the RSMv2 is constructed to predict annual surface-level PM concentrations, there are no temporal or vertical dimensions to the model.

2.3 The CMAQ Model

CMAQ is a three-dimensional Eulerian photochemical air quality model that simulates the chemistry and transport of many species of air quality concern in the troposphere, producing hourly gridded concentrations of speciated particulate matter and ozone (amongst other species). CMAQ is used by the EPA for various policy and regulatory impact analyses ([20], [21], [22]) within the United States, and its fidelity and suitability in modeling regional air quality have been demonstrated. The CMAQ model is open source and freely available to the air quality modeling community, building upon the array of scientific knowledge and modeling techniques that exist within the community. CMAQ model version 4.7.1 [23] is utilized for the simulations, since it contains updates that represent state-of-the-science modeling techniques in aqueous and photo-chemistry, aerosol treatment, and numerical solution methods. Further details about the CMAQ model and its underlying components can be found in Byun et al. [24]. Several choices exist for the physics and chemistry modules built into the CTM; these model build parameters, including compiler details and computational architecture are listed in Appendix B.

Most of the model options are kept to their default settings, with the exception of the chemical mechanism and the aerosol module. The Carbon Bond 05 (CB05cltx) chemical mechanism (described in detail in Yarwood et al. [25]) and the AERO5_txhg aerosol module were used in the CMAQ simulations. CB05 represents atmospheric oxidant chemistry, providing a set of reactions and chemical mechanisms that form the basis for the study of air quality issues such as those involving ambient ozone and $PM_{2.5}$. Notable updates from the older Carbon Bond IV (CBIV) mechanism include several updates to chemical kinetics and photolysis rates, chlorine chemistry and explicit treatment of toxic volatile organic compounds (air toxics). The AERO5 mechanism includes enhanced treatment for secondary organic aerosol (SOA) formation and several other updates for aerosol treatment. The explicit air toxics option was used in the CMAQ build, and as such the relevant toxics modules ('tx') were enabled to track the air toxics species.

2.4 Inputs to CMAQ

The following section describes the inputs to CMAQ in greater detail. The three main components involved in modeling air quality are meteorological parameters, emissions of pollutants and initial and boundary conditions (IC/BC). These components are brought together in the CTM within CMAQ, which is responsible for the computations of advective transport,

photochemistry and dry/wet deposition of species. The meteorology, IC/BC and base and future-year background emissions that are used in the CMAQ simulations in this thesis were the same ones used in Woody et al. [8]; a brief description of these inputs is provided in this section, while the reader is referred to [8] for additional details pertaining to the processing and generation of these datasets. The generation of the base year aviation emissions as well as the projection of aviation activity into the future years, along with the associated uncertainties, is discussed in depth in Chapter 3. Background emissions trends, forecasts and uncertainties are discussed in Chapter 4. A summary of the CMAQ inputs is given in Appendix C.

2.4.1 Meteorology

The CMAQ simulations in this thesis utilize year 2005 meteorological conditions. The gridded meteorology was generated by the Meteorology-Chemistry Interface Processor (MCIP) v3.3 [26], which uses outputs from the Pennsylvania State University/National Center for Atmospheric Research Mesoscale Model (PSU/NCAR MM5) v3.7.1 [27]. Meteorological conditions are held fixed across all CMAQ simulations; doing so eliminates the additional variability in the CMAQ outputs due to changing meteorological conditions, and isolates the air quality impacts of aviation activity due to changes in aviation and background emissions scenarios alone. Since meteorology is prescribed, climate-air quality feedbacks from aviation, for example due to aerosol radiative forcing or induced precipitation [28], are not modeled.

2.4.2 Initial and Boundary Conditions

Initial and boundary conditions for the CMAQ simulations are obtained from atmospheric simulations performed using the GEOS-Chem global model [29]. Concentrations of chemical species from the global domain were interpolated onto the CMAQ computational domain boundaries for each day of the simulation period [30]. Initial and boundary conditions from the GEOS-Chem year 2000 simulations are used for the CMAQ year 2005 simulations. In the absence of 2025 specific GEOS-Chem simulations, IC/BCs from 2000 and 2050 simulations based on the Intergovernmental Panel on Climate Change's A1B emissions scenario are temporally interpolated to obtain 2025 IC/BC concentrations [31]. Anthropogenic emissions for GEOS-Chem simulations were derived from a variety of sources, drawing from global sources such as Emissions Database for Global Atmospheric Research (EDGAR) as well as regional sources such as European Monitoring and Evaluation Programme (EMEP) and US EPA. The

GEOS-Chem simulations include aviation emissions since global aviation emissions (including cruise emissions) play a role in setting the overall oxidative capacity of the atmosphere. These aviation emissions are different from the ones modeled in this thesis; monthly mean gridded inventories of aircraft NO_x (developed for the year 1992, reported in Wang et al. [32]) and aircraft SO_2 (also developed for the year 1992, presented in Park et al. [33]) were used in the global GEOS-Chem simulation.

2.4.3 Gridded Emissions

The third major component in the inputs to CMAQ is the emissions of pollutants. Aviation emissions are distinguished from other anthropogenic emissions, in order to obtain the changes in particulate matter and ozone concentration caused by aviation activity. As will be explained in Chapter 3, the aviation emissions inventory used for this analysis is processed from detailed datasets, promoting a deeper and fuller understanding of aviation emissions and their projections into the future. The understanding becomes especially useful in interpreting the aviation signal from the air quality model outputs. The non-aviation, background, emissions are processed from the US EPA's National Emissions Inventory (NEI), which not only catalogs emissions within North America (US, Canada and Mexico) every three years but also projects emissions into the future years. Further details on the background emissions processing are given in Chapter 4.

Emissions are input in units of moles/sec for gaseous species and grams/sec for primary aerosol emissions, and are gridded to the CMAQ modeling domain both spatially (148x112x34 grid-cells) and temporally (hourly emissions). The choice of chemical mechanism, CB05 in this case, dictates the types of chemical species accepted into the CTM. An important characteristic of the CB05 mechanism is that real organic compounds are not emitted as individual species but instead as "lumped" model species (such as PAR, OLE, ALD). Organic compounds are grouped based on the number and type of internal carbon bonds within a molecule that lead to differing rates of reactivity; for example, propylene (C_3H_6) comprises one fast reacting carbon double-bond and one carbon single bond, and as such one mole of propylene yields one mole of OLE (carbon fast double-bond) and one mole of PAR (carbon single-bond) [34]. This facilitates some of the generalized chemistry and surrogate reactions that are modeled in the CB05 reaction set, and leads to enhanced computational efficiency of the CTM ([25], [35]).

2.4.4 Other Inputs

For completeness, several other ancillary yet important inputs to CMAQ are presented here.

Photolysis lookup tables contain information on incoming solar radiation and photolysis rates, which drive the photochemistry within the CTM. The photolysis rates are generated specific to the CB05 mechanism, and the values are a function of solar angle, latitude and altitude. These rates are for clear-sky conditions, and are corrected through parameterizations for cloud cover [36]. The photolysis rates are generated using the default profile published with CMAQ4.7.1.

Sea-salt emissions are calculated based on wind speed and relative humidity, and are split up into chloride, sodium and sulfate ions. An OCEAN file, containing the fraction of each grid cell covered by open ocean, is used in these calculations. The OCEAN file was processed by UNC, using the SSMASK tool[1].

2.5 CMAQ Performance Evaluation

2.5.1 Need for Performance Evaluation

The usage of the CMAQ model in any analysis requires a comprehensive model performance evaluation in order to establish model credibility and improve the reporting of results. CMAQ performance evaluation validates the base year (2005) model outputs against ambient measurement data, and quantifies the model characteristics and biases before it is applied towards predicting aviation impacts.

The Atmospheric Model Evaluation Tool version 1.1 (AMET v1.1) is used alongside custom MATLAB scripts to perform the CMAQ model evaluation. AMET is a collection of utility scripts and analysis tools that have been developed to compare model predictions of meteorology and air quality with observed quantities [37], and its usage in performance analyses is illustrated in the US EPA's modeling guidance for air quality attainment analyses [38].

2.5.2 Observational Data and Monitors

Air quality monitoring stations have been set up across the country to collect measurements of ambient $PM_{2.5}$, its species, ozone and other toxic and Hazardous Air Pollutants (HAPs). These

[1] SSMASK tool available through instructions at
http://www.cmascenter.org/help/model_docs/cmaq/4.5/AEROSOL_NOTES.txt

monitors are part of distinct monitoring networks, and therefore have discrete sampling and operating procedures that vary both in terms of temporal frequency as well as species that are monitored. Table 2 lists the monitoring networks that are used in this study, as well as the species that are compared and the frequency of measurement.

Table 2: Monitor networks, species that are measured and the temporal frequency of measurement

Network	Species monitored	Temporal frequency
IMPROVE	$PM_{2.5}$, NO_3, SO_4, EC, OC	1-in-3 day average
STN	$PM_{2.5}$, NH_4, NO_3, SO_4, EC, OC	1-in-3 day average
CASTnet	NH_4, NO_3, SO_4	Weekly average
AQS	O_3	Hourly, 1hr max, 8hr max

Interagency Monitoring of Protected Visual Environments (IMPROVE) [39]: IMPROVE sites were first set up in 1985 to study the effects of ambient particles on visibility and to characterize trends in visibility both spatially and temporally [40]. Most of the sites are located in the Western US, and the monitors at these sites report 24-hour integrated samples. The model performance evaluation uses measurement data from 168 sites and 115 days (due to the 1-in-3 day monitoring frequency), for the year 2005.

Speciation Trends Network (STN): The STN is a part of the Chemical Speciation Network (CSN) and comprises roughly 200 monitors primarily located in urban areas [41]. The network was established in 2000 to support epidemiological studies, assessing control and mitigation strategies and capturing trends in $PM_{2.5}$ and its species. Monitors at STN sites attempt to split total carbon (TC) that is measured into its organic and elemental constituents. This is done through the National Institute of Occupational Safety and Health (NIOSH) method 5040 [42]. A total of 219 sites are used in the evaluation of CMAQ.

The $PM_{2.5}$ mass that is measured at many of these 219 sites is obtained by using the Federal Reference Method for $PM_{2.5}$ (FRM $PM_{2.5}$) [43]. The FRM method is prescribed by the EPA to be used in the determination of National Ambient Air Quality Standards (NAAQS) attainment status. The FRM specifies conditions for sample measurement and filter handling – filters should be temperature-controlled and cold-filter shipped, and $PM_{2.5}$ mass should be gravimetrically measured by the difference in pre- and post-sampling measurement filters that have been

equilibrated for at least 24 hours at 20-23°C and 30-40% relative humidity. It is noted in Frank (2006) [44] that FRM $PM_{2.5}$ exhibits losses in semi-volatile organic compounds and ammonium nitrate. Particle-bound water is also included in the $PM_{2.5}$ mass, in contrast with the "dry" PM that is predicted by the CMAQ model.

Clean Air Status and Trends Network [45]: The CASTnet network was borne out of the National Dry Deposition Network (NDDN), with the goal of determining trends in atmospheric nitrogen, sulfur and ozone concentrations and dry deposition in order to assess the impacts of regional and national air quality control programs [45]. The evaluation uses 86 CASTnet regional monitor sites nationwide, which are located primarily in rural areas (thereby complementing the predominantly urban STN network). CASTnet filters are exposed to ambient conditions over a 1-week period – this exacerbates volatility issues related to measured nitrate and semi-volatile organic carbon concentrations [46].

Air Quality System [47]: The US EPA AQS is a data repository of hourly aerometric concentrations, centralizing data from other networks such as IMPROVE and STN as well as Federal, State and Local agencies. Hourly ozone concentrations from over 1000 monitors for the year 2005 are obtained from the AQS, and subsequently post-processed into 1-hour and 8-hour daily maximum concentrations. Ozone performance evaluation is done during the ozone season, from 1 May to 30 September for the base year 2005, when ozone reaches sustained elevated concentrations; the model has to be able to capture these periods of high ozone in order to accurately represent the health impacts due to population exposure.

2.5.3 Metrics of Comparison

CMAQ model data and observation data are paired in space (by monitor location) and time (hourly, daily maximum, daily average). Visual methods such as timeseries, boxplots and scatterplots are used to gauge trends in a qualitative manner, and statistical tools are employed in order to perform quantitative, objective comparisons between the performance of the CMAQ4.7.1 model in this thesis and that of other studies. The following section outlines the comparison methods and statistical parameters that are used in this thesis.

A number of statistical parameters are calculated when performing the model evaluation, and two of these are presented in greater detail in this thesis. The equations for the two statistical indicators of Normalized Mean Bias (NMB) and Normalized Mean Error (NME) are given in Equations (2.2) and (2.3).

$$\mathrm{NMB} = \frac{\sum(\mathrm{Model} - \mathrm{Obs})}{\sum \mathrm{Obs}} \times 100\% \tag{2.2}$$

$$\mathrm{NME} = \frac{\sum |\mathrm{Model} - \mathrm{Obs}|}{\sum \mathrm{Obs}} \times 100\% \tag{2.3}$$

NMB is a measure of the average performance and overall bias of the modeling system. Normalizing the biases by the mean of the observations allows relative comparisons regardless of actual magnitudes of observations. NMB is a useful indicator since it avoids over-inflating performance at low values (compared with mean normalized bias, for example, where the biases are normalized before taking the average) [38].

NME is similar to NMB, except that the error is measured as the absolute value of the difference between model and observations. In this way over-predictions and under-estimations do not cancel each other out. Normalizing by the mean observation allows for relative comparisons without regard for the actual magnitudes of measurements.

Median statistics are often used in place of the averages (summations) in Equations (2.2) - (2.3), yielding Normalized Median Bias (NMdnB) and Normalized Median Error (NMdnE). Median values are useful in skewed datasets, or when outlying data points might cause a significant deviation in the mean value. In particular, hourly measurements of ozone and $PM_{2.5}$ might yield observations near zero as well as instantaneous peaks, yielding exceptionally high biases and errors. Taking the median instead of the mean places less emphasis on these outliers and focuses the analysis on the bulk of the data. The time averaging that is performed in computing annual $PM_{2.5}$ and seasonal 8-hour daily maximum ozone, however, smoothes the biases and errors thereby making the mean and median values comparable; therefore, only the mean values are considered in this thesis.

Statistical measures are compared against several prior modeling efforts by the US EPA. This provides a basis with which to compare model biases and errors and quantitatively judge the model's performance.

In addition to looking at statistical measures, timeseries, boxplots and scatterplots are also utilized to understand the model behavior. Time-series show the model output as a function of time (hourly, daily or monthly) and illustrate the model's ability to capture pollution episodes or temporal variations in concentrations. In addition, they are well-suited to assess performance over specific monitor sites. Boxplots are useful for assessing the performance over multiple sites, where the spread of observations within each period is represented as interquartile ranges. Scatterplots provide information on model performance at specific ranges of observations (for example, model performance at high ozone observations), and are generated by plotting model predictions against all available observation data.

2.5.4 $PM_{2.5}$ and Ozone Evaluation

Table 3 provides the magnitudes of NMB and NME for the 2005 control case (Simulation #1).

Table 3: CMAQ NMB and NME for the 2005 background scenario

	NMB (%)	NME (%)
STN $PM_{2.5}$	3.0	42.9
IMPROVE $PM_{2.5}$	10.3	57.8
AQS 8hr maximum O_3	5.8	18.5

Model $PM_{2.5}$ outputs at STN and IMPROVE monitors have relatively low NMBs but high NMEs, indicating that the model performs better at capturing annual-averaged mean concentrations than temporal fluctuations. It is observed that IMPROVE sites have higher NMBs and NMEs compared with STN sites, attributable to different spatial coverage of the two networks as well as differences in filtering and processing methodologies [48]. Ozone NMB is lower than NME, similar to $PM_{2.5}$, indicating that seasonal averages are represented better than peak values. The ozone NME is comparatively lower with respect to $PM_{2.5}$, partly due to the computation of 8-hour daily maximum ozone which smoothes hourly fluctuations.

The statistics are compared with prior modeling performance evaluations in order to gauge the relative performance of the current CMAQ4.7.1 modeling platform. Foley et al. [49] evaluated CMAQv4.7 for a 12 km nested Eastern US grid for two months in 2005, using Weather Research and Forecasting (WRF)-derived meteorological inputs. The EPA's Light-Duty Vehicle Greenhouse Gas Emissions Final Rule (LDV-GHG) Regulatory Impact Analysis [22] evaluated CMAQ4.7.1 for their application using 12km Eastern and Western US grids for a base year of 2006. The statistics from these evaluations are shown in Table 4 and Table 5. Note that Foley et al. used median statistics instead of mean values for all species, and the LDV-GHG evaluation applied a 40 ppb threshold on seasonal average 8-hour daily maximum ozone to restrict the assessment of model performance to days with relatively high observed ozone levels.

Table 4: Statistics from the CMAQ model evaluation performed by Foley et al. [49]

Foley et al.		**NMdnB (%)**	**NMdnE (%)**
STN $PM_{2.5}$	January	19.1	39.1
	August	-6.4	29.1
IMPROVE $PM_{2.5}$	January	9.5	39.7
	August	-28.4	37
AQS 8hr maximum O_3	January	3.9	13.2
	August	6.9	14.5

Table 5: Statistics from the CMAQ model evaluation performed in the EPA's LDV-GHG Final Rule Regulatory Impact Analysis [22]

	STN $PM_{2.5}$		**IMPROVE $PM_{2.5}$**		**AQS 8hr maximum O_3 (40ppb threshold)**	
EPA LDV-GHG	**NMB (%)**	**NME (%)**	**NMB (%)**	**NME (%)**	**NMB (%)**	**NME (%)**
Northeast	16.6	38.1	9.1	39.4	2.4	12.6
Midwest	19.5	45.6	21.5	52.9	-0.9	11.1
Southeast	-7.2	34.1	-10.5	37.2	2.3	12.3
Central	0.6	41.7	-5.5	42.4	-4.8	13.2
West	-10.9	46.1	-13.3	45	-0.2	13.5

CMAQ performance for $PM_{2.5}$ is comparable with the Foley et al. and EPA LDV-GHG simulations. The NMB falls within the range of seasonal and spatial values provided by Foley and EPA's LDV-GHG assessments respectively for both STN and IMPROVE sites. CMAQ NME for $PM_{2.5}$ lies towards the upper range of the values reported in the two tables. For ozone, the CMAQ NMB of 5.8% falls within the range of Foley et al. and is marginally higher than the spatial range of statistics in the LDV-GHG comparison. CMAQ NME's for ozone are higher than both comparisons. These errors could arise due to the differing grid resolution (36 km as opposed to 12 km), or, in the case of LDV-GHG ozone, the application of a 40ppb minimum threshold which filters out poorer performance of CMAQ at low ozone concentrations.

Scatterplots for annual $PM_{2.5}$ from both networks and seasonal ozone are shown in Figure 2-3 (a)-(c). $PM_{2.5}$ is spread about the 1-to-1 line in comparison with STN monitors, giving rise to the low mean bias observed in Table 3. For IMPROVE sites the positive bias is seen in the cluster of points near the 2-to-1(upper) line, where CMAQ tends to over-predict low and high observation values. For 8hr daily maximum ozone, low values are over-predicted while high values are under-predicted, which is a known source of error within the CMAQ model [49].

Figure 2-3 (d)-(e) shows annual box-plots for FRM (STN) $PM_{2.5}$ and a seasonal box-plot for AQS 8-hour daily maximum ozone respectively. CMAQ-predicted $PM_{2.5}$ follows the overall seasonal trends in FRM $PM_{2.5}$, with over-predictions in the winter and under-predictions in the summer. This is similar to the biases observed by Foley et al. (statistics reproduced in Table 4). Ozone performance shows a small but consistent over-prediction throughout the ozone season, which is expected given the positive bias of 5.8% as shown in Table 3.

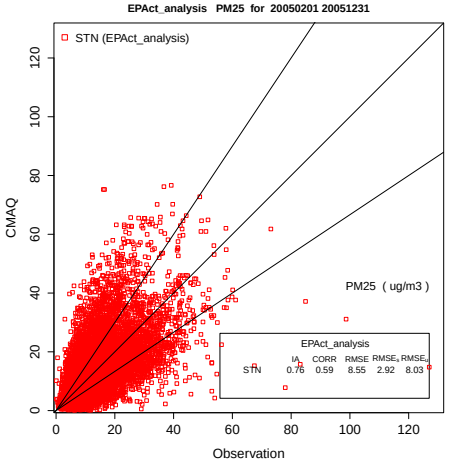

(a) STN $PM_{2.5}$ scatterplot

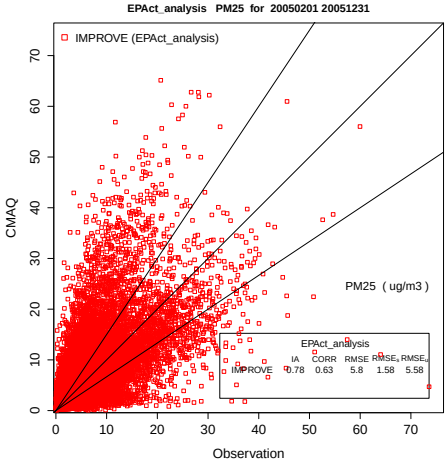

(b) IMPROVE $PM_{2.5}$ scatterplot

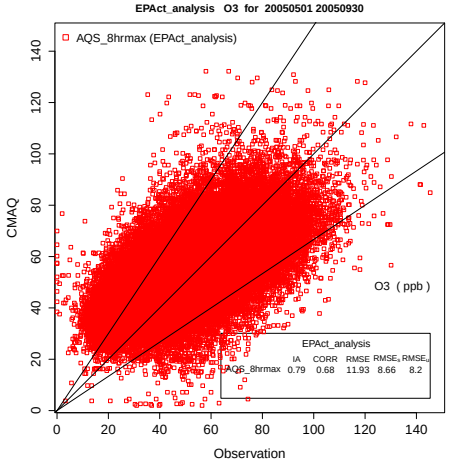

(c) AQS 8hr maximum ozone scatteplot

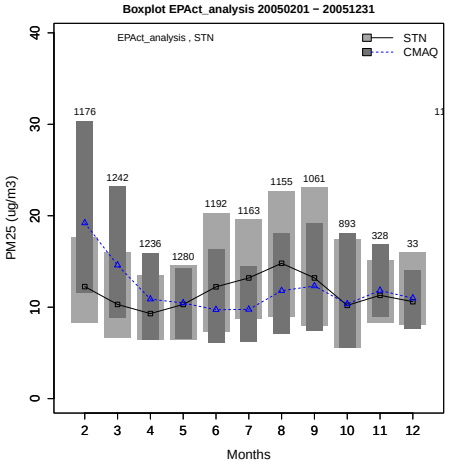

(d) FRM (STN) $PM_{2.5}$ boxplot

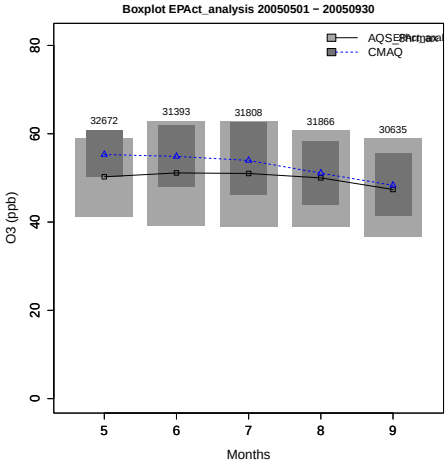

(e) AQS 8hr maximum ozone boxplot

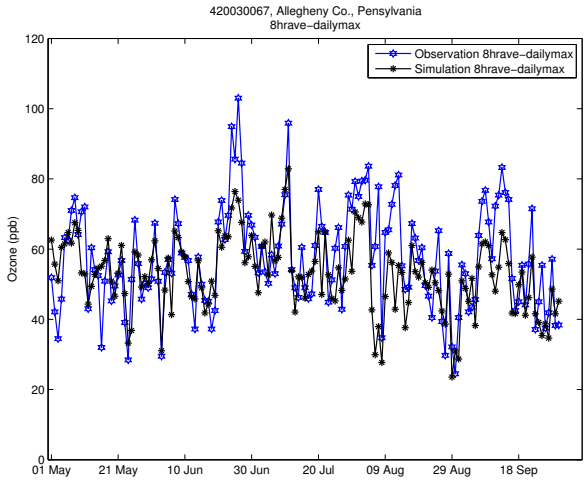

(f) AQS 8hr maximum ozone timeseries

Figure 2-3: CMAQ performance evaluation plots

Time-series plots are analyzed to determine model performance at specific monitor sites. An example of a time-series plot of 8-hour daily maximum ozone (during the ozone season) is illustrated in Figure 2-3 (f) for a site in Allegheny County, Pennsylvania. CMAQ captures the mean trends during the season, but misses several peak values, a behavior characteristic of the model as explained by the scatterplot.

Overall the CMAQ model performs within expectations and the performance statistics are similar to those reported in the two other studies, bearing in mind differences in grid resolution, range of domain and model inputs. While the quantification of the model biases on the aviation signal may not be straightforward, it is assumed that the biases do not significantly impact the model's ability to capture the aviation-attributable air quality impacts.

2.6 The Response Surface Model

2.6.1 Model Description

The RSM [10] is a reduced order air quality model designed as part of the FAA's Aviation Environmental Portfolio Management Tool (APMT) [50] to model the impact pathway from aviation emissions to air quality and (ultimately) human health impacts. Its high computational speed and reduced-form structure make it a suitable tool for multi-scenario policy analyses with quantification of uncertainty ranges and probabilistic analyses.

The APMT RSM model consists of modules which translate aviation emissions into monetary damages. This process is described by the flowchart in Figure 2-4. Airport-level LTO emissions are derived from aviation operation scenarios, often times generated by external programs/agents such as the FAA's Aviation Environmental Design Tool (AEDT) managed by Department of Transportation Volpe Center, or consulting agencies such as CSSI and Metron. These emissions are then input into an air quality module, which forms the core component of the RSM that computes the marginal change in ambient $PM_{2.5}$ concentrations (speciated PM in RSMv2) attributable to aviation emissions.

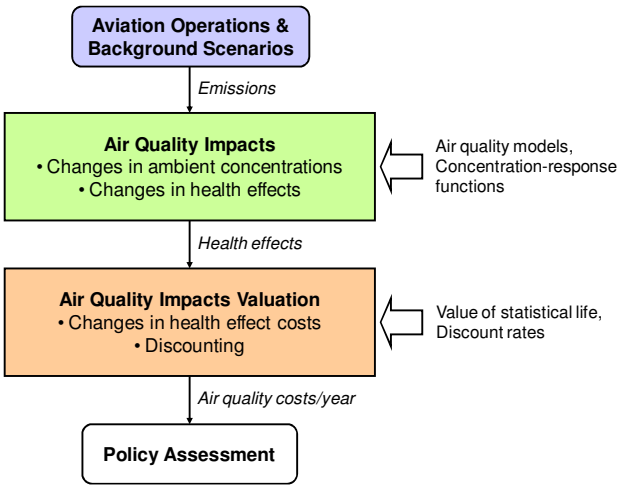

Figure 2-4: APMT-Impacts Response Surface Model (RSM) process flow

Concentration-response functions (CRFs) relate changes in ambient PM exposure to several health endpoints or incidences (further details are included in Brunelle-Yeung's thesis [11]). The health endpoints are monetized in the final step, the largest cost typically arising from premature adult mortalities. For scenarios extending into the future, future costs are discounted according to a 2%, 3%, or 5% discount rate [50].

The strength of the RSM lies in its speed in estimating PM concentrations due to aviation emissions. Firstly, the expeditious nature of the code allows uncertainty propagation through the model. Many sources of uncertainty exist within the model: input emissions variability in fuel sulfur content (FSC), uncertainties in health impact CRFs, distribution of monetary valuations, are a few examples of potential sources of variability. These uncertainties are described in terms of probability distributions that are sampled via a Monte-Carlo simulation within the RSM. Whereas an annual CMAQ simulation (with a deterministic set of emissions) has a runtime on the order of days to weeks, a probabilistic RSM run with 10,000 random draws requires on the order of hours to finish. A second advantage of a fast model is the ability to simulate multiple "what-if" scenarios, as required by many policy analyses [15]. The ability to assess a policy with multiple scenarios, and estimate the range of effectiveness of the policy through uncertainty propagation, are key characteristics of the RSM that make it a well-suited policy decision-making and analysis tool. The efficiency of the RSM is achieved through the design of the core module, which approximates the CMAQ CTM by generating a response surface through linear regressions. The regression model is described in further detail in the following section.

2.6.2 Response Surface Regression Model

The core of the RSM lies in the air quality model – translating aviation LTO emissions into changes in ambient concentrations of the PM species. This is done through a response surface, which comprises a linear regression of the $PM_{2.5}$ concentrations (and, in version 2 of the RSM, the five major PM species impacted by aviation: Nitrates (NO_3^-), sulfates ($SO_4^=$), ammonium (NH_4^+), elemental carbon (EC) and organic carbon (OC)) against four emission species: fuel burn (FB), NO_x, SO_x, and black carbon (BC). Equations (2.4) through (2.8) illustrate the form of the regression:

$$[NH_4^+] = \beta_1(FB) + \beta_2(SOx) + \beta_3(NOx) + \beta_4(BC) \quad \textbf{(2.4)}$$

$$[EC] = \beta_5(FB) + \beta_6(SOx) + \beta_7(NOx) + \beta_8(BC) \quad \textbf{(2.5)}$$

$$[SO_4^=] = \beta_9(FB) + \beta_{10}(SOx) + \beta_{11}(NOx) + \beta_{12}(BC) \quad \textbf{(2.6)}$$

$$[NO_3^-] = \beta_{13}(FB) + \beta_{14}(SOx) + \beta_{15}(NOx) + \beta_{16}(BC) \quad \textbf{(2.7)}$$

$$[OC] = \beta_{17}(FB) + \beta_{18}(SOx) + \beta_{19}(NOx) + \beta_{20}(BC) \quad \textbf{(2.8)}$$

An ensemble of CMAQ simulations is used to derive the β coefficients in the equations. The four aviation emissions inputs are perturbed by scaling factors that are carefully chosen to span the RSM design space. The design space, given in Table 6, is defined to incorporate not only present-day aviation scenarios, but also future year scenarios and the potential policy measures that might be implemented. A set of 27 sample points (with each sample point consisting of one scaling factor for each of the four inputs) is selected through a low-discrepancy Halton sampling sequence that efficiently samples the 4-dimensional design space. The combination of scaling factors in each sample point is applied to the aviation emissions, and a CMAQ simulation is conducted to isolate the impact of aviation on $PM_{2.5}$ (through the difference of annual-averaged surface-level PM concentrations, similar to the methods described in this thesis). The 27 data points are then regressed against the corresponding input scale factors to obtain the coefficients in the equations. The regression is performed for each grid-cell in the CMAQ modeling domain.

Table 6: RSM design space ranges (taken from Masek [10])

Variable	Min	Max
Fuel burn multiplier	0	2.5
Fuel sulfur content multiplier	0.025	5
Inventory NO_x EI multiplier	0.7	1.1
Inventory nvPM EI multiplier	0.25	3.6

The CMAQ simulations were performed using 2001 meteorology, IC/BCs and background emissions scenario. Due to the long runtime of CMAQ (on the order of days to weeks), the four months of February, April, July and October were modeled. LTO aviation emissions from 325 airports in the US were used in the baseline case, with vertical profiles applied to distribute emissions vertically. The RSM domain is similar to the one used in the current CMAQ model in this thesis, differing only in grid origin and vertical layer coordinates.

Chapter 3 Aviation Scenarios

This chapter describes the methodologies behind current and future aviation activity and emissions generation. National emissions totals are presented for each of the three years: base year 2006, and future years 2020 and 2030 A characterization of the uncertainties in the base year and future year emissions is presented at the end of the chapter, to illustrate the possible ranges of values which the emissions could take on.

3.1 Base year 2006 LTO Aviation Activity

3.1.1 Landing and Take-Off (LTO) Cycles

The LTO cycle consists of several modes of flight: Ground idle, ground taxi, takeoff, climb-out and descent, and is defined as operations at or below 3000ft. Traditionally aviation emissions have been regulated only within the LTO phases of flight [51] with the reasoning that local air quality is affected by aviation primarily due to emissions within the atmospheric mixing layer (or planetary boundary layer). This is because the mixing layer contains turbulent eddies and vertical motion of the air [16], transporting emissions and particulate matter to the surface layer and impacting local air quality. A recent study by Barrett et al. [52] demonstrated that the inclusion of full-flight emissions could lead to up to 5 times the health impacts globally, as a result of long-range atmospheric transport at cruise altitudes and large-scale motions of the atmosphere (such as the Hadley and Ferrell cells). Consistent with the existing aviation regulatory impact analysis practice, this thesis assesses current and future air quality impacts of aviation LTO activity only.

The definition of LTO cutoff height requires further explanation. The FAA defines a categorical exclusion for all flights over 3000ft above ground level (AGL) in modeling local air quality impacts [14]. The International Civil Aviation Organization (ICAO) defines LTO as being at or below 3000ft above the field elevation of the airport (AFE). In an environment without geographic features such as mountains or valleys these definitions are interchangeable; however, in the presence of a cliff, for example, emissions may be underestimated if a cutoff with respect to ground level is used instead of an airport reference. This happens as since the aircraft's altitude AGL would jump once the aircraft passes over the cliff and the aircraft thus spends less

time below 3000ft AGL than 3000ft AFE. Similarly, for the case when an airport is close to a mountain, using a cutoff of 3000ft AFE would lead to lower emissions than if AGL were used. This concept is illustrated in Figure 3-1:

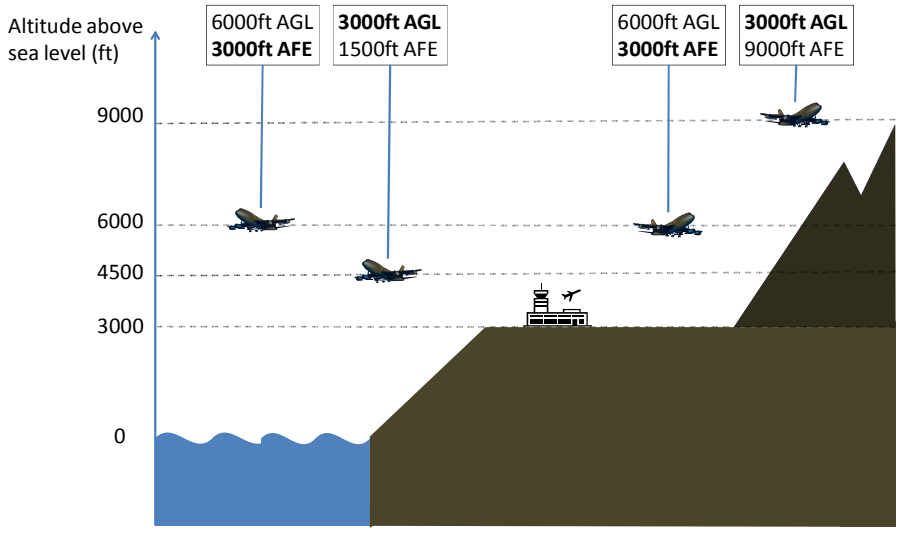

Figure 3-1: Illustration of altitude above ground level (AGL) and above field level (AFE)

The emissions processing methods used in this thesis employ the AFE definition to filter flight activity. Note that, even though FAA defines LTO as 3000ft AGL, this methodology is consistent with the implementation in the FAA's Emissions Dispersion and Modeling System [53], which is required by the FAA in regulatory air quality modeling. In some sense, the airport elevation is used as an approximation of the ground level elevation surrounding the airport (encompassing the range within which aircraft climb or descend to 3000ft). The use of AFE also provides a conservative estimate of LTO emissions, and amounts to approximately 3% greater LTO totals than AGL; the cause for the differences in emissions likely arises from more airports being located next to valleys and cliffs rather than elevated obstacles such as mountains.

3.1.2 Aviation Activity Data

Base year aviation activity is computed by the US Department of Transportation (USDOT) John A. Volpe National Transportation Center using data from Enhanced Traffic Management System (ETMS) [54], Enhanced Tactical Flow Management System (ETFMS) [55] and Official Airline Guide (OAG) [56]. ETMS is a compilation of radar tracks and flight plans for flights under the FAA's radar system and includes commercial aviation, scheduled cargo, general aviation and

charter flights within all of North America and parts of Western Europe, serving as the FAA's repository for electronic flight position recording and flight plan information for use in air traffic management [57]. ETMS data is combined with data from the ETFMS from EUROCONTROL to include coverage of the European airspace. An estimated 50-60% of worldwide commercial aviation activity is thus captured via radar coverage. Gaps in radar coverage are filled through consultation of schedules listed in the Official Airline Guide (OAG), and other unscheduled flights are accounted for by scaling known flights [55].

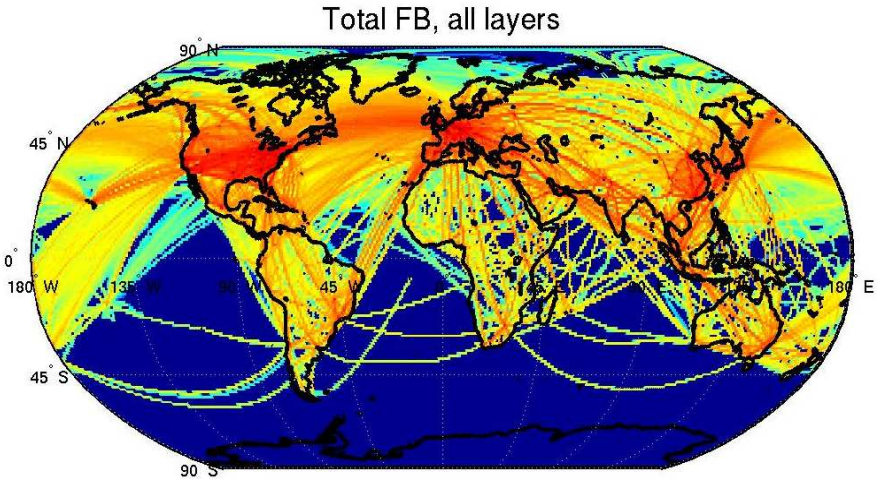

Figure 3-2: Global flights modeled in AEDT (Fuel burn in kg plotted on a log scale)

Flight radar tracks and trajectories are discretized into segments both temporally and spatially. The length of each chord varies, depending on the rate of change of the physical state parameters such as flight speed, altitude or horizontal deviation [55]. The discrete spatial steps are refined within the LTO phase, given the relatively high rate of change of the state of the aircraft (i.e., maneuvering, climb restrictions, etc.) compared with other flight phases. Short flight segments within the LTO regime also enable accurate spatial allocation of flight emissions into the CMAQ grid, especially since the vertical grid structure is dense within the PBL.

3.1.3 Flight Selection

The global flight activity data is filtered to exclude certain flights. First, military, helicopter and piston-engine aircraft are excluded. Military flights rarely operate on regular schedules, and their flight tracks are not made public, and as a result both current and future activity cannot be estimated. Piston-engine aircraft and rotorcraft are not subject to similar certification standards

as general aviation or commercial aviation, and emissions characterization for these aircraft are difficult due to lack of emissions models and emissions measurement data for validation. A list of the aircraft types that were filtered out is provided in Appendix D.

Due to the regional nature of the air quality study performed in this thesis, global flight activity data is filtered to include US flights only. International flights arriving at or departing from a US airport are included in the LTO inventory, since emissions from these flights will have an impact on the regional air quality. It is important to note that even through the CMAQ domain includes several major airports in Canada and Mexico, aviation activity at these airports is not included in the aviation inventory. While this may lead to localized under-representation of air quality over the US (for example, downwind of major Canadian airports such as Vancouver and Toronto), its effects on the domain-averaged impacts are assumed to be small. Flights into and out of Alaska and Hawaii are treated in a similar fashion as international flights, given that these states are located outside the modeling domain. A list of excluded airports in Alaska and Hawaii is presented in Appendix E .

3.2 Emissions Methodology

The FAA's Aviation Environmental Design Tool (AEDT) was utilized to compute aircraft emissions from the base year flight activity data. The overall methodology in converting aviation activity into emissions is as follows: flight track segments are combined with actual/estimated aircraft takeoff gross weight and aircraft performance characteristics such as thrust-specific fuel consumption (TSFC) and drag. AEDT then dynamically models aircraft performance in space and time and computes fuel burn estimates for each flight segment. Fuel burn forms the basis for modeling other emission species for the flight segment, through multiplicative factors known as Emissions Indices (EIs) and correlations that rely upon the rate of fuel burn.

3.2.1 CO, HC and NO_x

The Boeing Fuel Flow Method version 2 (BFFM2, [58]) is used to compute CO, HC and NO_x emissions. This method has been reviewed by the ICAO WG3 and deemed to be an acceptable modeling method of CO, HC and NO_x, and as such forms the "de-facto standard" [57] in aviation emissions characterization. BFFM2 computes CO, HC and NO_x EIs as a function of ICAO databank fuel flows, including various correction factors for installation effects and atmospheric adjustments. The correlations are either log-linear (for NOx EI) or log-bilinear (for CO and HC

EI), as depicted in Figure 3-3 (taken from Kim et al. [57]). Low fuel-flow corresponds to lower combustion temperatures, resulting in lower amounts of nitrogen in the air being thermally dissociated and oxidized to form NO_x, and vice-versa for high fuel-flow rates. The converse relationship is true for CO and HC: at low fuel-flow settings combustion is less efficient, leading to higher CO and HC emissions.

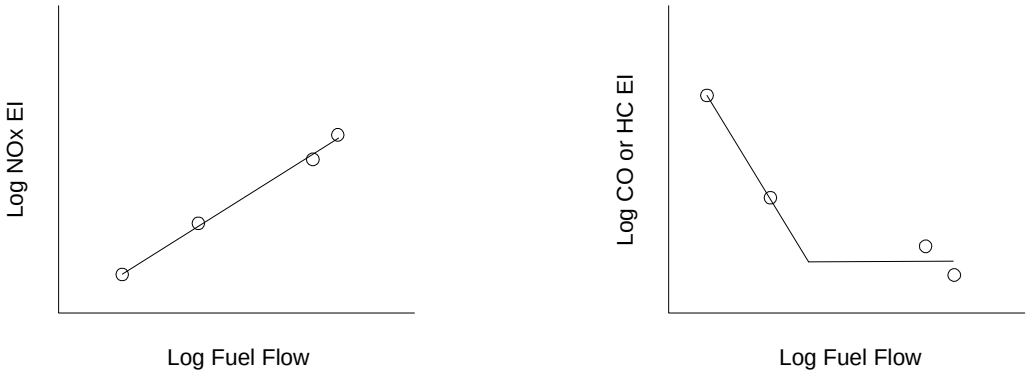

Figure 3-3: Boeing fuel-flow method version 2 NO_x EI and CO/HC EI as a function of fuel flow (figure taken from [57])

Aircraft fuel-flow rates, taken from EUROCONTROL's Base of Aircraft Data (BADA) during the aircraft performance modeling, are used look up EIs from these charts. The final emission values are computed by multiplying the EIs with fuel burn during that segment, as shown in equation (3.1):

$$Emis = EI_{emis} * FB = EI_{emis} * ff * dt = EI_{emis}(ff) * ff * dt \quad \textbf{(3.1)}$$

where "emis" represents the distinct emissions species NO_x, CO and HC, and *ff* represents the fuel flow rate.

3.2.2 Primary $PM_{2.5}$

Primary $PM_{2.5}$ are aerosols that are emitted by aircraft engines, in contrast with secondary $PM_{2.5}$ which are formed in the atmosphere via the reactions of gaseous precursor emissions of NO_x, SO_2 and some unburned hydrocarbons with ambient oxidants and compounds such as ammonia. Primary $PM_{2.5}$ emissions estimates are made using the First Order Approximation v3a (FOA3a) methodology. The PM composition includes:

$$PMvols = PM_{primary\ sulfates} + PM_{primary\ OC} + PM_{lubrication\ oil} = f(FSC) + f(EI_{HC}) + 1.4g \quad \textbf{(3.2)}$$

$$PMnvols = "Smoke\ Number: Mass"\ relationship = f(SN) \quad \textbf{(3.3)}$$

$$Primary\ PM = PNvols + PMnvols \quad \textbf{(3.4)}$$

Primary sulfate and organic carbon (OC) aerosols are not present directly at a jet engine's exhaust nozzle because the high temperature of the exhaust plume prevents formation of these kinds of particles; only non-volatile PM exists at the engine exit plane. However, FOA3a is intended to estimate PM from aircraft jet engines as observed in near-field aircraft plumes; thus, the methodology considers some amount of sulfate and organic PM to be "primary" PM. FOA3a estimates PM from aircraft jet engines only, and therefore PM from turboprop engines was not computed for this study. The FOA3a methodology is a conservative extension of the FOA3 methodology that is based on work done by Wayson et al. [59]. Therefore, many of the steps that are taken in computing FOA3a $PM_{2.5}$ estimates are similar to that prescribed by FOA3. Additional details of the modifications to the FOA3 methodology can be found in the Partnership for AiR Transportation Noise and Emissions Reduction project 15 (PARTNER-15) report [7].

PMnvols represents black carbon PM (BC), or soot that is emitted from the engine. Soot forms as a result of incomplete combustion, and is highly dependent on the geometry and characteristics of the combustion process within the engine. The methodology that is used for non-volatile PM is the same as that prescribed by FOA3. FOA3 uses correlations between measured mass data and engine smoke number (SN, an engine certification parameter originally developed to address concerns over visible smoke from aircraft jet engines) in the ICAO engine emissions databank [60] to compute the soot concentration index (CI). The CI is multiplied with core exhaust flow volume (computed based on modal air-to-fuel mass ratio (AFR)) and fuel burn to calculate non-volatile PM (PMnvols) emissions. A correction factor of (1+bypass ratio) is applied to the core exhaust flow volume for SNs that are measured from internally mixed[2] exhaust flows [59]. It should be noted, though, that there have been new measurement data which suggest that errors in

[2] The Energy Policy Act Study by Ratliff et al. utilized the FOA3a version of this methodology, which applied the bypass ratio correction factor to all engines regardless of measurement flow conditions. The BC methodology used in AEDT (and therefore, used in this thesis) implements .FOA3 (where the correction factor is applied to internally-mixed flows only).

non-volatile PM estimates could be as high as an order of magnitude [61]. As such, the FOA3a BC correlation coefficients may have to be revised in light of these new findings.

Primary OC aerosols, are formed as unburnt hydrocarbons condense onto non-volatile particulates in the exhaust of the engine [62]. In FOA3a, primary OC is estimated using aerosol measurement data from APEX-1 [63] for the CFM56-2-C5 engine which are weighted by ICAO LTO time-in-mode statistics [64] (listed in Table 7), and the hydrocarbon emissions index (HC EI) for the flight segment. FOA3a estimates roughly 10 times more primary organic PM than FOA3, as a result of the conservative assumptions used in generating the emissions indices. As with PMnvols, the derivations for primary OC need to be updated to reflect new measurement data from recent campaigns [61].

PM from lubrication oil arises due to losses due to engine wear and tear, which occur predominantly when the engine is operated at high power settings [7]. Therefore primary organic aerosols from engine lubrication oil are added at a fixed rate of 1.4g per takeoff operation. It is assumed that no lube oil is converted into PM during aircraft approach and idle/taxi modes.

Table 7: ICAO Times-In-Mode (TIM) and proportion of LTO duration

Phase	Time (s)	Proportion of LTO duration
Takeoff	42	2%
Climb-out	132	7%
Taxi (Split equally between taxi-out and taxi-in)	1560	79%
Approach	240	12%

Primary sulfates are computed as a function of fuel sulfur content (FSC), sulfur oxidation efficiency ($S^{(IV)}$ to $S^{(VI)}$) and fuel burn. The amount of sulfur in the fuel governs the amount of SO_2 emitted, since that is the only major source of sulfur in the combustion process (atmospheric sulfur is not as abundant, compared to nitrogen, for example). The value for FSC is chosen to be 600ppm, which is a nominal value for jet fuel FSC within the US [65]. SO_2 emissions are oxidized into sulfuric acid downstream of the engine exit plane, which is then neutralized by atmospheric constituents to form sulfate PM. The degree to which SO_2 gets oxidized into sulfates is represented by the oxidation efficiency parameter, chosen to be 5% for this study. The

conversion efficiency is at the upper bound of measured values [66], which adds to the conservative nature of this inventory. Primary sulfate aerosols are assumed to be non-hydrated.

3.2.3 Speciation of NO_x and HC

The NO_x emissions calculated from BFFM2 are an aggregation of nitric oxide (NO) and nitrogen dioxide (NO_2) reported on an NO_2-mass basis. In order to appropriately treat the chemistry that each of these three compounds participates in, they need to be speciated into their individual constituents before being input to CMAQ. There have been several studies which have attempted to speciate NO_x by flight mode and/or altitude ([67], [68]). Measurement campaigns ([67], [69]) have indicated that engines produce relatively high NO_2 at low thrust settings, while NO dominates at high thrust settings, with a small fraction (~1%) of HONO present. The focus on LTO emissions allows the simplification from a modal speciation to a general split fraction apportionment: 23% NO_2, 76% NO and 1% HONO [68]. The NO, NO_2 and HONO values derived from this speciation scheme is approximately equal to the apportionment calculated by Wood et al. [67], based on the ICAO standard LTO cycle.

Similar to NO_x, unburnt hydrocarbon (HC) emissions are an aggregate of several organic gaseous compounds and need to be speciated for the chemistry. HCs are first converted into Total Organic Gases (TOG) using a conversion factor of 1.16, then speciated into their chemical constituents and aggregated into lumped species used by the CMAQ CB05 chemical mechanism. The FAA-EPA May 2009 Total Organic Gas (TOG) Speciation profile (shown in Appendix F) is employed to speciate the hydrocarbons into their chemical constituents. Aviation emissions are mapped to several extra toxic species in addition to the standard CB05 lumped species, since CMAQ is built with the explicit air toxics module enabled. The final list of conversion factors that map HC emissions (in g) into the lumped species (mol) is shown in Appendix G.

3.3 Future-Year Aviation Activity Forecast

The base year 2006 LTO inventory is projected via scaling factors to model the aviation activity in 2020 and 2030. Aviation activity and emissions scaling factors are derived from the year 2009 FAA Terminal Area Forecast (TAF) projections as well as ICAO NO_x stringency controls. Explicit changes in fleet mix and route structure are not implemented in the activity forecasts (as will be explained in the following section, however, some of these effects are implicitly included

in the TAF projections). This section describes the flight activity data projection and characteristics as predicted by the TAF.

3.3.1 FAA TAF Methodologies

The FAA's TAF system serves as the official outlook for aviation activity at FAA facilities [70], designed to meet budget and planning needs of the FAA, the industry, state and local agencies and the public. It contains aircraft activity and passenger enplanement forecasts for currently active airports as identified in the National Plan of Integrated Airport Systems (NPIAS) [71]. FAA forecasts are required by mandate to be representative of local conditions at airports, based on the latest available data, and provide justification for airport planning and development [72], and this is reflected in their forecasting methodologies.

Aviation activity forecasts are developed based on historical trends of aviation activity (which include data on passenger enplanements, operational factors such as average seats per aircraft and load factors, peak hour activity and based aircraft) with respect to national and local conditions (such as national socioeconomic data, FAA's Aviation System Performance Metrics (ASPM) data for specific large airports and OPSNET) that affect aviation activity. Data for these regression analyses come from a variety of sources, as described in the FAA TAF report [70]. The TAF assumes that the demand for aviation will not be subject to new constraints in the future; it is developed independent of an airport's current ability to handle increased demands. While the TAF is updated infrequently to include significant shifts due to major airline decisions (i.e. a merger or dissolution), the activity projection does not explicitly include the incorporation of new aircraft into the fleet nor any effects of changing network structure. Constraints and long-term fleet and network evolution effects are represented only to the extent they exist in historical trends.

3.3.2 FAA TAF Activity Data

Itinerant and local operations contained within the 2009 TAF dataset were processed by Eastern Research Group (ERG)[3] to calculate the LTO activity at each airport in the aviation inventory, for the base year 2006 as well as future years 2020 and 2030. Aviation activity is categorized into four TAF bins: general aviation (GA), air taxi (AT), air carrier (AC) and military. Military

[3] ERG processed the FAA TAF as part of the EPAct Follow-on project aviation inventory modeling activities.

operations were removed (since they are not in the scope of aviation activity modeling as described in Section 3.1.3), and airport aviation activity scaling factors for each TAF bin, relative to base year LTO operations, were calculated for each of the two future years. Table 8 shows the total growth in aviation activity at all airports in the inventory, as projected by the 2009 TAF. Growth is reported in the table as percentages relative to 2006 levels, rounded to two significant digits. In general, air carrier activity is expected to grow by approximately 24% by 2020 and by 55% by 2030 relative to base year levels. Air taxi and general aviation operations are expected to first decrease by 2020, and then increase by 2030.

Table 8: Aggregate TAF growth for all airports in the aviation inventory

Arrival Airports TAF LTO Activity (Number of LTOs)				Departure Airports TAF LTO Activity (Number of LTOs)		
Air Carrier						
Baseline 2006	2020	2030		Baseline 2006	2020	2030
6,387,751	7,884,670	9,898,474		6,373,391	7,884,670	9,898,474
growth (w.r.t 2006)	23%	55%		growth (w.r.t 2006)	24%	55%
Air Taxi						
Baseline 2006	2020	2030		Baseline 2006	2020	2030
6,640,197	6,253,281	7,164,746		6,610,209	6,176,969	7,088,434
growth (w.r.t 2006)	-5.8%	7.9%		growth (w.r.t 2006)	-6.6%	7.2%
General Aviation						
Baseline 2006	2020	2030		Baseline 2006	2020	2030
37,468,092	37,056,657	40,158,907		37,497,261	37,093,462	40,198,852
growth (w.r.t 2006)	-1.1%	7.2%		growth (w.r.t 2006)	-1.1%	7.2%
Total						
50,496,039	51,194,607	57,222,127		50,480,861	51,155,100	57,185,760
growth (w.r.t 2006)	1.4%	13%		growth (w.r.t 2006)	1.3%	13%

Note that even though the TAF comprises LTO operations (and hence does not make a distinction between flight legs), there is a slight difference between arrival and departure airport activity; this occurs since in the base year inventory, the number of airports for each flight leg is slightly different (3566 arrival airports vs. 3540 departure airports).

3.4 Future year Emissions Projection

Base year emissions are scaled up to future-year levels by incorporating airport activity growth information from the TAF. It should be noted that, apart from NO_x stringency reductions in NO_x emissions, no other changes in engine technology, alternative fuels or implementation of new aviation policy measures are considered when generating future year emissions.

The TAF scaling of the base year 2006 LTO inventory is performed on an aircraft-airport basis; that is, the TAF bin of each aircraft at a given airport is used to identify the scaling of emissions for that flight, instead of applying an average scale factor for all aircraft at each airport. Doing so weights the scale factor in each TAF bin based on the amount of emissions in that bin. NO_x stringency scenario 6 is applied to NO_x emissions forecasts in 2020 and 2030 to account for the implementation of NO_x stringency measures proposed by ICAO CAEP/8.

3.4.1 CAEP/8 NO_x Stringency

The changes in NO_x emissions due to the implementation of an ICAO CAEP/8 NO_x stringency policy are implemented in the future emissions forecasts. The ICAO CAEP/8 NO_x stringency rules, as well as policy scenarios specifically considered by CAEP/8, are listed in Mahashabde et al. [12]. NO_x stringency Scenario 6 was selected by CAEP/8 during the committee meeting in February 2010 [73]; this stringency is therefore applied to future aviation inventories.. The CAEP/8 NO_x stringency emissions inventory is provided by Volpe Center and includes NO_x emissions for each airport - flight leg combination, for various stringency levels, modeling the years 2006, 2016, 2026 and 2036.

Table 9: ICAO CAEP/8 NOx Stringency #6 vs. Stringency #0 NO_x emissions

	NO_x Emissions (short tons/year)		Change in NO_x (%)
Year	Stringency 0	Stringency 6	(Str6 – Str0) / Str0
2016	9.52×10^4	9.37×10^4	-1.6%
2020	$\mathbf{1.08 \times 10^5}$	$\mathbf{1.05 \times 10^5}$	**-3.0%**
2026	1.28×10^5	1.21×10^5	-5.1%
2030	$\mathbf{1.46 \times 10^5}$	$\mathbf{1.37 \times 10^5}$	**-6.0%**
2036	1.75×10^5	1.62×10^5	-7.3%

Table 9 lists the aggregate (arrival + departure, summed over all airports) emissions from the CAEP/8 NO_x stringency dataset. If an airport exists in the base year 2006 inventory, but not in the CAEP/8 inventory, an average factor is assumed depending on the flight leg. All other emissions species are assumed to be unchanged. Emissions from the CAEP inventory are linearly interpolated in time to obtain NO_x emissions estimates for the target modeling years of 2020 and 2030 (shown in bold font in Table 9). Stringency 0 represents the baseline emissions levels (i.e. without any NO_x stringency policies enacted). The ratios of NO_x levels between Stringency 6 and Stringency 0 are computed on an airport-flight leg level and applied to the NO_x emissions calculated from TAF growth alone.

3.5 Aviation Emissions Totals

Table 10 provides a national inventory summary of the base year 2006 LTO emissions inventory, as well as the projected future year inventories. Aggregate aircraft operations are also given. Net growth percentages are given in Table 11. The base year inventory presented here is a product of the aforementioned filtering and elimination procedures, and the future year inventories are a result of the scaling factors discussed above. For the 60 busiest airports (ranked by amount of fuel burn), airport-level emission totals as well as TAF scaling factors and NO_x stringency reduction ratios for each airport are given in Appendix H.

The emission growths align well with the projected air carrier activity growths of 23-24% by 2020, 55% by 2030 as shown in Table 8; the notable exception to this trend is HC emissions (and as a consequence, primary OC emissions). This suggests that air carriers are responsible for a comparatively smaller percentage of HC emissions relative to AT/GA aircraft, in comparison with other emission species such as CO or SO_2; thus the net change in HC emissions is weighted more towards AT/GA activity.

Table 10: Base year 2006 and future years 2020 and 2030 aviation LTO inventory

	Baseline 2006				Future 2020				Future 2030		
Short Tons / Year	**Arrival**	**Departure**	**Total**		**Arrival**	**Departure**	**Total**		**Arrival**	**Departure**	**Total**
Fuel Burn	$2.61x10^6$	$4.78x10^6$	$7.40x10^6$		$3.26x10^6$	$6.03x10^6$	$9.28x10^6$		$4.05x10^6$	$7.54x10^6$	$1.16x10^7$
CO	$4.52x10^4$	$7.24x10^4$	$1.18x10^5$		$5.41x10^4$	$8.85x10^4$	$1.43x10^5$		$6.63x10^4$	$1.10x10^5$	$1.76x10^5$
NO_x (as NO_2)	$1.66x10^4$	$6.22x10^4$	$7.88x10^4$		$1.99x10^4$	$7.56x10^4$	$9.55x10^4$		$2.43x10^4$	$9.21x10^4$	$1.16x10^5$
SO_2	$2.98x10^3$	$5.45x10^3$	$8.43x10^3$		$3.71x10^3$	$6.87x10^3$	$1.06x10^0$		$4.62x10^3$	$8.59x10^3$	$1.32x10^4$
HC	$8.57x10^3$	$1.31x10^4$	$2.17x10^4$		$9.41x10^3$	$1.48x10^4$	$2.43x10^4$		$1.12x10^4$	$1.80x10^4$	$2.92x10^4$
BC	$8.02x10^1$	$2.62x10^2$	$3.42x10^2$		$1.08x10^2$	$3.56x10^2$	$4.64x10^2$		$1.33x10^2$	$4.38x10^2$	$5.71x10^2$
Primary sulfates	$2.40x10^2$	$4.40x10^2$	$6.80x10^2$		$2.99x10^2$	$5.54x10^2$	$8.53x10^2$		$3.72x10^2$	$6.92x10^2$	$1.06x10^3$
Primary OC	$4.95x10^2$	$1.19x10^3$	$1.68x10^3$		$5.44x10^2$	$1.35x10^3$	$1.89x10^3$		$6.49x10^2$	$1.63x10^3$	$2.28x10^3$
Operations	13,060,683	13,067,060	26,127,743		15,469,931	15,468,817	30,938,748		18,725,815	18,721,358	37,447,172

Table 11: Net growth of future year aviation emissions

Growth w.r.t base 2006	**Future 2020**				**Future 2030**		
	Arrival	**Departure**	**Total**		**Arrival**	**Departure**	**Total**
Fuel Burn	25%	26%	26%		55%	58%	57%
CO	20%	22%	21%		47%	51%	50%
NO_x (as NO_2)	20%	22%	21%		47%	48%	48%
SO_2	25%	26%	26%		55%	58%	57%
HC	10%	13%	12%		31%	37%	35%
BC	35%	36%	36%		65%	67%	67%
Primary sulfates	25%	26%	26%		55%	58%	57%
Primary OC	10%	14%	12%		31%	37%	36%
Operations	18%	18%	18%		43%	43%	43%

3.6 Uncertainty in Aviation Emissions

3.6.1 Base Year Uncertainty

The methods used to develop the base year aviation inventory represent current, widely used and well-accepted emissions modeling techniques, incorporating actual air traffic information, realistic aircraft performance modules and emissions characterization methodologies such as FOA3a and BFFM2, as described in Section 3.2. These methods, however, have several sources of uncertainty inherent in them, which are important to quantify using error bounds.

Uncertainty estimates in the base year 2006 aviation emissions are derived from the uncertainty quantification performed by Stettler et al. [61] for UK airports. Stettler performs a Monte-Carlo simulation using 1000-member ensembles, with probability distributions on emissions characterization parameters such as aircraft LTO Time-In-Mode, fuel flow and thrust settings, in addition to the emissions parameters (EIs, NO_2/NO_x ratio, FSC, …). The probability distribution ranges are obtained through reviews of existing literature and new experimental data. It is important to note that the probability distributions not only capture the lack of knowledge (for example, uncertainty in hydrocarbon emissions at low power settings) but also characterize the natural variability or spread in the parameter (such as variable thrust setting, or spread in FSC).

These distributions are propagated through an emissions model, which uses methods similar to that of AEDT to compute emissions species. Specifically, the model utilizes the BFFM2 for NO_x, CO and HC emissions, FSC and sulfur conversion efficiency to compute SO_2 and primary sulfate aerosol emissions, and FOA3 to compute POA and PEC (note that PEC is computed using re-estimated modal coefficients for the FOA3 functional). Although the nominal values that are assumed in the paper are different from those used in this study, the output of interest is the relative range between the 5^{th} and 95^{th} percentile.

The error ranges from Stettler et al. are presented below, as applied to the base year 2006 aviation inventory. The ranges are reported as percentages relative to the median value of each emissions species. The exceptionally high 95^{th} percentile value for hydrocarbon emissions is a result of highly uncertain aircraft taxi thrust setting and EI(HC), as demonstrated by the sensitivity analysis conducted in the paper.

Table 12: Uncertainty bounds on emissions species (adapted from Stettler et al. [61])

Emissions Species (short tons per year)	Lower (5%ile) range	Total LTO Emissions	Upper (95%ile) range
CO	(-47%) 6.25×10^4	1.18×10^5	2.21×10^5 (87%)
NO_x (as NO_2)	(-26%) 5.83×10^4	7.88×10^4	1.07×10^5 (36%)
SO_2	(-29%) 5.99×10^3	8.43×10^3	1.12×10^4 (33%)
HC	(-66%) 7.38×10^3	2.17×10^4	5.92×10^4 (173%)
BC	(-49%) 1.74×10^2	3.42×10^2	5.99×10^2 (75%)
Primary sulfates	(-56%) 2.99×10^2	6.80×10^2	1.29×10^3 (89%)
Primary OC	(-66%) 5.71×10^2	1.68×10^3	2.89×10^3 (72%)

For all of the emissions species, the upper threshold of uncertainty in the base year 2006 emissions is in fact greater than the projected increase in emissions in the future year 2020, and for some species, even greater than the projected growth in 2030. The uncertainties in the base year aviation emissions were not propagated through CMAQ to quantify the variability in air quality impacts due to the infeasible computational resource requirements that would be involved in conducting a full Monte-Carlo simulation using CMAQ.

3.6.2 Projection Uncertainty

The aviation emissions projections are dependent on several forecast datasets including the FAA TAF and improvements in technology such as NO_x emissions reductions. It is thus difficult to generate specific bounds on emissions forecasts for each species. It is possible, however, to consider the variability in the various components that feed into the projection, as well as prior projections that have been performed, to obtain an idea of the range of projections.

The FAA NPIAS states that airport forecasts generated by airport planners and sponsors will be accepted if it is within 10% of the TAF forecast for that airport over the next 5, 10 and 15 years. The metrics for evaluation include activity data such as total airport operations, total commercial operations and number of passenger enplanements [72]. This suggests that there could be at least a 10% variability in the airport-level activity data contained in the TAF.

There are a few airport forecasting studies which include probabilistic assessments of airport activity forecasts. A study done for the San Diego International Airport [74] considers a high and a low scenario, with discrete values of real personal income growth, income elasticity, and

business travel substitutions. Total passenger airline aircraft operations forecast for KSAN in 2030 range from a low estimate of 272,890 to a high estimate of 326,970 (an increase of roughly 20%). In an airport forecast performed for Portland International Airport [75], high, median and low estimates for aircraft operations forecasts are 438,200, 275,000 and 172,400, representing a [-37% , 60%] bound. While these ranges reflect airport-specific uncertainties, it becomes clear that other major airports will have similar or higher variability (especially at international airports, where aviation activity is further dependent on the highly uncertain global economy and demand for air travel).

At an aggregate level, the national emissions forecast totals are compared with those used in other studies. The FAA Aerospace Forecast 2011 [76] predicts an increase in total US aviation fuel burn from a 2006 value of 21,241 million gallons to 24,606 in 2020 (increase of 16% w.r.t 2006 levels) and 29,876 in 2030 (increase of 41% w.r.t 2006 levels). These growths are markedly lower than the forecasts performed in this thesis, due to anticipated enhancements in aircraft and engine technology that are incorporated into the Aerospace Forecast.

Woody et al. [8] utilized a growth scenario developed for the Interagency Portfolio and Systems Analysis Division of NextGen's Joint Planning and Development Office (JPDO) based on the methodologies of Gawdiak et al. [77]. The aviation inventory included emissions below 10,000ft from 99 airports in the US. In that study, net aviation activity is projected to increase by 117% from their base year of 2004 to their future projection year of 2025, a growth that is reflected in the future-year emissions as described by Table 13.

Table 13: Future aviation emissions forecasts as compared with Woody et al. [8]

Percent Increase	**CO**	**HC**	**NO_x (as NO_2)**	**SO_x**	**BC**	**Fuel burn**
Woody et al., 2004-2025	103%	79%	119%	112%	77%	112%
Thesis, 2006-2020	21%	12%	21%	26%	36%	26%
Thesis, 2006-2030	50%	35%	48%	57%	67%	57%

As such there exists significant variability in future aviation activity and emissions forecasts; however, as with base year emissions, these uncertainty ranges are not propagated through the air quality model to generate a range of air quality impacts.

Chapter 4 Background Emissions Scenarios

Background emissions complement the aviation emissions dataset as inputs to the CMAQ modeling system, and provide a complete scenario of the ambient conditions into which aviation emissions are emitted. Background emissions are essential to quantifying the air quality impacts of aviation, since they provide the necessary compounds (such as ammonia) and oxidative capacity of the atmosphere (ozone, OH radical) with which aviation precursor gaseous emission react to form secondary PM.

Background emissions contain both anthropogenic emissions, from industrial and other man-made activities, as well as biogenic emissions from natural processes occurring in vegetation (primarily VOCs) and soils (NO and CO emissions). The focus of the discussions in this chapter, however, is centered upon the data assimilation and trends of anthropogenic sources only, given the anticipated change in these emissions over the next two decades and their effect on aviation air quality impacts. As such, in this thesis, background emissions are meant to refer to non-aviation anthropogenic emissions only. Further information on biogenic emissions processing can be found at the US EPA's BEIS website[4].

The development of background emissions datasets is discussed in the next section, following which past and projected trends in background emissions are studied. Finally, the uncertainties in these emissions are characterized, and a sensitivity study to understand the effects of uncertain background emissions is proposed.

4.1 US EPA NEI Data Gathering Methodologies

Anthropogenic emissions are obtained from the US EPA National Emissions Inventory (NEI). The NEI is a comprehensive emissions inventory that reports emissions of all Criteria Air Pollutants (CAPs) and several Hazardous Air Pollutants (HAPs) within the US as well as parts of Canada and Mexico, and is compiled in a three-year cycle (the latest NEI being 2005, at the time of this writing). Data from the NEI is developed for use in air quality modeling for State Implementation Plans (SIPs), regulatory compliance assessments and emissions trading and modeling activities [78].

[4] More information found at: epa.gov/AMD/biogen.html

The NEI is created as part of a mandate pursuant to the Clean Air Act (CAA) of 1970 (amended in 1990) [79] which requires the EPA to report estimates for CAP and HAP emissions such that permit requirements may be set by regulatory agencies. Emissions are reported by source sectors, depending on the nature of the emissions and are classified as point sources, non-point (stationary area) sources, non-road mobile, on-road mobile and fire sources. EPA relies upon data gathered and reported by the numerous state, local and tribal agencies to compile the NEI. Models are used to derive some of the emissions based on other measured quantities such as electricity usage and road activity, and these are discussed below.

The EPA uses the Integrated Planning Model (IPM) to obtain emissions from Electricity Generating Units (EGUs) and other sources in the electric power sector. The IPM is a dynamic power sector model which incorporates demand for electricity, dispatch strategies and emissions control options in the form of technological changes or market-based measures, to model emissions from power generation facilities [80]. Utility data from the National Electric Energy Database System (NEEDS) is fed into the IPM along with model power-plant characteristics to obtain CAP emissions at the location of each existing plant.

Emissions from mobile sources are split into three sectors: onroad, nonroad and aircraft, locomotive and marine (alm). Mobile source emissions are derived using the EPA's National Mobile Inventory Model (NMIM), which runs the MOBILE6 program for onroad emissions, and the NONROAD2005 model for nonroad emissions. MOBILE6 utilizes annual vehicle miles travelled (VMT) and uses scaling factors based on VMT to calculate vehicular emissions. NONROAD2005 models evaporative, refueling and exhaust emissions from nonroad vehicles excluding marine, aircraft and locomotive sources, based on equipment populations, emission factors and activity levels [81].

Aviation emissions within the ALM category are excluded from the base year and future year emissions inventories. These emissions are replaced with the more detailed AEDT emissions as described in Chapter 3.

As set forth in the 2006 PM NAAQS study, emissions in the future can change due to a number of reasons including economic and activity growth, a mix in production activities between sectors, technological innovation and emissions controls [82]. These effects are incorporated in

the NEI through a variety of projection and growth factors, and implementation of current and anticipated emissions control measures [83]. The IPM is run with forecasts of energy demand (for example, from the Energy Information Administration Annual Energy Outlook (EIA AEO)) [84], proposed power plant establishments and power plant characteristics that incorporate future designs, technologies and controls to estimate changes in IPM-point sources. Estimated livestock growth rates are applied for area source ammonia emissions. Projections for VMT, activity data, fuel properties and emissions factors are input to the NMIM for future-year projections of mobile source emissions.

The 2005 base year emissions platform utilizes the 2005v2 NEI [78], while the 2025 future scenario is based on an interpolation between the 2020 and 2030 emissions from the 2002v3 CAPHAP platform projections [83]. The background inventory contains the following CAPS: CO, fine and coarse PM, NO_x, SO_2 and VOCs and ammonia [78]. Approximately 43 HAPs are considered, including HCl, Hg, benzene, acetaldehyde, formaldehyde, methanol, acrolein, 1,3-butadiene, naphthalene, toluenes and xylenes [85]. VOCs are speciated according to the EPA's SPECIATE database, which includes VOC speciation profiles based on source classification codes (SCCs).

NEI emissions are published as raw text files containing emissions by SCC. This allows for tracking of data by its origin (for example, emission from wood burning in residential fireplaces has a unique SCC of 2104008001). The application of speciation profiles (in the case of VOCs), and diurnal or seasonal temporal profiles (since most datasets are annual or monthly totals) is facilitated through SCCs as the profiles are likely similar for all sources sharing an SCC. These steps are accomplished through the Sparse Matrix Operator Kernel Emissions (SMOKE) program[5], which comprises a set of scripts and tools that are used to read, manipulate and aggregate the raw text files to produce a set of spatially and temporally allocated model-ready emission files.

The CMAQ-ready emissions files for the base and future year background scenarios are the same as the ones used in Woody et al. [8].

[5] SMOKE program available online at: http://www.smoke-model.org/index.cfm

4.2 Historical Trends and Future Projections of Anthropogenic Emissions

Anthropogenic emissions have been recorded by the EPA since its inception in 1970. Figure 4-1 shows the trends[6] of the CAPs in the NEI since this time, as well as projected future year emission inventory forecasts until the year 2030. The projected emissions are obtained using the 2002v3 CAPHAP modeling platform for the years 2009, 2014, 2020 and 2030.

The time history of CAP emissions shows that there has been a general decline in the national emission levels over the past 30 years. This decrease in emissions is brought about by the implementation of various local, state and national emissions control strategies and programs, mandated by environmental laws the most notable of which the Clean Air Act (CAA). The CAA is aimed at cleaning up commonly-found pollutants in the air (CAPs and ozone), lowering the emissions of HAPs which have serious health impacts and phasing out the production and use of chemicals that destroy stratospheric ozone.

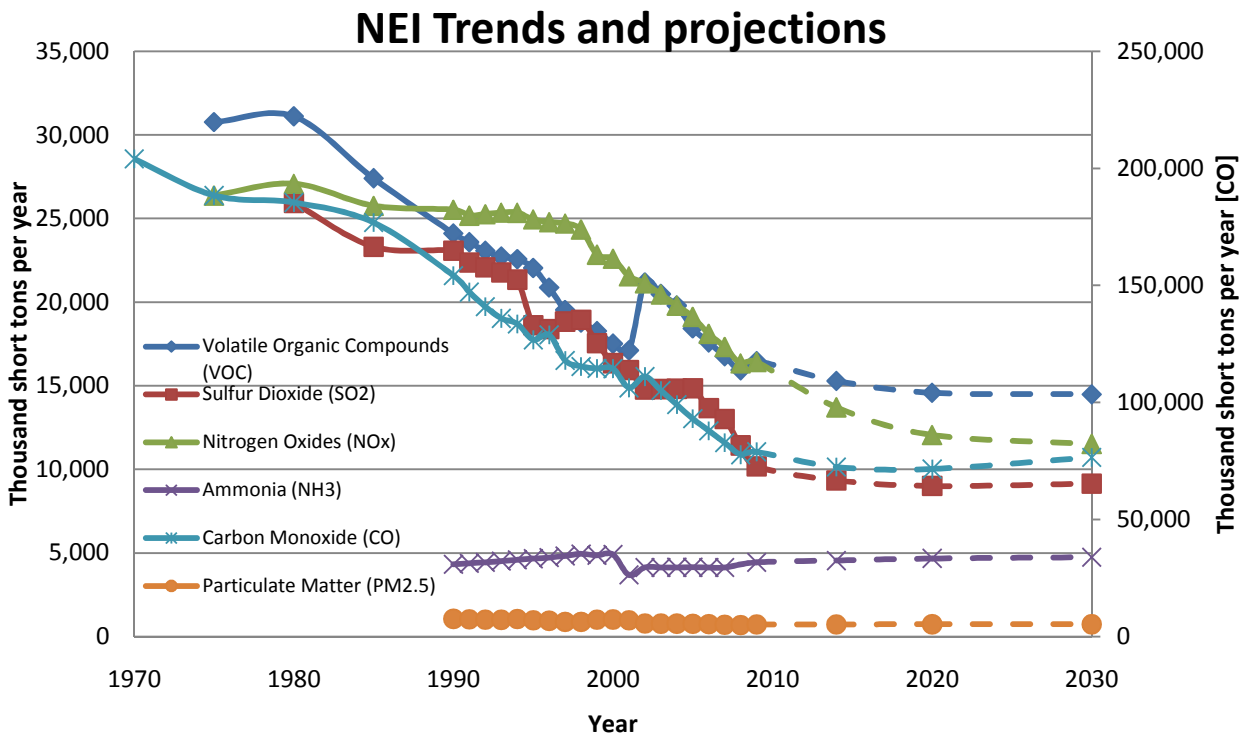

Figure 4-1: Past trends and future projections in the National Emissions Inventory (NEI)

[6] Based on National Emissions Inventory (NEI) Air Pollutant Emissions Trends Data, available online at: http://www.epa.gov/ttn/chief/trends/trends06/nationaltier1upto2008basedon2005v2.xls, June 2011

The EPA sets limits on ambient concentrations of pollutants, known as National Ambient Air Quality Standards (NAAQS). Locations where ambient levels are above the threshold are identified as non-attainment areas, and State/Tribal implementation plans (SIPs) aimed at reducing pollutant concentrations to acceptable levels are developed in consultation with local and state agencies. Emissions goals are achieved through market-based measures, permits, and technological solutions that control emissions from industrial sources such as power plants and factories. The CAA mandates air quality control strategies on a national level in addition to SIPs: The production and use of cleaner-burning engines to reduce emissions, the development and implementation of cleaner alternative fuels, the enforcement of passenger vehicle inspection and maintenance programs and the implementation of transport policies that regulate highway and transit rail line construction, are a few such examples.

The NEI forecasts a continuing decline of emissions out to 2014, 2020 and 2030, with the trend becoming approximately stagnant between 2020 and 2030. Marginal increments in certain emissions species (CO, VOC and SO_2, for example) are caused by the growth in vehicular activity (and therefore, an increase in mobile source emissions). Apart from the mobile sector (which includes onroad and nonroad emissions), other sectors use emissions from the year 2020 as a proxy for the year 2030. Specifically, the IPM model was run only till the future year 2020, and as such the EGU emissions for 2020 are used in the 2030 scenario. Resource limitations and uncertainty in the projection methodologies and capabilities are the main reasons[7] for employing 2020 emissions in the 2030 scenario. The latest compliance dates for currently proposed emissions control programs fall by 2015, and therefore no further controls beyond this date are applied to the 2020 and 2030 inventories. These factors explain the apparent stagnation in background emissions between 2020 and 2030. .

Background emissions for CMAQ modeling activities are developed for the years 2005 and 2025. The 2005 emissions are based on the 2005 NEI Data, while the 2025 scenario is linearly interpolated between the NEI forecasts for 2020 and 2030. The 2025 emissions dataset was selected to be used in place of the 2020 and 2030 emissions scenarios since it was readily available (and in the appropriate format) at the time of this study. This approximation is justified,

[7] Based on email communication with Marc Houyoux, Group Leader, Emission Inventory and Analysis Group, Office of Air Quality Planning and Standards US EPA, March 4 2011.

however, since the best estimate for future-year background emissions (the US EPA NEI) is forecast to remain approximately constant over 2020-2030 timeframe.

4.3 Uncertainties in Emissions (Present-day and Future)

The quantification of uncertainty in background emissions is not a new field of research - there have been numerous attempts in the past to quantify the errors and variability in present-day emissions ([86], [87]). Hourly NO_x emissions from coal-fired power-plants have been characterized by Abdel Aziz and Frey [88] to have an uncertainty range of -15% to 20% for daily emissions, and a 20 to 40% uncertainty for hourly emissions depending on the hour of the day. Frey et al. [89] analyzed highway (onroad) emissions of CO, HC and NO_x from the EPA's MOBILE6 tool, accounting for variability in drive cycles, ambient conditions such as temperature and fuel Reid vapor pressure. The uncertainties in average emissions ranged from ±35% for HC, ±46% for CO, and ±38% for NO_x. Wisner et al. [90] considered the uncertainty in NO_x emissions from EGUs, comparing the US EPA's Compilation of Air Pollutant Emission Factors AP-42 with measurement data from Continuous Emissions Monitors (CEMs) for specific SCCs. The study found that 13 out of the 21 SCCs that were considered had an uncertainty range greater than 25%, and six of the SCCs had variability greater than 50%. Emissions factors are utilized in the modeling of EGU emissions, and tend to have high variability due to the limited number of sample points per SCC over which the factors are averaged. Further examples of uncertainties in emissions are given in chapter 8 of NARSTO [87]. It becomes clear, though, that although there are studies aimed at characterizing uncertainty in specific source sectors, there has not been much research in aggregating these uncertainties for the background scenario as a whole.

Emissions forecasts further compound the uncertainties. Bollman et al. [91] analyzed AEO natural gas consumption forecasts in the Lake Michigan Air Director's Consortium (LADCO) region relative to actual consumption records, and found an over-estimate of the annual growth rate between 1996 and 2004 of 3.25%. AEO projections of natural gas consumption in 2004 (based on 1999 values) differed by 28% in comparison with actual usage in the region. The use of these energy forecasts in estimating future emissions, along with equally or even more uncertain economic and demand estimates, lead to a high degree of uncertainty in the forecast emissions outputs.

Examples of the levels of uncertainty in the NEI can be found within the future-year forecast estimates of the US EPA's prior regulatory analyses. Table 14 shows relative differences in future-year CAP emissions forecasts between four EPA Regulatory Impact Analyses (RIAs) and the 2002v3 CAPHAP platform. Even though some of the analyses may include emissions projections for several future years, only the two target years of 2020 and 2030 were selected for the comparison. The first RIA was prepared in 1999 for the final rule of the Tier 2 Motor Vehicle Emissions Standards and Gasoline Sulfur Control Requirements [20], and estimated future year emissions for 2030. The second RIA was performed for the Clean Air Nonroad Diesel Final Rule of 2004 [92], and includes emissions estimates for the year 2020 and 2030. The national emissions estimates from this RIA are computed based on the fractions of the national inventory that mobile emissions contribute to, as reported in Tables 3.2-1 through 3.2-6 of the Final Rule report [92] . The third analysis was performed for the Clean Air Interstate Rule (CAIR) of 2005 [93], which calculated national emissions out till 2020. The CAIR inventories are based on the 2001/2002v1 NEI modeling platform. The final inventory used for comparison is the Light-Duty Vehicle Greenhouse Gas Emissions (LDV-GHG) Standards [48] Proposed Rule of 2010. The LDV-GHG study estimates the national inventory for the year 2030. This inventory is projected from the 2005v4 NEI modeling platform.

Forecasts differ on a species-to-species basis, with projections being both higher and lower than those predicted by the 2002v3 emissions modeling platform. As the datasets are developed later in time, the estimates have lower variability since more is known about the effects of a proposed rule and socioeconomic forecasts are updated. Though the CAIR and LDV-GHG emissions inventories are based on 2002v1 and 2005v4 NEIs, emissions forecasts are also tailored to the specific study they are employed within, potentially contributing to the variability seen here. These changes and modifications are described in the respective emissions modeling Technical Support Documents (TSDs).

Table 14: Background (non-aviation anthropogenic) emissions forecasts from previous EPA Regulatory Impact Analyses

(tons/ year)		2002v3 CAPHAP	2010 LDV-GHG	2006 CAIR	2004 NONROAD DIESEL	1999 Tier2 Motor
2020						
	CO	64,912,870		28%	49%	
	NH_3	4,241,636		-3%	-	
	NO_X	10,930,663		31%	38%	
	PM_{10}	12,671,074	-	16%	-	-
	$PM_{2.5}$	4,768,531		13%	-56%	
	SO_2	8,171,411		77%	81%	
	VOC	13,220,304		-1%	5%	
2030						
	CO	69,431,177	-22%		58%	-
	NH_3	4,297,455	-1%		-	-
	NO_X	10,452,858	10%		46%	86%
	PM_{10}	12,680,651	0%	-	-	162%
	$PM_{2.5}$	4,764,633	-15%		-53%	93%
	SO_2	8,295,030	11%		87%	108%
	VOC	13,138,328	-8%		22%	40%

It would be a challenge to fully characterize the uncertainty in the ambient concentration outputs of the model due to the uncertainty in background emissions. First, the development of a probability density function for each emissions species would require a far greater number of future-year predictions, and a complete understanding of all the uncertainties inherent in the inputs not only to base year emissions models but the forecast models as well. Assuming the distributions are available, such an assessment might involve a Monte-Carlo simulation approach (as suggested by Frey [86]), wherein the emission species distributions are sampled and the CMAQ model run for each set of inputs. As with the uncertainties in aviation emissions, the long runtime of CMAQ renders this infeasible.

In order to achieve an understanding of the sensitivity of aviation impacts to an uncertain background, a sensitivity study is conducted. The study is only aimed at estimating the variability in the outputs for a given (deterministic) change in the inputs; it is not used to provide confidence intervals or obtain probabilistic distributions of the CMAQ model outputs. Two new

background scenarios are developed for this purpose: 0.5xDelta and 1.5xDelta, to represent 50% of the change and 150% of the change between the 2005 and 2025 background scenarios respectively. These two scenarios describe situations where (1) the NEI forecasts are aggressive and the actual changes in emissions are lower in magnitude (0.5xdelta), and (2) the NEI forecasts are conservative, and the changes in emissions are greater than that predicted by the NEI (1.5xDelta). The difference in emissions (the "Delta") is calculated on an hourly, grid-cell basis. The "Delta" is multiplied by 0.5 and 1.5, and added to the base year 2005 inventory to obtain the sensitivity background scenarios. This is shown in Equations (4.1) and (4.2) below.

$$\{0.5xDelta\}_{i,j,k,t} = \{2005\}_{i,j,k,t} + 1/2 * \left(\{2025\}_{i,j,k,t} - \{2005\}_{i,j,k,t}\right) \quad \textbf{(4.1)}$$

$$\{1.5xDelta\}_{i,j,k,t} = \{2005\}_{i,j,k,t} + 3/2 * \left(\{2025\}_{i,j,k,t} - \{2005\}_{i,j,k,t}\right) \quad \textbf{(4.2)}$$

where the indices *i*, *j* and *k* refer to spatial grid cells, *t* refers to the time dimension (hourly time steps), and {2005} refers to all emissions species in the year 2005.

In the 1.5xDelta inventory, values which become negative are floored to 0, and as such the net change in emissions totals in some cases is not symmetric with the 0.5xDelta scenario. Emission totals are reported in Table 15. These aggregates represent domain totals and therefore include background emissions from Mexico and Canada as they are included within the modeling domain. It is also noted that the changes in emissions relative to the 2025 scenario are not homogenous across emissions species, as seen from the changes expressed as percentages relative to the nominal 2025 totals.

Table 15: Sensitivity study background emissions domain totals and relative changes

Species (short tons/year)	**2005**	**0.5xDelta**	**(% w.r.t. 2025)**	**2025**	**(% w.r.t. 2025)**	**1.5xDelta**
CO	104,980,184	93,366,976	(14%)	81,753,760	(-14%)	70,521,992
NO_x	23,256,954	19,179,110	(27%)	15,101,264	(-23%)	11,605,371
BC	423,480	345,569	(29%)	267,658	(-25%)	200,789
SO_2	17,871,268	14,648,293	(28%)	11,425,319	(-11%)	10,155,329
NH_3	4,825,689	5,009,940	(-4%)	5,194,189	(4%)	5,384,823

Performing the scaling on a grid-cell basis takes into account the changes in magnitude of emissions (which can be brought about by changes in demand, technology or emissions controls) as well as any spatial changes that may occur. This can happen when, for example, a power-plant closes at one location and a new plant with more efficient technology and stringent controls opens in another. In this case specifically, the 0.5xDelta scenario would represent a situation where both power-plants operate at half their regular capacities and the load is proportionally shared between them.

As described in Table 1 in Chapter 2, the two future-year aviation scenarios of 2020 and 2030 will be paired with each of the two background sensitivity scenarios. Initial and boundary conditions are set to 2025 conditions since the sensitivity study is performed for future-year scenarios, necessitating that the global concentrations reflect future conditions. Other model parameters are set to their default settings as defined in Chapter 2.

Chapter 5 CMAQ Simulation Results

This section of the thesis presents the results of the CMAQ simulations performed to (A) quantify the impact of aviation in future emissions scenarios and (B) ascertain the sensitivity of aviation impacts to the variations in the background emissions scenario. The post-processing steps are first outlined, following which aviation $PM_{2.5}$ and ozone future-year impacts are presented. The effect of the US EPA's Speciated Model Attainment Test (SMAT) on the PM and ozone concentrations is shown. Finally, the results of the sensitivity study are presented.

5.1 Post-processing of Model Outputs

The impacts of aviation on ground-level, annual concentrations of $PM_{2.5}$ and ground-level seasonal concentrations of ozone are assessed, since long-term exposure to these pollutants are strongly linked to adverse health risks and mortalities [6]. The CMAQ model (as configured for this study) outputs the concentration of 192 chemical species, reporting both end-of-the-hour instantaneous values as well as hourly-averaged concentrations. The raw CMAQ model outputs contain ionic concentrations of inorganic $PM_{2.5}$ species (sulfates, nitrates, and ammonium) as well as several lumped organic aerosol compounds and EC. The organic aerosol groups are aggregated to form total Organic Carbon (OC) PM. CMAQ outputs PM2.5 as three distinct modes of aerosol formation: Aitken (I), Accumulation (J) and Coarse (K), and $PM_{2.5}$ is taken as the sum of 'I' and 'J' modes. The CMAQ species and the formulae that are used to compute total $PM_{2.5}$ and ozone are listed in Appendix I.

For each modeled scenario, hourly $PM_{2.5}$ values from the full year of simulation are averaged, on a grid-cell basis, to obtain an annually-averaged quantity. For the ozone season starting May 1 through September 30, 8-hour daily maximum ozone is computed using standard EPA methodologies[8], which involves taking running 8-hour averages of ozone and selecting the highest such quantity as the maximum value for any particular day [94] . Seasonal average 8-hour daily maximum ozone is computed by averaging the 153 daily maxima for each grid cell. The annual (or seasonal) aviation contribution at each grid cell is isolated by taking the difference of the aviation scenario and the corresponding non-aviation (background-only) simulation.

[8] Ozone post-processing routines were obtained from EPA and implemented for the CMAQ simulation outputs.

5.2 Future-year Aviation Impacts

5.2.1 $PM_{2.5}$

The domain-averaged aviation-attributable surface level annual $PM_{2.5}$ is shown in Figure 5-1 for all three aviation scenarios.

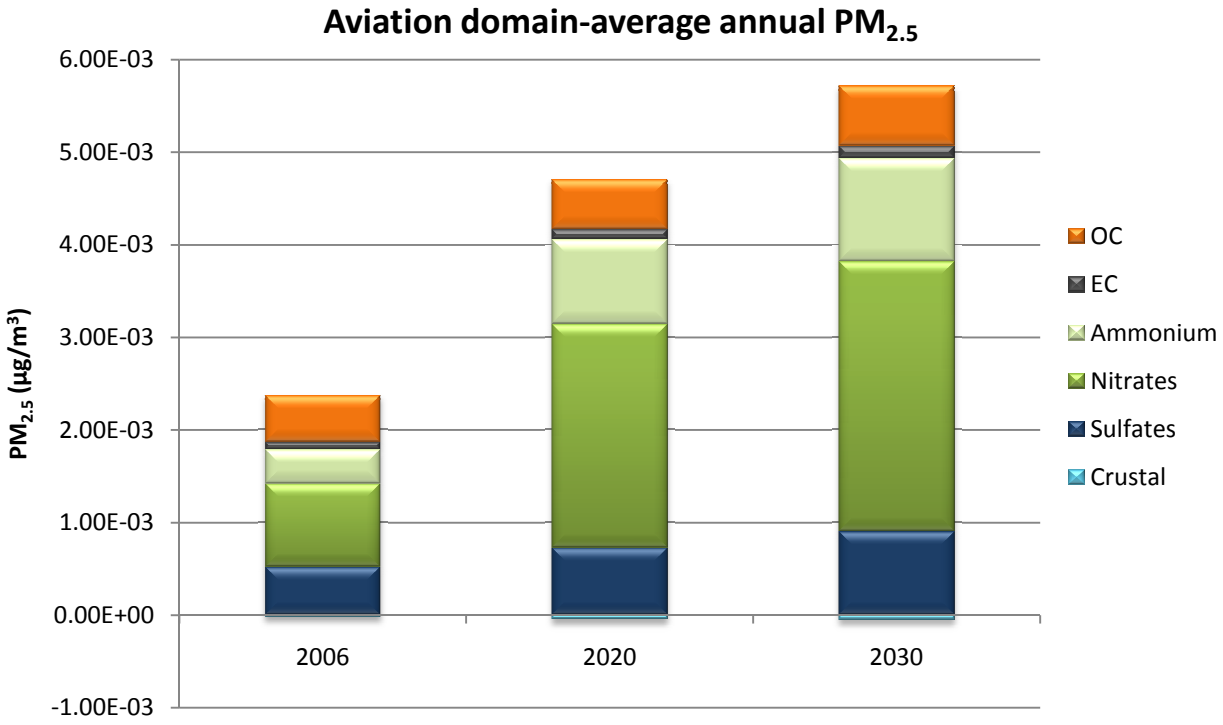

Figure 5-1: Domain-averaged annual $PM_{2.5}$ (and species) concentrations for LTO aviation in 2006, 2020 and 2030

Aviation $PM_{2.5}$ is seen to increase in the future scenarios relative to the base year. This is consistent with the modeled future year aviation emissions being larger in magnitude compared to present-day levels: as seen in Table 11, aviation LTO fuel burn increases by 26% from 2006 to 2020, and by 57% from 2006 to 2030 (2030 grows by 25% relative to 2020 levels). However, the changes in aviation PM are not constant across the three cases. This is shown in Table 16, which contains the growth in PM species relative to the base year 2006 and future year 2020 concentrations. The total PM concentration in 2020 is almost double that in 2006, and increases by 141% in 2030. Notably, nitrates grow by 169% from 2006 to 2020 and 224% from 2006 to 2030, accompanied by a similar change in ammonium. While the increases in crustal PM are

relatively high compared to the other species, its contribution to total PM2.5 is negligible and therefore its growth does not have a significant impact on total $PM_{2.5}$ concentrations in future years.

Table 16: Growth of $PM_{2.5}$ species relative to 2006 and 2020 concentrations

	Sulfates	Nitrates	Ammonium	EC	OC	Crustal	Total PM
% increase w.r.t. 2006							
2020	40%	169%	148%	37%	7%	83%	99%
2030	74%	224%	202%	68%	29%	122%	141%
% increase w.r.t. 2020							
2030	24%	21%	22%	23%	21%	21%	22%

In going from the base year to the 2020 scenario, it is important to note that there are two factors involved: a change in aviation emissions as well as a change in background emissions scenario from 2005 to 2025. The background scenario is kept fixed at 2025 conditions for both the 2020 and 2030 simulations, and therefore the change in aviation-attributable $PM_{2.5}$ concentrations between 2020 and 2030 is due solely to aviation emissions. This is reflected in the bottom row of Table 16, which demonstrates that the growth in total PM (and its constituent species) is closer to the growth in aviation fuel burn between 2020 and 2030 of 25%.

There exists a disproportionate increase in aviation-attributable $PM_{2.5}$ relative to growth in aviation activity between 2006 and 2020. From Figure 5-1 and Table 16, it is clear that the growth in future-year PM is dominated by inorganic $PM_{2.5}$ species (ammonium, nitrate and sulfate ions). The reason for this growth lies in the interaction of background emissions with the PM formation pathway for aviation emissions. The pathway from SO_2 and NO_x emissions to $PM_{2.5}$ has two major phases: (a) the oxidation from SO_2 (NO_x) to H_2SO_4 (HNO_3) and (b) the neutralization of H_2SO_4 (HNO_3) by ammonia to form ammoniated sulfate (ammonium nitrate) particulate matter. The background emissions scenario impacts each of these two processes, the combined effect of which leads to the disproportionate increase in aviation-attributable PM.

First, the effect of the background emissions on the oxidative capacity of the atmosphere is discussed. Background emissions levels are forecast to decrease, as shown in Figure 4-1; the reasons for this decrease are discussed in Chapter 4. The decreased rate of emission leads to higher ambient levels of oxidants in the atmosphere; this could occur since emissions that would otherwise have reacted with these oxidants are no longer present. Higher levels of oxidants, in turn, mean that more of the aviation emissions are oxidized into their acidic forms. This hypothesis is proven by considering the removal rates of aviation-attributable SO_2 and SO_4.

The annual-averaged dominant removal processes for SO_2 (dry deposition) and SO_4 (wet deposition) are shown in Table 17 for the three aviation scenarios. Note that the rates represent annual domain-averaged aviation deltas (that is, the change in deposition as a result of aviation emissions). The table also contains the relative growth of deposition rates with respect to 2006 and 2020. Between 2006 and 2020, deposition rates of SO_2 and SO_4 increase by 23% and 36% respectively relative to 2006, despite an increase in aviation fuel burn of 26% that occurs during this time. Between 2020 and 2030, however, the increase in both dry and wet deposition rates (relative to 2020) are very close to the projected increase in aviation fuel burn of 25%, illustrating the sole effect of added aviation emissions on the deposition rates since the background emissions scenario is held fixed in the two simulations. The fact that, in 2020 the increase in SO_4 wet deposition is higher than 26%, and the increase in SO_2 dry deposition is lower than 26%, suggests that a greater fraction of aviation SO_2 has been oxidized into SO_4, thus implying that the atmosphere into which 2020 aviation emissions are emitted has a higher oxidative potential.

Table 17: Aviation-attributable SO_2 and SO_4 annual-averaged deposition rates

	Annual aviation delta		**% increase w.r.t 2006**		**% increase w.r.t 2020**	
	SO_2 Dry Dep. (kg/hectare)	**SO_4 Wet Dep. (kg/hectare)**	**SO_2 Dry Dep.**	**SO_4 Wet Dep.**	**SO_2 Dry Dep.**	**SO_4 Wet Dep.**
2006	1.85×10^{-6}	1.80×10^{-6}	-	-	-	-
2020	2.26×10^{-6}	2.43×10^{-6}	23%	36%	-	-
2030	2.82×10^{-6}	3.05×10^{-6}	53%	70%	25%	25%

Spatial maps of ozone and the hydroxyl radical (OH) further support this argument. Ozone is an important species in setting the oxidative potential of the atmosphere. It is the main precursor for the hydroxyl radical which is one of the most potent oxidizers in the atmosphere which reacts with a large number of compounds and has a short chemical lifetime [95]. Figure 5-2 shows the difference in annual-averaged ambient ozone concentrations between the 2005 and 2025 background scenario simulations (Sims. #1 and #3). Over most of the urban areas, ozone levels are higher in 2025 than 2005. This is due to the fact that urban areas are predominantly VOC-limited, and thus a decrease in the amount of NO_x background emissions leads to an increase in ozone concentrations [96]. The higher ozone concentrations yield more OH, through photodissociation and reaction with water vapor; this is illustrated in Figure 5-3, which plots the difference in OH concentrations between 2005 and 2025. Note that, even though OH decreases on a domain-average basis, OH peaks exist at many urban locations. The majority of large airports are co-located near these urban areas, and as a result much of the aviation LTO emissions occur amidst elevated levels of ambient OH, allowing a greater fraction to be oxidized.

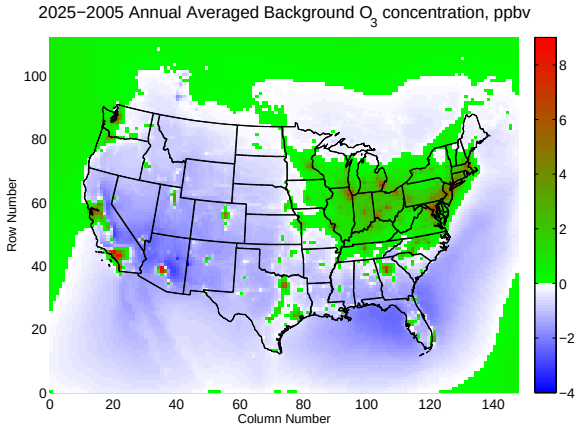

Figure 5-2: Background Delta (2025-2005) surface-level annual O_3

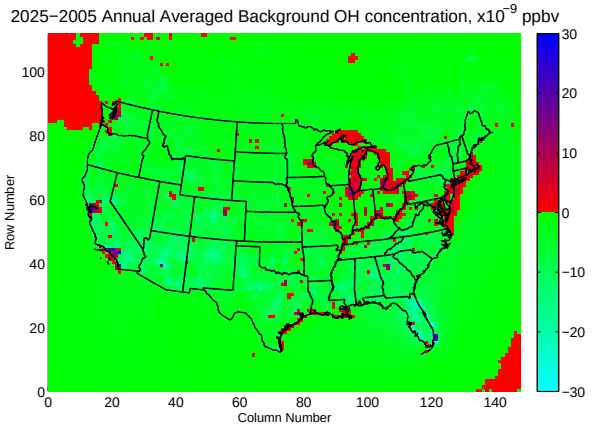

Figure 5-3: Background Delta (2025-2005) surface-level annual OH

The second part of the PM formation pathway involves reaction with ammonia to form ammonium nitrate and ammoniated sulfate compounds. There is a significant increase in the proportion of aviation-attributable $PM_{2.5}$ that is ammonium nitrate in going from the 2006 aviation case to 2020 (38-52%), as shown in Table 18. The reason for this is found in a quantity known as free ammonia (FA), following the explanation given in Woody et al. [8]. FA is an indicator of the amount of ammonia available to the atmospheric system, and is a measure of the

left-over ammonia once background nitrates and sulfates have been neutralized. Figure 5-4 shows the spatial plot of FA in 2005 and 2025.

Table 18: Aviation-attributable domain-averaged annual $PM_{2.5}$ composition

	Sulfates	Nitrates	Ammonium	EC	OC	Crustal
2006	22%	38%	16%	3%	22%	-1%
2020	16%	52%	20%	2%	12%	-1%
2030	16%	52%	20%	2%	12%	-1%

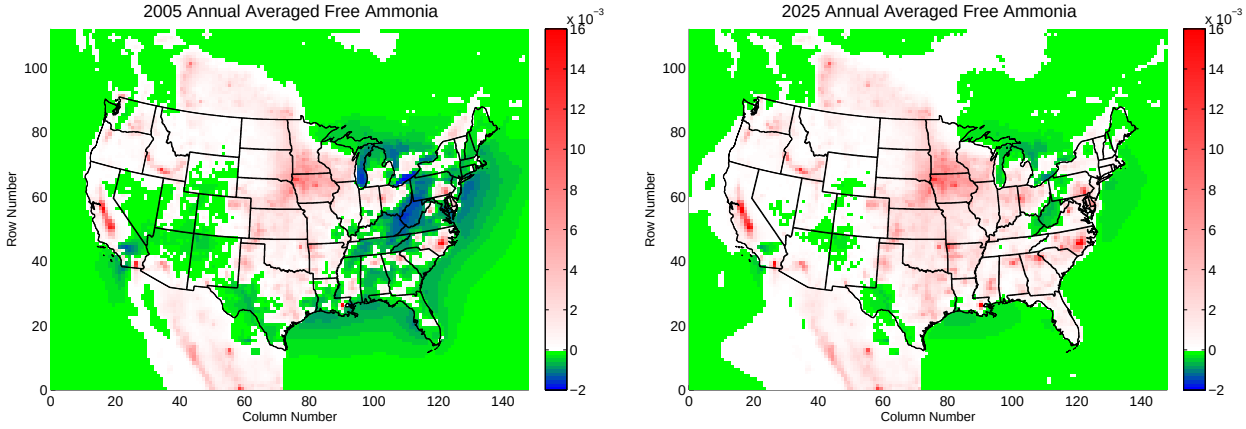

Figure 5-4: Spatial plots of annual free ammonia in 2005 and 2025

Larger portions of the US have FA in 2025 compared to 2005. The reduction of NO_x background emissions result in lower concentrations of HNO_3, and this, combined with the fact that ammonia emissions have risen by 8% from 2005 to 2025, free up ammonia to react with aviation emissions. Sulfates react preferentially with ammonium under most conditions and are thus mostly neutralized; the increase in aviation sulfate PM is therefore attributable only to increase in aviation SO_x emissions and enhanced oxidation from the atmosphere. However, the excess ammonia in the background allows for a greater percentage of the aviation NO_x emissions to react with ammonia (after being oxidized to HNO_3) and form ammonium nitrate aerosols.

The effect of changing background is eliminated when considering the 2020 and 2030 aviation scenarios, since the modeled background was held constant at 2025 levels, and therefore the growth in PM is solely due to increased aviation emissions. The increase in annual-average aviation-attributable PM is about 22% relative to 2020 levels, with near-uniform increments of

21-24% in all $PM_{2.5}$ species. These changes are proportional, in general, to the increase in aviation emissions.

As seen in Table 18, the proportion of organic PM is relatively large in the base year 2006 (contributing to 22% of total $PM_{2.5}$) compared with prior air quality analyses of aviation impacts ([97], [12]). This arises from the FOA3a methodology that is used to compute aviation emissions of primary organic PM. As noted in Section 3.6, FOA3a estimates primary organics to be an order of magnitude larger than the conventional FOA3 method. It is re-iterated that these methodologies need to be updated to reflect the latest findings and measurement information available [61].

The spatial concentration plots of total $PM_{2.5}$ are given in Figure 5-5, Figure 5-6 and Figure 5-7 for the years 2006, 2020 and 2030, respectively. Aviation LTO impacts in 2006 are observed locally within the airport grid-cells, evidenced by peaks in aviation $PM_{2.5}$ located near cities and airports. Aviation impacts are also prevalent over large areas of the Midwest and the Eastern seaboard regions of the country, as well as California. These areas generally correspond to areas with high free ammonia, as shown previously in Figure 5-4. Aviation LTO emissions, which mostly occur within the surrounding grid cells of its arrival or departure airport, are oxidized and advected into these regions through strong mixing within the PBL, where they react with ammonia to form PM.

Looking into the future years of 2020 and 2030, airport grid-cells become more prominent hotspots due to highly localized effects from growth in aviation as well as increased oxidation brought about by the declining emissions from non-aviation sources. The additional availability of FA in 2020 and 2030 over Appalachia and the Southeastern US enables aviation emissions to form $PM_{2.5}$ over these areas. The maximum $PM_{2.5}$ concentration occurs in the Los Angeles area in 2006; however in 2020, the New York Metroplex area contains the highest concentration. While the magnitude of PM increases from 2020 to 2030, the spatial distribution of $PM_{2.5}$ changes very little.

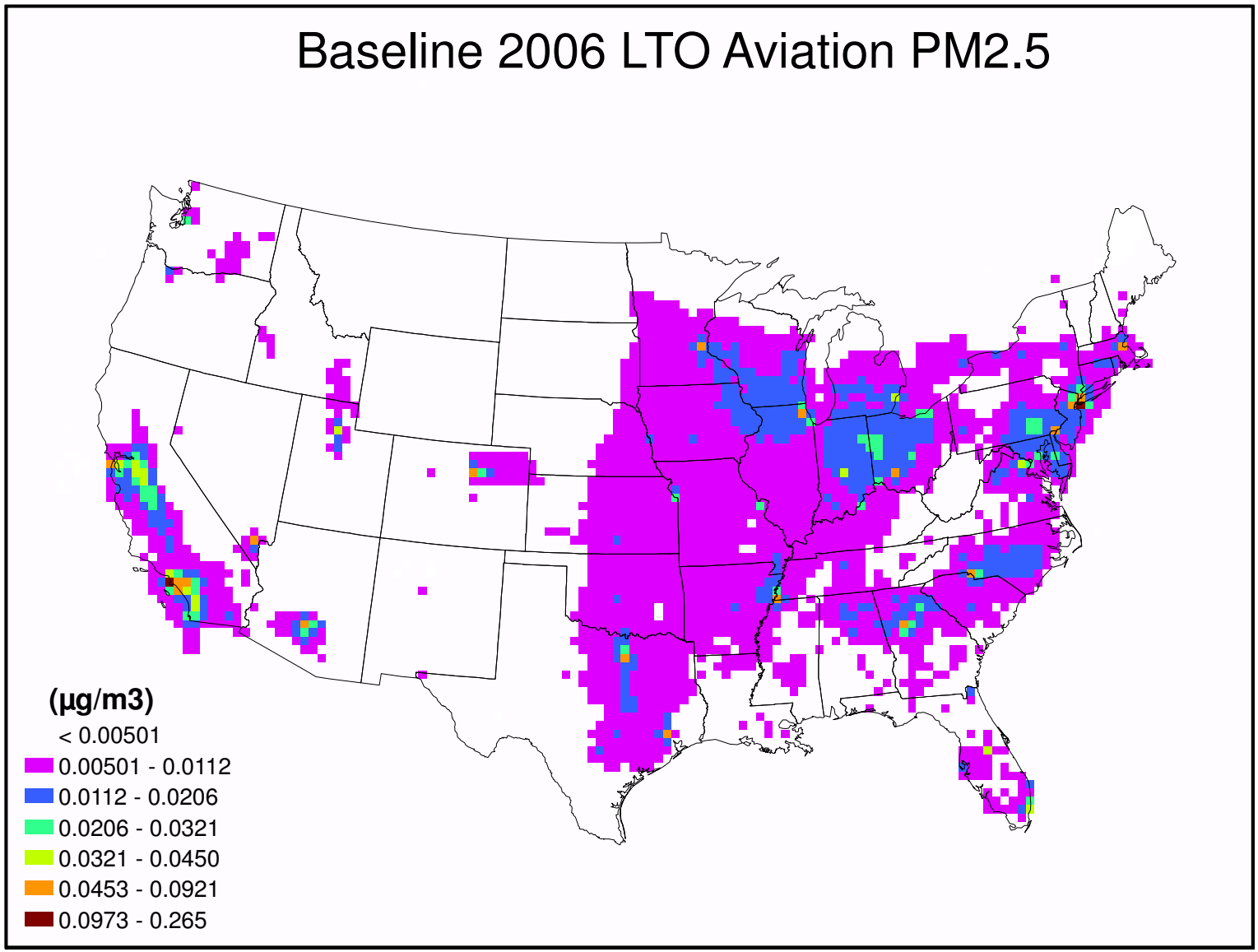

Figure 5-5: Baseline 2006 LTO aviation annual $PM_{2.5}$ spatial plot

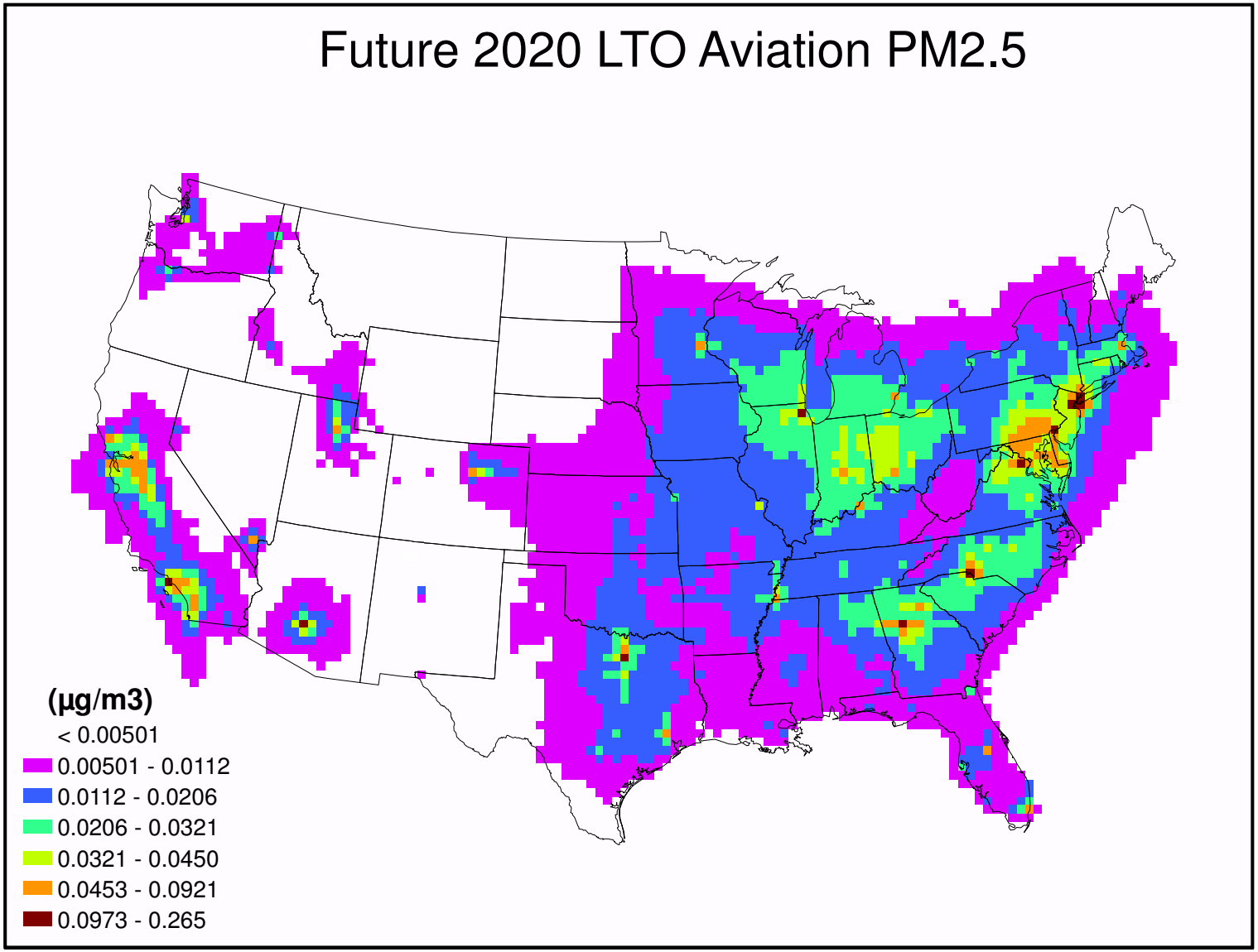

Figure 5-6: Future 2020 LTO aviation annual $PM_{2.5}$ spatial plot

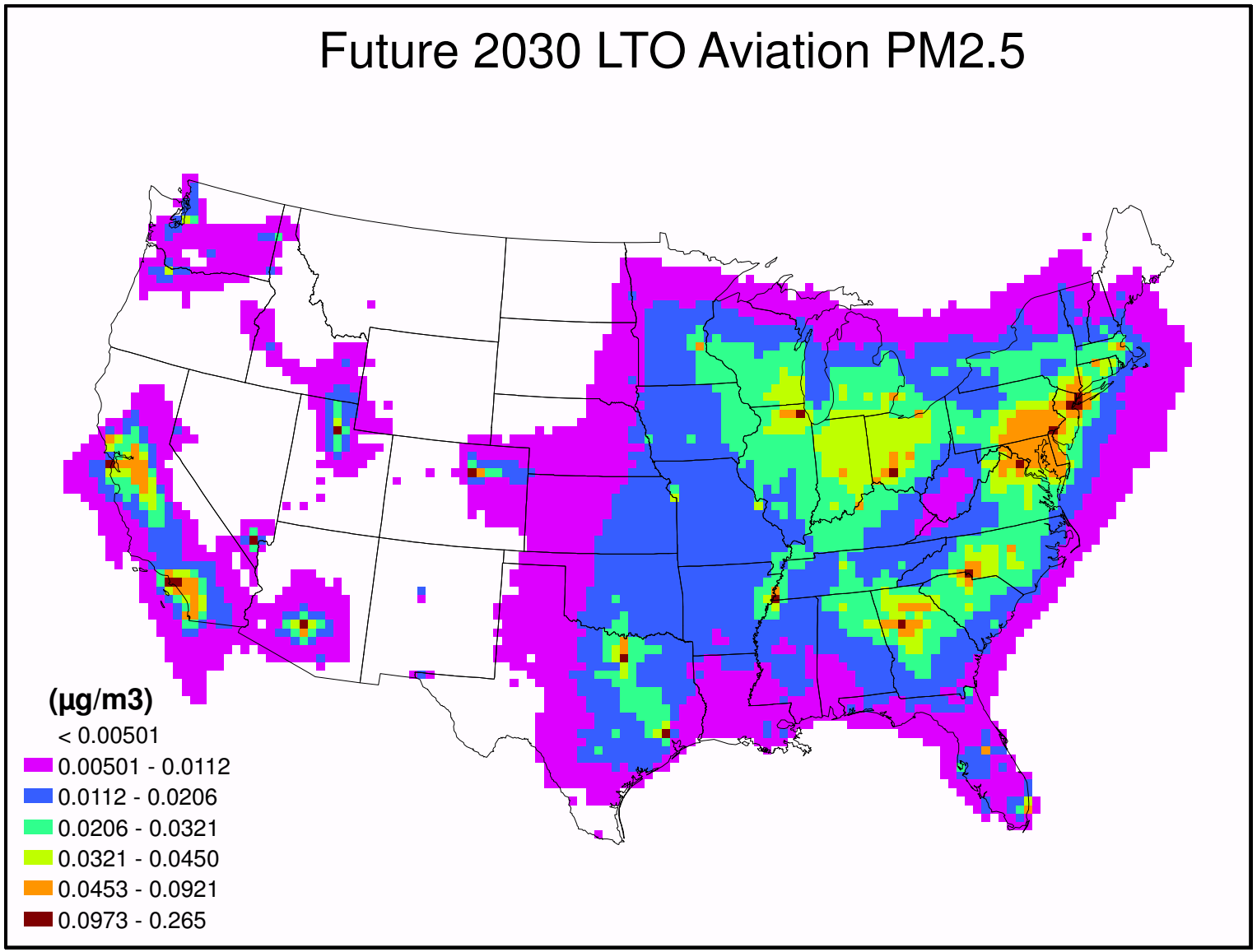

Figure 5-7: Future 2030 LTO aviation annual $PM_{2.5}$ spatial plot

5.2.2 Ozone

On a domain-averaged basis there is an increase in surface-level seasonal 8-hour daily maximum ozone levels caused by aviation, as illustrated by the bar chart in Figure 5-8. Aviation-attributable ozone increases by 1.9 times from 2006 to 2020, and 2.2 times from 2006 to 2030.

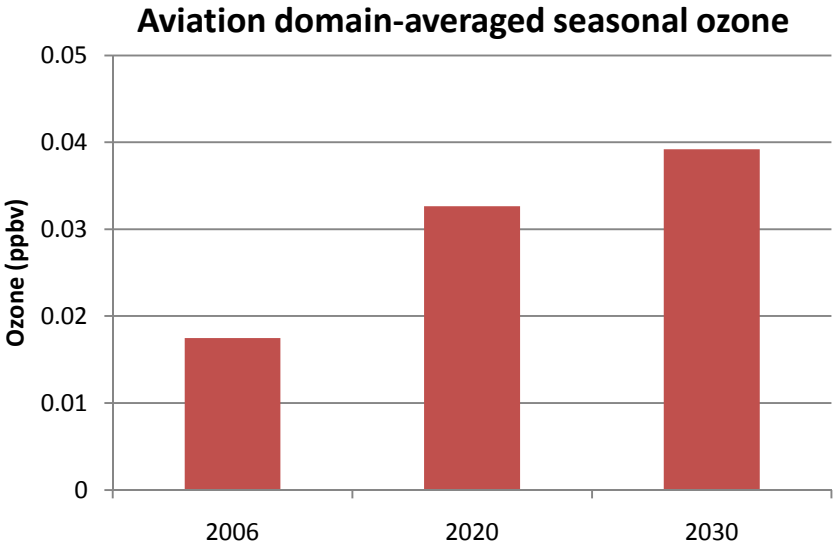

Figure 5-8: Domain-average seasonal ozone concentrations from LTO aviation in 2006, 2020 and 2030

The behavior of aviation-attributable ozone is not, however, homogeneous throughout the domain. The spatial plot in Figure 5-9 shows baseline 2006 LTO aviation activity causes a decrease in seasonal 8-hour ozone concentrations at airports and surrounding regions in the upper latitudes. At lower latitudes, the decrease in ozone (if any) is confined to the airport grid cell, with the surrounding regional impacts (often occurring over rural areas) yielding a net increase in ozone.

The localized decrease in ozone concentration is attributed to NO_x-VOC-O_3 photochemistry which is summarized in an ozone isopleth (an example of which can be found in Sienfeld and Pandis [96]). The behavior of ozone to additions or reductions of NO_x emissions is governed by the mixing ratio between NO_x and VOCs. The majority of urban regions has polluted atmospheres, since ambient NO_x levels are higher than VOC concentrations, and is thus VOC-limited; under these conditions, the incremental addition of NO_x emissions from aircraft inhibits

the rate of ozone formation[9]. On the other hand, rural areas, being relatively unpolluted, have comparatively lower NO_x mixing ratios; in this regime, incremental addition of aviation NO_x increases ozone.

Future year aviation impacts on ozone retain similar trends in the spatial distribution as compared to the base year impacts in the upper latitudes, with the magnitude of impacts becoming larger and more spread out. This is seen in Figure 5-10 and Figure 5-11. Towards the southern regions, the ozone deltas become predominantly positive even within the airport grid cell. It is noteworthy that much of the regional impacts are located downwind of the airports, as observed in the California area and the Northeast and Southern US. The effects of atmospheric advection and chemical transport are evident here, since aviation LTO emissions only occur within the 2-3 grid-cells surrounding the airport and yet its impacts are felt much farther out to hundreds of kilometers. It is observed again that aviation impacts change most significantly between the base year and the future year 2020 compared with the changes from 2020 to 2030, due to simultaneous variation of both aviation and background emissions.

[9] The reverse phenomenon is observed with changes in background emissions, wherein a reduction in NO_x emissions from 2005 to 2025 leads to an increase in O_3 as seen in Figure 5-2.

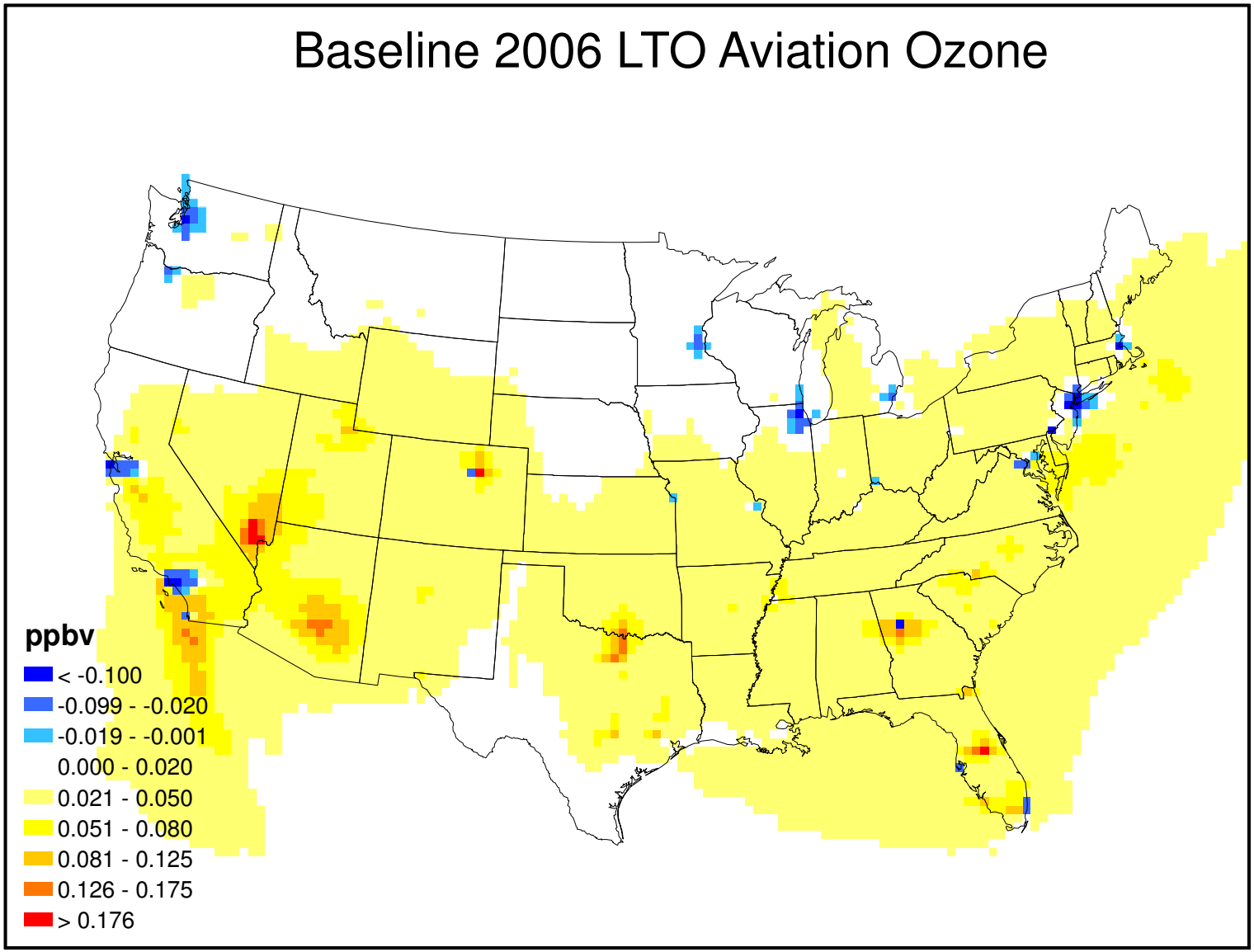

Figure 5-9: Baseline 2006 LTO aviation seasonal ozone spatial plot

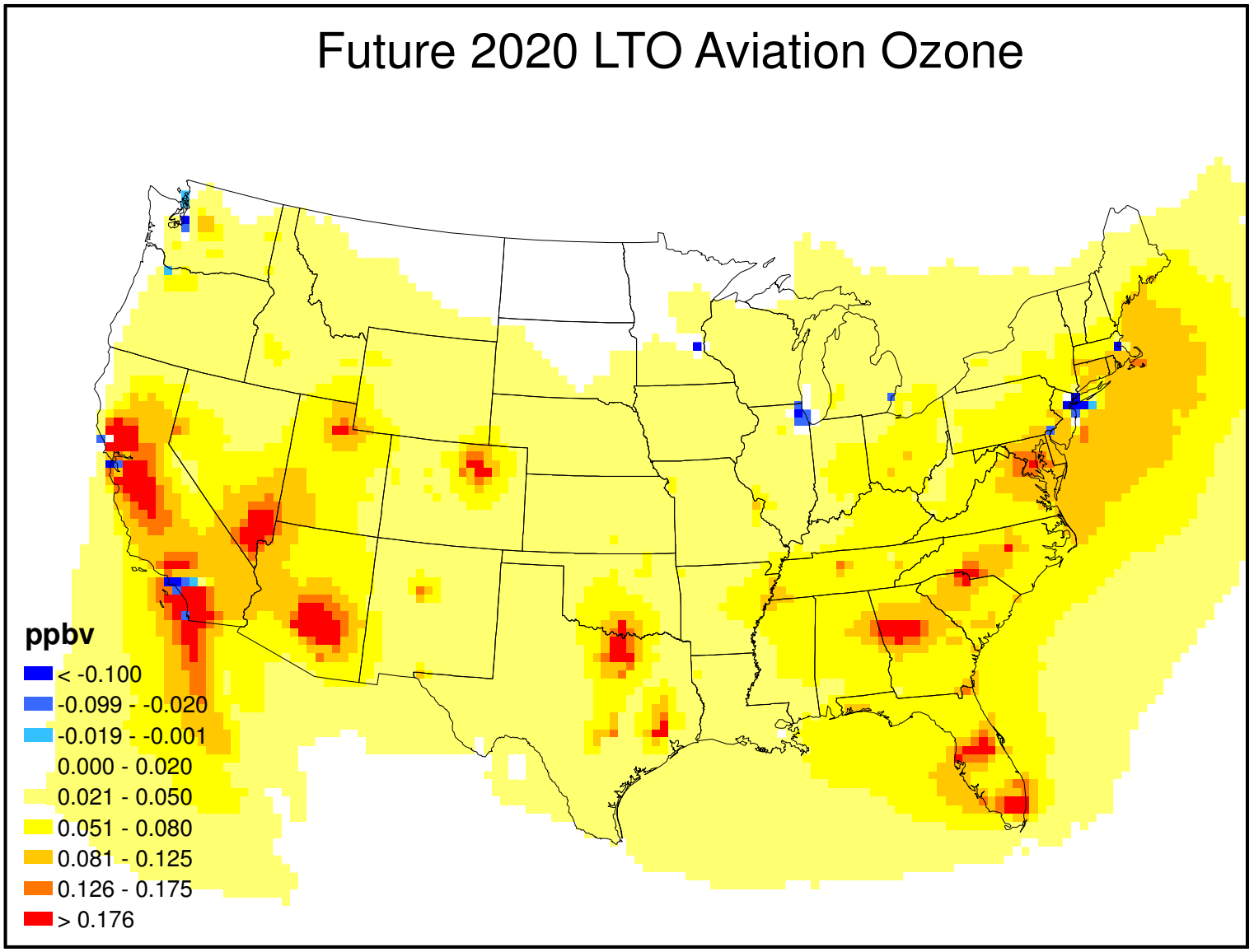

Figure 5-10: Future 2020 LTO aviation seasonal ozone spatial plot

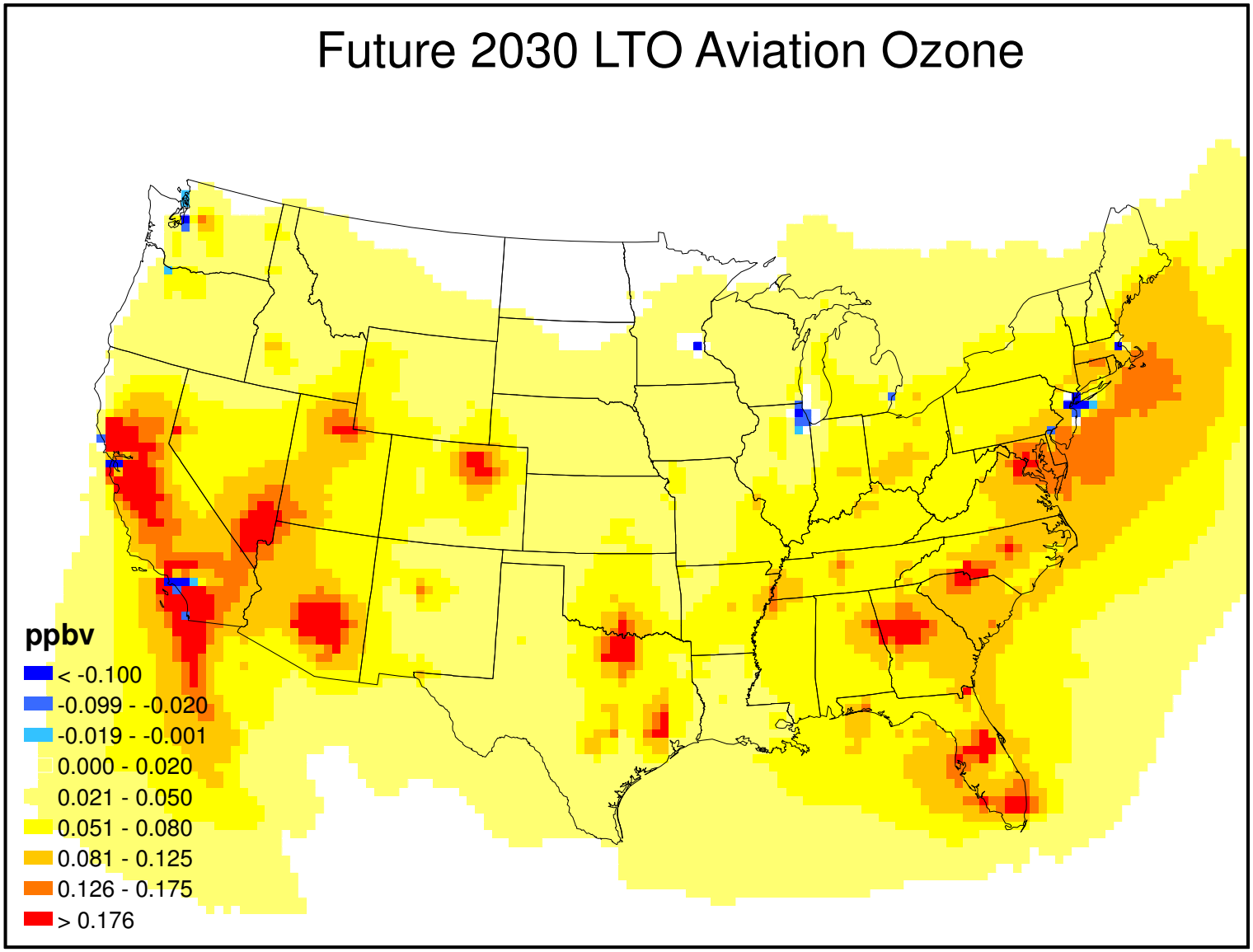

Figure 5-11: Future 2030 LTO aviation seasonal ozone spatial plot

5.3 SMAT Process

The EPA's Speciated Modeled Attainment Test (SMAT [38]) procedure is applied to the CMAQ outputs to reconcile model outputs to PM and ozone measurement monitors located throughout the country. The overall methodology is similar for $PM_{2.5}$ and ozone, however key differences in the implementation exist, which will be highlighted. The Modeled Attainment Test Software (MATS, [98]) is used to perform the SMAT process.

The methodology behind SMAT lies on the argument that atmospheric photochemical models such as CMAQ possess inherent biases which do not allow them to accurately predict absolute ambient concentrations, but they are well-suited for predicting relative changes as a result of a policy or control measure [99]. The relative changes from the model are applied to baseline measurements of current conditions from air quality monitoring networks to project the changes into ambient concentrations.

Ambient concentration measurements from monitors are converted into Monitor Design Values (DVs) through an averaging process. Ozone design values are calculated as the 3-year average of the fourth highest monitored 8-hour daily maximum value at each monitor location. The annual average $PM_{2.5}$ DV is taken as the 3-year average of the annual mean PM observed at the monitor [38]. The baseline DV that is used in the MATS software is computed by taking a further average of the DVs computed for each analysis period; that is, for a baseline year of 2005, the baseline DV is obtained by averaging each of the three DVs computed for the 2003-2005, 2004-2006 and 2005-2007 periods. Doing so weights the DV towards the middle (analysis) year of 2005, while incorporating meteorological and emissions variability that occur during the 2003-2007 period. Additional details for the DV calculation are found in 40CFR Part 50 [43].

The SMAT process makes use of the model results to calculate the relative changes through a ratio known as the Relative Response Factor (RRF). The RRF is a ratio between a future (or scenario) case and the base (or control) case. In this thesis, the base year is chosen to be the 2005 background simulation (Sim #1 in Table 1), and RRFs for all other scenarios are computed relative to this simulation. Note that the term 'future case' does not necessarily imply temporal differentiation, and even though Sims #2-5 are in fact future years compared to 2005, RRFs are also calculated for the 2006 base year aviation case (Sim #2). Baseline DV's from 2005 is used to multiply with the respective RRFs to obtain post-SMAT absolute concentrations for each

scenario. Aviation impacts are estimated, as before, by taking the difference of the post-SMAT scenario and control case.

MATS computes RRFs from quarterly-averaged $PM_{2.5}$ on a grid-cell basis, thereby producing a gridded field of future PM design values. Official FRM $PM_{2.5}$ Design Values at each monitor for the year 2005 are used to estimate $PM_{2.5}$ concentrations, which are interpolated to the gridded field using a Voronoi Neighbor Averaging (VNA) interpolation scheme that uses a weighted averaging method to obtain gridded FRM concentrations. Unofficial speciation data from the STN monitor network are also used to compute RRFs for each species. Further details on speciation and the caveats that accompany these methods are discussed in the MATS manual [98]. The discussion of post-SMAT results in this thesis will be limited to the official FRM $PM_{2.5}$ outputs. Ozone is input to MATS as seasonal averaged 8-hour daily maximum values for each grid-cell.

Data from off-domain $PM_{2.5}$ monitors (such as Hawaii, Alaska and Puerto Rico) was removed to prevent erroneous interpolation artifacts; all other program options were set to their default values (see Appendix J for a list of MATS options). MATS settings for ozone are also tabulated in the appendix. A custom monitor dataset[10] which contains seasonal average DVs for each monitor is used instead of the daily 8-hour daily maximum DVs that are packaged with a default copy of MATS. The precision level of MATS was increased to 7 decimal places for both $PM_{2.5}$ and ozone calculations, since the objective is to analyze small changes in concentrations that arise from the aviation cases. Gradient-adjusted MATS outputs were used for annual $PM_{2.5}$, as they were generally smoother in nature than those without gradient adjustment.

5.4 Post-SMAT Aviation Air Quality Impacts

Figure 5-12 provides a comparison of the pre- and post-SMAT aviation-attributable ambient $PM_{2.5}$, averaged over the modeling domain.

[10] Custom seasonal average DV dataset provided by Brian Timin of US EPA

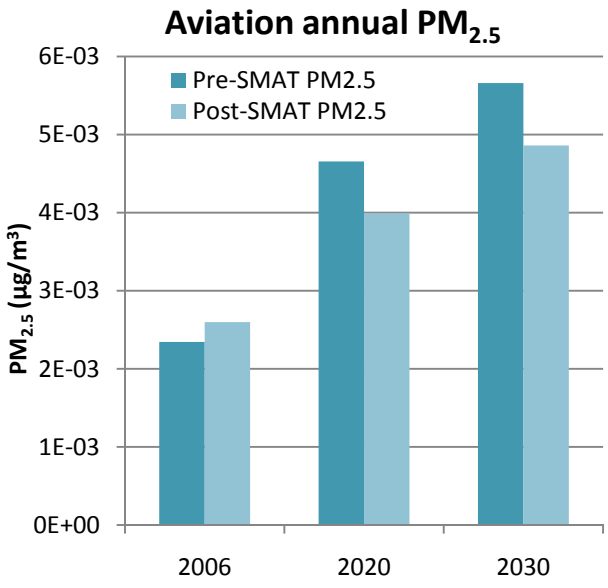

Figure 5-12: Pre-SMAT and post-SMAT annual domain-averaged aviation $PM_{2.5}$

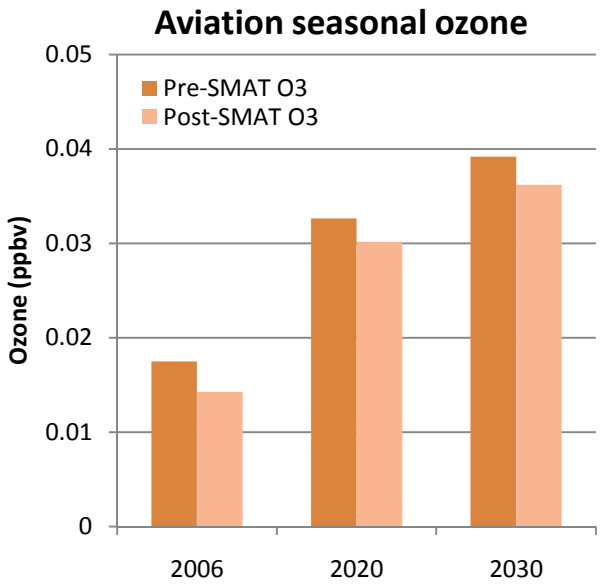

Figure 5-13: Pre-SMAT and post-SMAT seasonal domain-averaged aviation ozone

The SMAT process increases domain-averaged concentrations in 2006 by 11%, and decreases future-year concentrations by 14%. Spatial maps of total post-SMAT $PM_{2.5}$ are shown in Figure 5-14, Figure 5-15 and Figure 5-16. Reductions in $PM_{2.5}$ are seen in the Northeastern and Midwestern rural regions, while $PM_{2.5}$ concentrations at the airport hotspots (and surrounding urban areas) are seen to increase. Regional impacts in California are seen to grow as well. These changes also exist in the future years, although the magnitude of reductions is higher than the increments in PM, on average.

Post-SMAT domain-averaged concentrations of seasonal 8-hour maximum ozone are shown in Figure 5-13. Post-SMAT ozone is decreased by 18% in 2006, and by 8% in 2020 and 2030. The spatial distribution of ozone, shown in Figure 5-17 - Figure 5-19, is not changed significantly compared with pre-SMAT seasonal ozone. Marginal reductions in magnitude are seen, though, towards the Northeast and Southern regions of the US, leading to the decrease in average ozone impacts that is observed.

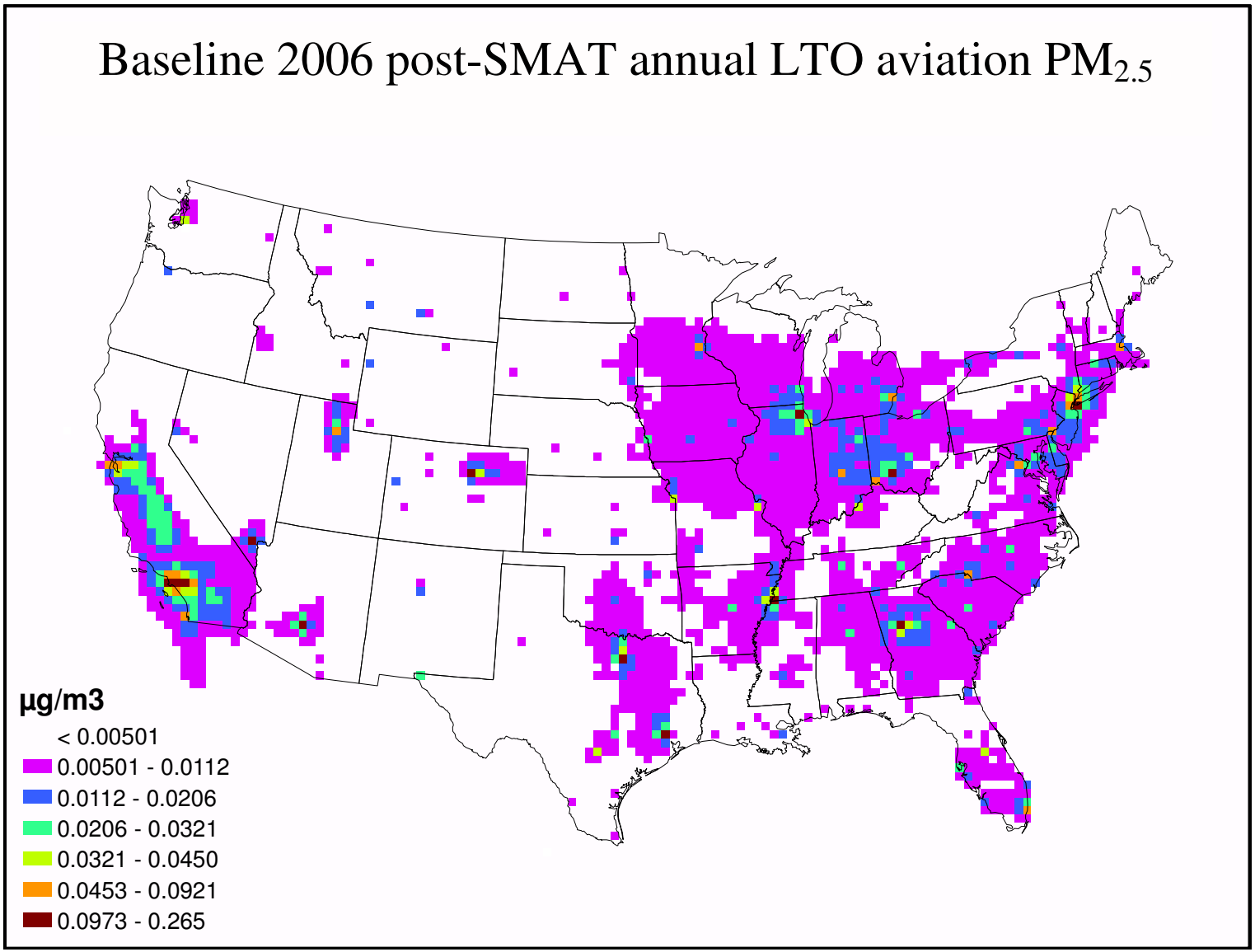

Figure 5-14: Baseline 2006 LTO aviation post-SMAT annual $PM_{2.5}$ spatial plot

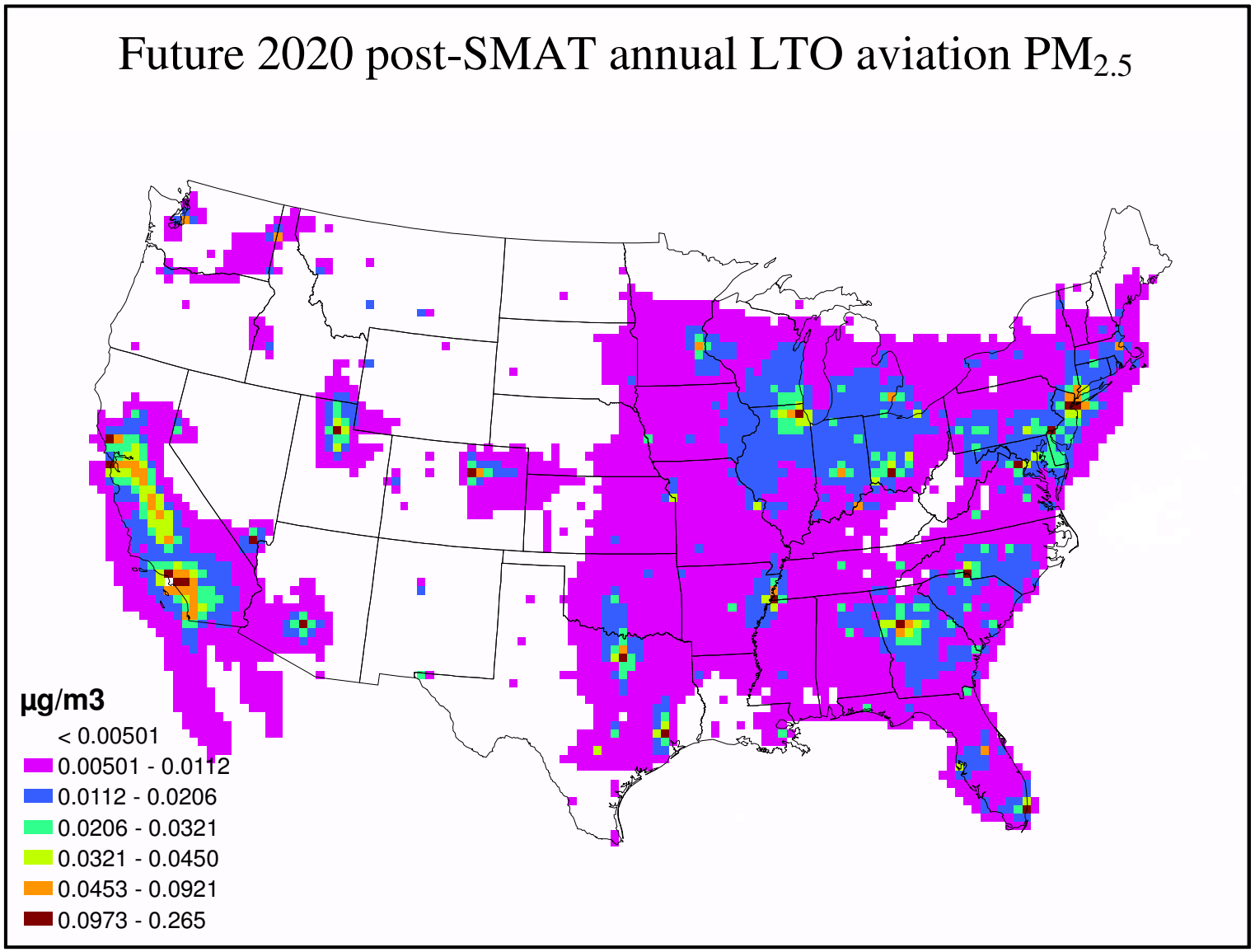

Figure 5-15: Future 2020 LTO aviation post-SMAT annual $PM_{2.5}$ spatial plot

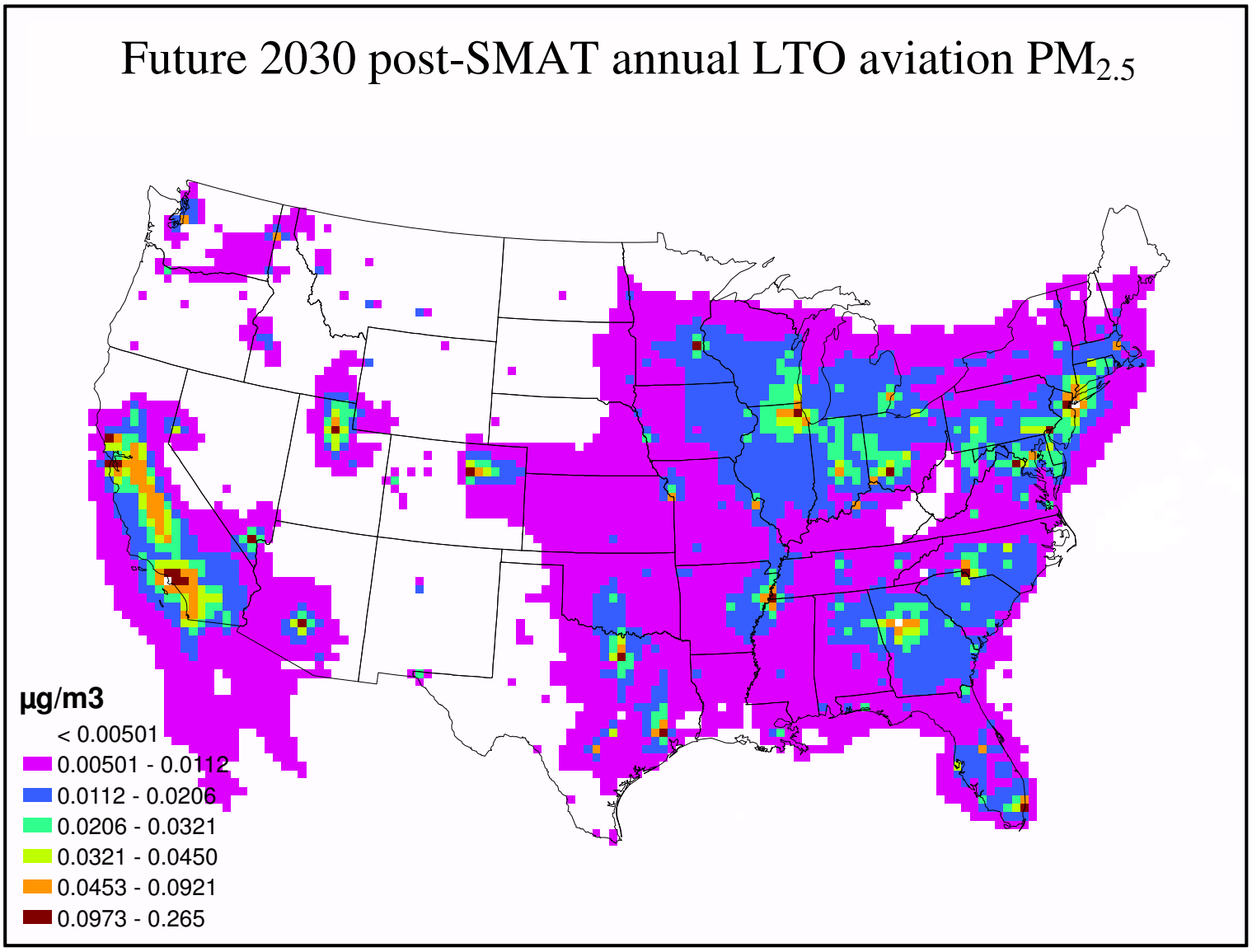

Figure 5-16: Future 2030 LTO aviation post-SMAT annual $PM_{2.5}$ spatial plot

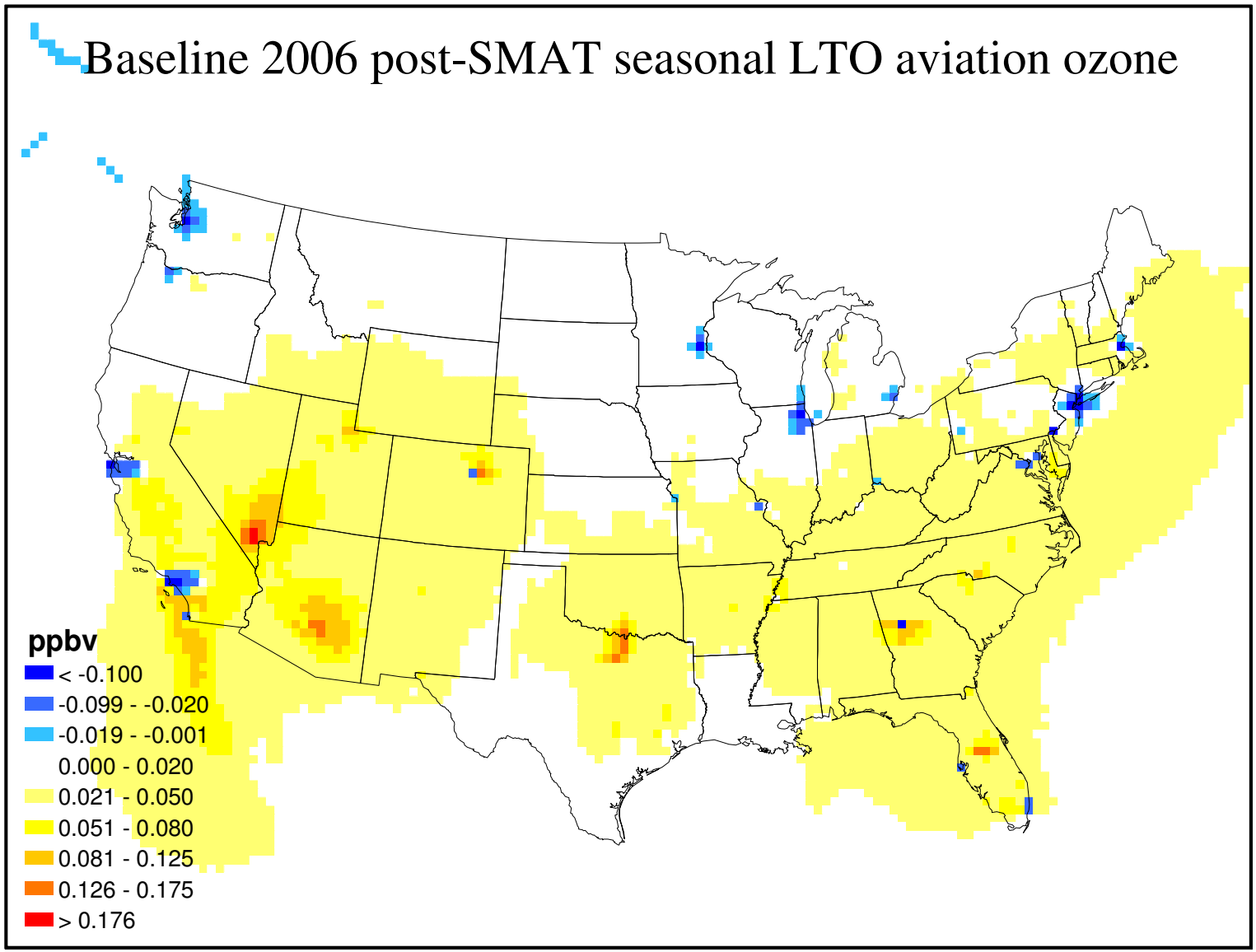

Figure 5-17: Baseline 2006 LTO aviation post-SMAT seasonal ozone spatial plot

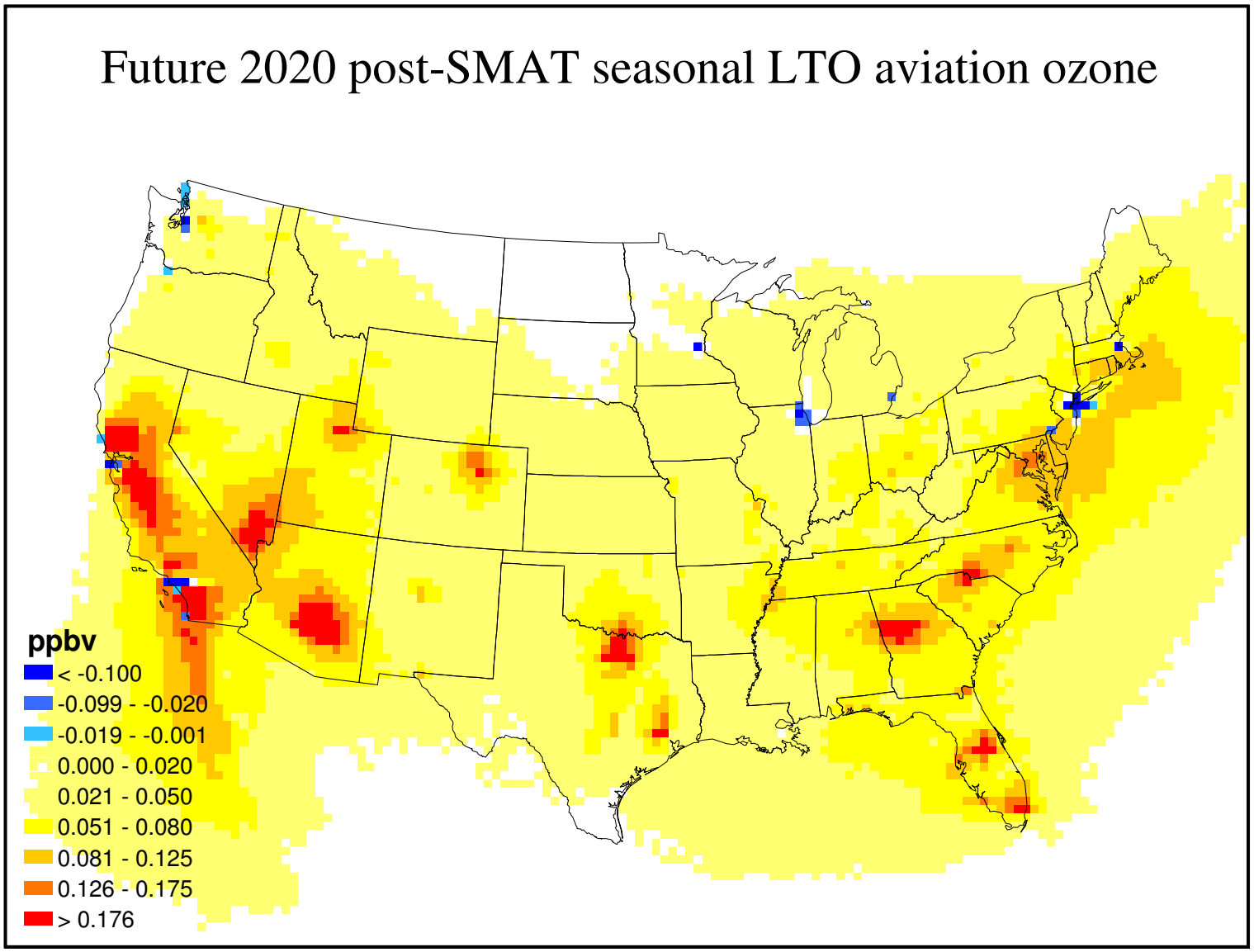

Figure 5-18: Future 2020 LTO aviation post-SMAT seasonal ozone spatial plot

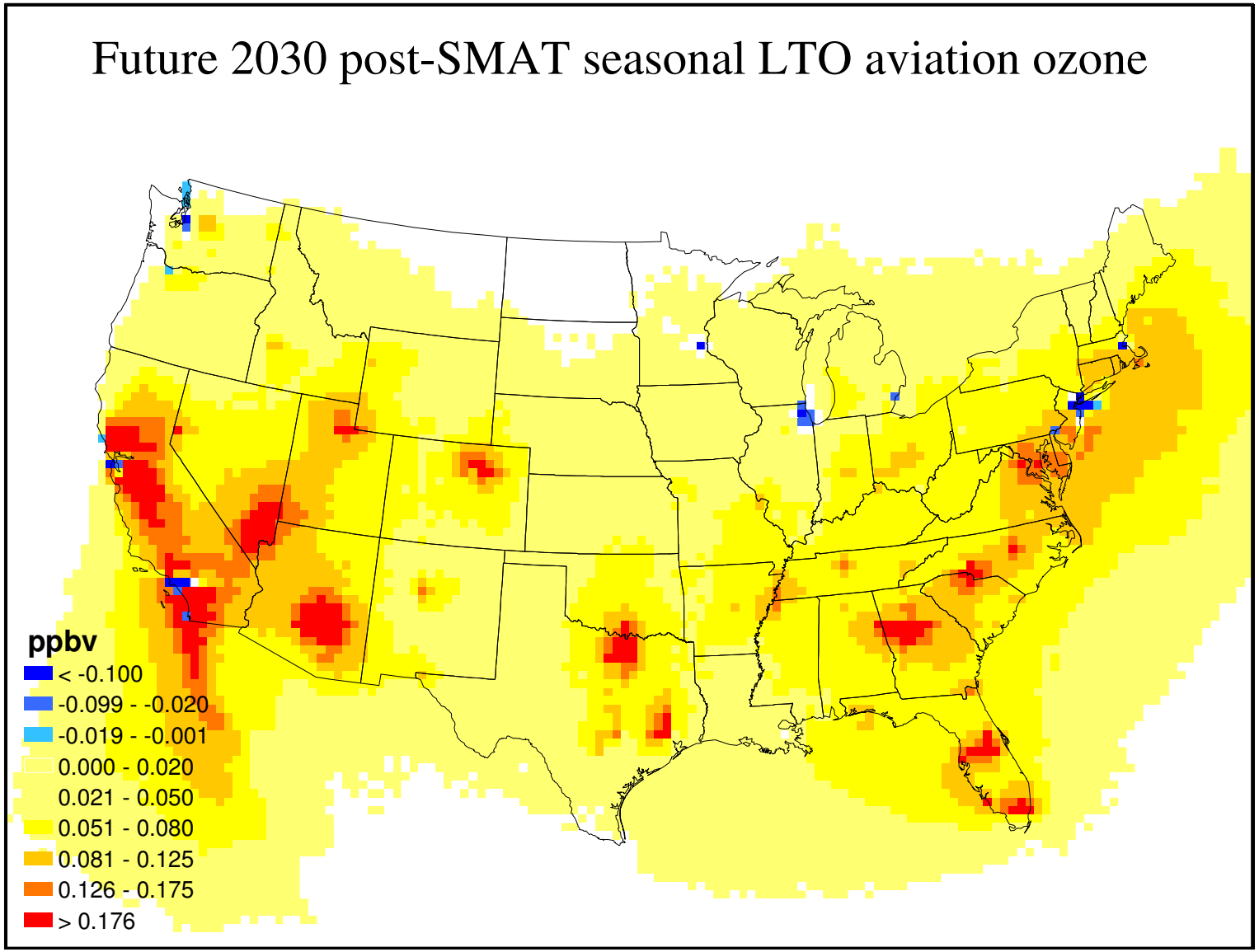

Figure 5-19: Future 2030 LTO aviation post-SMAT seasonal ozone spatial plot

5.5 Sensitivity Study

5.5.1 $PM_{2.5}$ Sensitivity

The future-year background emissions are varied to represent a less-than-predicted change (0.5xDelta case) and a greater-than predicted change (1.5xDelta case) in forecast background emissions as described in Section 4.3. The magnitude of emissions in each background scenario is given in Table 15 in Section 4.3, with the 1.5xDelta (0.5xDelta) scenario containing lower (higher) aggregate emissions than the 2025 case. The aviation-attributable domain-averaged annual $PM_{2.5}$ concentrations from simulations #6-#11 are shown in Figure 5-20. The solid line corresponds to the simulation with the nominal 2025 background scenarios (from simulations 3-5), while the upper and lower dashed lines represent the greater-than-expected (1.5xDelta) and less-than-expected (0.5xdelta) change in background emissions from 2005 to 2025.

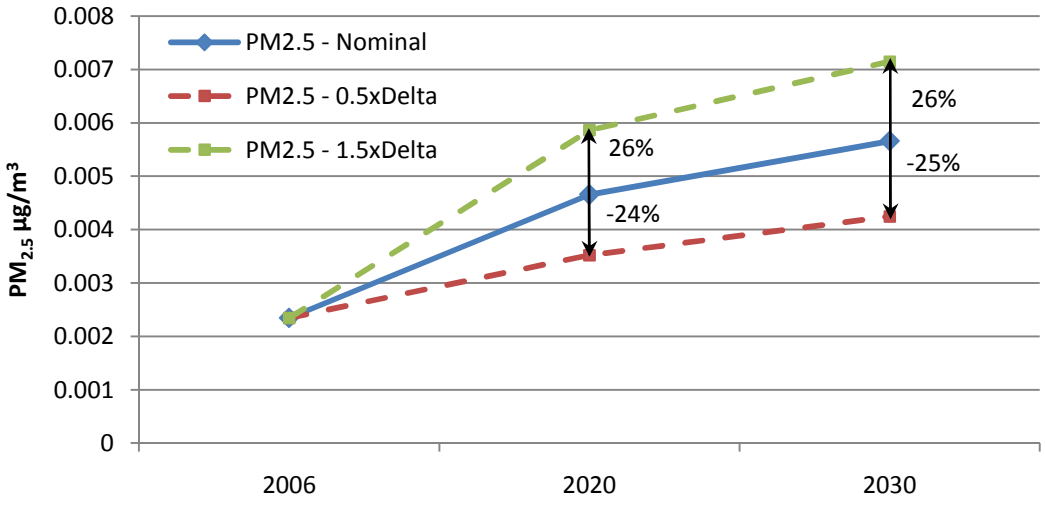

Figure 5-20: Future-year aviation annual $PM_{2.5}$ sensitivity to background emissions

Considering the magnitude of changes (expressed as percentages relative to the nominal concentrations for each of the two future year aviation scenarios), it is evident that the aviation impacts change by approximately ±25% in both future years. The changes are close to symmetric with the change in background emissions: an increase or decrease in the background emissions yields similar magnitude of change in the aviation impacts, with the only difference being the direction of change. While changes in aviation impacts appear to be linear with changes in background emissions, it should be noted that all background emissions species are changing

concurrently and the amount by which each species changes is not uniform (ranging from -4% to 29%); the apparently linear relationship holds only for the specific cases modeled herein.

Table 19 shows the relative composition of aviation $PM_{2.5}$, expressed as percentages of total $PM_{2.5}$ for each of the three background scenarios for both 2020 and 2030 aviation cases. The relative compositions of $PM_{2.5}$ are similar between the 2020 and 2030 aviation cases, exhibiting nitrate dominance of $PM_{2.5}$ in all background scenarios. Nitrates become more dominant with decreased background emissions (45% in the 0.5xDelta case rising to 55% in the 1.5xDelta case), lowering the proportion of sulfates in the process.

Also given in Table 19 are the $PM_{2.5}$ species concentrations for the 2020 and 2030 aviation scenario for all three background scenarios considered in this sensitivity study. Examining the sensitivity of each aviation case, it is seen that the inorganic secondary PM species concentrations (sulfates, nitrates and ammonium) increase in magnitude as the aggregate background emissions decreases ("High" to "Low"). This behavior is consistent with that observed between the 2006 and 2020 nominal case that is analyzed in Section 5.2.1, extending the scenario to a situation where the aviation emissions stay constant and only the background emissions vary. It is therefore not surprising that the 1.5xDelta background scenario (with relatively lower aggregate emissions) yields more aviation-attributable $PM_{2.5}$ than the nominal case, while the 0.5xDelta background emissions scenario yields relatively lower concentrations.

Spatial variability is examined by considering a histogram of relative change per grid cell (expressed as a percentage of the nominal 2020 aviation scenario) for the 2020 annual-averaged aviation-attributable $PM_{2.5}$ (the 2030 aviation case is not shown, given its similarity to the 2020 aviation case). Figure 5-21(a) shows the relative frequency of percent change in grid-cell values in the 0.5xDelta case, while Figure 5-21(b) shows the same for the 1.5xDelta scenario. The average percentage change amongst the grid cells in the 0.5xDelta case is -17% and +18% in the 1.5xDelta case. This is expected since the domain-averaged aviation $PM_{2.5}$ is reduced in the 0.5xDelta background case and increased in the 1.5xDelta case.

Table 19: Future-year annual aviation $PM_{2.5}$ sensitivity to background emissions

(Relative) Background Emissions		Sulfates		Nitrates		Ammonium		EC		OC		Crustal	
2020 Aviation $PM_{2.5}$ ($\mu g/m^3$)													
(High)	**0.5xDelta**	6.93×10^{-4}	(20%)	1.58×10^{-3}	(45%)	6.24×10^{-4}	(18%)	1.08×10^{-4}	(3%)	5.59×10^{-4}	(16%)	-4.18×10^{-5}	(-1%)
(Mid)	**Nominal**	7.24×10^{-4}	(16%)	2.42×10^{-3}	(52%)	9.16×10^{-4}	(20%)	1.09×10^{-4}	(2%)	5.40×10^{-4}	(12%)	-4.89×10^{-5}	(-1%)
(low)	**1.5xDelta**	8.46×10^{-4}	(14%)	3.21×10^{-3}	(55%)	1.23×10^{-3}	(21%)	1.10×10^{-4}	(2%)	5.02×10^{-4}	(9%)	-3.92×10^{-5}	(-1%)
2030 Aviation $PM_{2.5}$ ($\mu g/m^3$)													
(High)	**0.5xDelta 2030**	8.62×10^{-4}	(20%)	1.87×10^{-3}	(44%)	7.50×10^{-4}	(18%)	1.33×10^{-4}	(3%)	6.75×10^{-4}	(16%)	-4.85×10^{-5}	(-1%)
(Mid)	**Nominal 2030**	9.01×10^{-4}	(16%)	2.92×10^{-3}	(52%)	1.11×10^{-3}	(20%)	1.33×10^{-4}	(2%)	6.52×10^{-4}	(12%)	-5.94×10^{-5}	(-1%)
(low)	**1.5xDelta 2030**	1.05×10^{-3}	(15%)	3.90×10^{-3}	(55%)	1.50×10^{-3}	(21%)	1.35×10^{-4}	(2%)	6.06×10^{-4}	(8%)	-4.82×10^{-5}	(-1%)

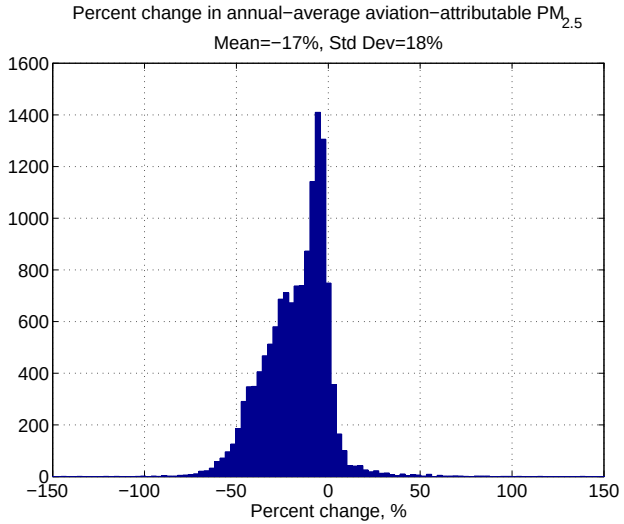

(a) 0.5xDelta ÷ nominal 2020 aviation

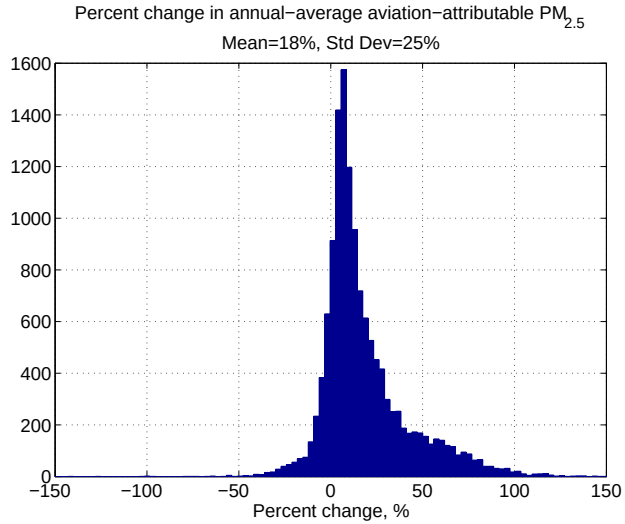

(b) 1.5xDelta ÷ nominal 2020 aviation

Figure 5-21: Grid cell changes (percentages) of 2020 aviation $PM_{2.5}$ between the nominal background and (a) 0.5xDelta background and (b) 1.5xDelta background

There exists a high degree of variability in the grid-cell changes, as evidenced by the high coefficients of variation (CV[11]) of 1.06 and 1.39 for the 0.5xDelta and 1.5xDelta cases respectively. Specifically for the 0.5xDelta case, this suggests that there exist a significant number of grid cells (in a normally-distributed statistical sense, about 32 percent) which experience either a growth in $PM_{2.5}$ or a greater than 35% reduction (this interpretation can be extended vice versa to the 1.5xDelta case). The spread in the magnitude of relative change is higher in the 1.5xDelta case compared with the 0.5xDelta case (25% vs. 18% standard deviation), and is evident visually from the histograms as well. It is noted that the spread in relative changes could arise from the inhomogeneous (spatial) changes in background emissions, as well as nonlinear chemistry between the background and aviation emissions.

5.5.2 Ozone Sensitivity

The sensitivity of aviation-attributable seasonal-average 8-hour daily maximum ozone to background is shown in Figure 5-22. The trends are similar to that of $PM_{2.5}$, with aviation contribution to ozone decreasing amid the 0.5xDelta background scenario and increasing in the 1.5xDelta background case. It is notable that, unlike the $PM_{2.5}$ concentrations, the magnitude of change is not symmetric between the two background scenarios; ozone decreases in the 0.5xDelta background by 21%, while it experiences a growth of 34% in the 1.5xDelta background.

The spatial distributions of change in aviation ozone concentrations exhibit some variability in the magnitude of changes that occur, characterized by a standard deviation of 9 and 20 percent for 2020 aviation amidst 0.5xDelta and 1.5xDelta background emissions respectively. This is demonstrated in Figure 5-23(a) and Figure 5-23(b), which show the relative frequency of grid-cell change in ozone for 2020 aviation expressed as a percentage relative to the nominal 2020 aviation case (the similarity of the 2030 aviation case to the 2020 aviation case is noted, as before, and therefore not shown). The variability of grid-cell level change is attributed to the inhomogeneous spatial changes in background emissions and non-linear NO_x-VOC-O_3 chemistry (as explained in Section 5.2.2).

[11] Coefficients of Variation (CV) are defined as the standard deviation divided by the absolute value of the mean.

Changes in ozone concentrations exhibit more consistency compared with the change in $PM_{2.5}$. The CV for both cases are less than 1 (0.5 for the 0.5xDelta case and 0.67 for the 1.5xDelta case), indicating that the majority of grid-cells experience unidirectional changes in magnitude; that is, for the 0.5xDelta background scenario, most positive grid-cells become less positive and most negative grid-cells become less negative. A similar outcome is seen for the aviation perturbation in the 1.5xDelta background scenario, although the larger CV results in greater variation in magnitude of changes that occur.

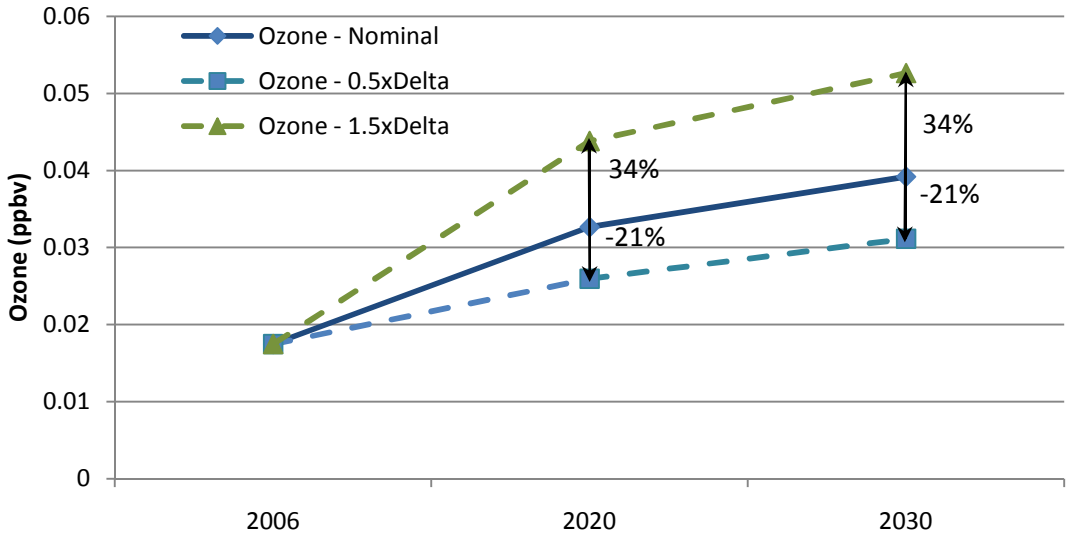

Figure 5-22: Future-year aviation seasonal ozone sensitivity to background emissions

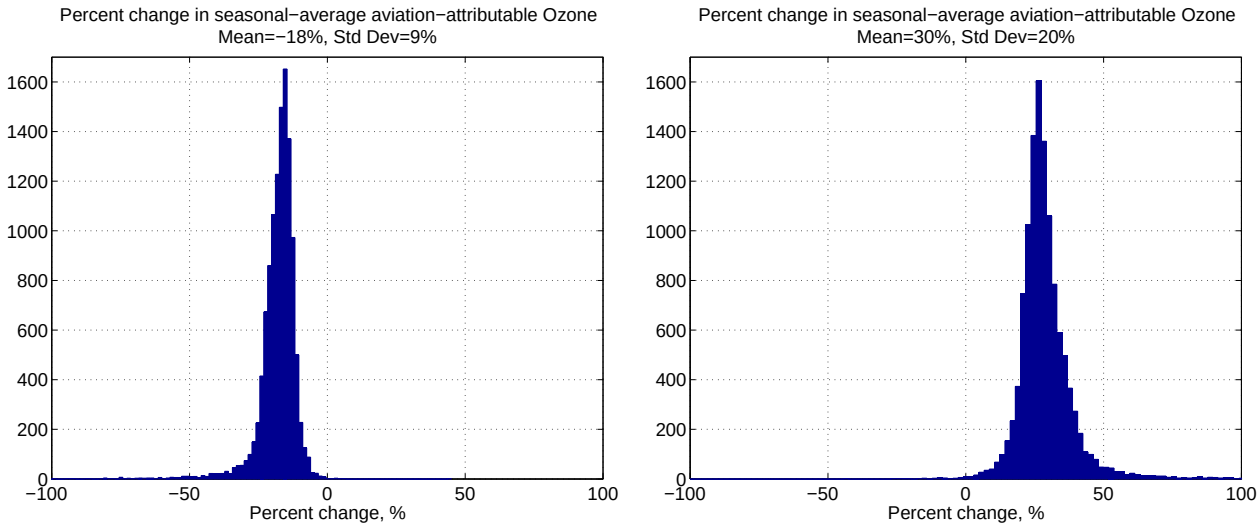

(a) 0.5xDelta ÷ nominal 2020 aviation

(b) 1.5xDelta ÷ nominal 2020 aviation

Figure 5-23: Grid cell changes (percentages) of 2020 aviation O_3 between the nominal background and (a) 0.5xDelta background and (b) 1.5xDelta background

Chapter 6 Discussion of Results

The following section discusses some of the conclusions that can be drawn from the modeling results and analyses in the previous sections. Specifically the discussion will be focused on addressing the three objectives of the thesis, as set forth in Section 1.3:

A Quantify the future-year impacts of LTO aviation emissions on regional air quality in the US – this is done through the base-year implementation and future-year projection of aviation activity and emissions, and the simulation of the atmospheric response to these emissions amid a present-day and future-year background emissions scenario

B Estimate the sensitivity of the air quality impact of LTO aviation emissions to the background emissions forecasts – a sensitivity study is performed, perturbing the background emissions to ascertain their influence on the resulting aviation-attributable $PM_{2.5}$ and ozone concentrations

C Identify the implications of a changing background emissions scenario on the current policy analysis methodology – the current aviation air quality policy analysis tool, the RSMv2, is used to calculate future-year aviation $PM_{2.5}$ concentrations, and subsequently compared against the outputs from the CMAQ model

6.1 Future-year Impacts

Figure 5-5 - Figure 5-7 and Figure 5-9 - Figure 5-11 in Chapter 5 provide clear evidence that, at a national level, the future-year air quality impacts of aviation LTO emissions are expected to increase in magnitude: $PM_{2.5}$ concentrations grow to by factor of 2 and 2.4 relative to base year 2006 levels by 2020 and 2030, while ozone concentrations grow by 90% and 120% in 2020 and 2030 respectively. Through the analysis in Chapter 5, it is shown that the increase in impacts is brought about not only due to growth in aviation activity, but also as a result of changes in background (non-aviation anthropogenic) emissions. The spatial distributions of the impacts are not uniform: most of the future growth in PM arising in regions with positive free ammonia, while ozone levels may actually decrease due to aviation emissions locally while becoming elevated regionally.

Mitigation strategies will be required to address the rising impacts of aviation in the future. At the most fundamental level, net aviation emissions need to be reduced in order to control the present-day and future contribution of aviation to ambient levels of PM and ozone. A key aspect that is not accounted for in this study is the application of improved future technologies. Improvements in engine efficiency and advancements in airframe design can lead to lower amount of fuel being required for a given mission, thereby lowering emissions from each aircraft engine. System-level enhancements in air traffic management (for example, allowing for more direct routings and continuous descent approaches (CDAs) [100]) and surface operations (reducing engine idling and taxi times) [101] also lead to savings in fuel burn, and therefore a reduction in emissions. Alternative fuels which reduce EIs for emissions species (soot, fuel organics and NO_x for instance [65]), and Ultra-Low Sulfur (ULS) jet fuel [97] are another promising avenue for mitigation of specific pollutants.

Examining the trends in PM species, it becomes clear that particle nitrates form the majority of PM in the base year simulation and drive the growth in future-year PM concentrations. Nitrate PM, as explained in Section 5.2, form as a result of aviation NO_x emissions being oxidized and subsequently neutralized by ammonia to form ammonium nitrates. Therefore, in addition to reducing overall emissions from aircraft, special attention must be given to NO_x emissions and ways to reduce them. A potential approach to combat aviation NO_x is through NO_x Stringency measures. In this analysis, a NO_x stringency policy, Scenario #6 from ICAO CAEP/8 which aims to reduce NO_x emissions from large engines by 15% [15], is implemented in the emissions inventories. As shown in Table 9, though, this policy results in only a 3-6% reduction in fleet-wide NO_x emissions – reasons for this include the fleet inertia of the national aviation fleet and other barriers to implementation (discussed in Mahashabde et al. [12]) which reduce the effectiveness of the policy. This might imply the need for stricter stringency goals that are set early enough, such that airframe and engine manufacturers are able to roll out new technologies in time to meet the goals more effectively. Penalties could also be imposed for non-compliance of in-service aircraft to incentivize the change.

Modifications/implementation of new technology or policies aimed at reducing a specific emissions species might have undesired side-effects on other emissions species or on the overall environmental impact of aviation. Specific examples include tradeoffs between NO_x and

CO/unburnt HC emissions (as seen in Section 3.2.1), the implementation of ULS jet fuel decreasing sulfate PM but giving rise to more nitrate PM in certain regions as a result of bounce-back effects [97], or the possibility of raising ozone concentrations by lowering NO_x emissions due to nonlinear NO_x-VOC-O_3 interactions. In addition, policies aimed at reducing air quality impacts could have a negative impact on noise or climate. A clear example of this is seen in Mahashabde et al. [12], wherein the implementation of a NO_x stringency policy provides air quality benefits but is found to cause increased climate and noise damages. Thus, care must be taken to evaluate each proposed emissions reduction policy using well-accepted modeling methods and under an integrated environmental impacts framework (such as APMT-Impacts), considering both aggregate as well as local impacts in order to fully characterize the effects of the policy.

The growth of aviation emissions in future years is well-aligned with projected increases in commercial (air carrier) aircraft activity, suggesting that emissions from commercial aviation are responsible for the majority of aviation emissions. While the local air quality impacts of aviation may be more dependent on aircraft activity in all categories (as might be the case for primary nonvolatile PM emissions), gaseous emissions of NO_x and SO_x that act as precursors for the dominant secondary PM are driven by changes in air carrier activity. As such, in order to effectively manage aviation impacts, any proposed improvements (be it technological, system-level or fuel-oriented) should be geared towards commercial aviation. This is indeed the case with the majority of the current aviation environmental research, and the findings presented herein lend further support to this argument.

6.2 Sensitivity of Aviation Impacts to Background Emissions Scenarios

The analysis presented in Section 5.2 shows that aviation impacts are sensitive to background emissions by demonstrating the effect that a change in background emissions from 2005 to 2025 has on aviation $PM_{2.5}$ and ozone formation. The sensitivity of future-year aviation impacts to over/under predictions of background emissions forecasts is shown by the sensitivity study, where aviation impacts on particulate matter concentrations vary by approximately ±25% and impacts on ozone change by +34% & -21% amid a ±50% variation in the predicted change in background emissions between 2005 and 2025. A high degree of variability, characterized by a coefficient of variation greater than unity, is seen in the relative grid cell changes for $PM_{2.5}$ as

shown in Figure 5-21 for both the less-than-predicted change (0.5xDelta case) and the greater-than-predicted change (1.5xDelta case), while a lower (but still significant) spread is observed for seasonal 8-hour maximum ozone. These results hold three key implications from an aviation air quality policy analysis perspective, which will be described below.

First, the efficacies of aviation air quality policy measures could potentially be over-estimated or under-represented if future-year background emissions are not accounted for in the air quality analysis. This occurs since the future-year background emissions cause a change in aviation impacts that are disproportionate to the predicted change in aviation emissions alone. For instance, the effects of a reduction in aviation NO_x emissions on aviation-attributable $PM_{2.5}$ might be under-represented amid a background scenario that gives rise to lower baseline aviation nitrate concentrations due to a lack of free ammonia and reduced oxidative capacity. In a cost-benefit analysis policy decision-making framework such as APMT-Impacts where a break-even (costs=benefits) solution is often assessed, the changes induced by the background emissions might yield a new optimum. Therefore, a complete and accurate characterization of future-year aviation impacts needs to take into account the effects of future-year background emissions scenarios.

Second, aviation policies need to be developed in conjunction with the proposed plans and policies of other anthropogenic emissions sectors. As seen in the sensitivity study performed in this thesis, variation in the background emissions scenario leads to significant changes in the magnitude, spatial distribution and relative composition of chemical species of aviation air quality impacts (as shown in Table 19, Figure 5-21 and Figure 5-23). These changes could potentially alter the direction of aviation emissions policies to focus on different mitigation strategies. For example, more aggressive SO_x emission reductions from the IPM sector could cause create “hotspots” that encourage PM formation (such as regions of elevated FA around airports) and might necessitate the need for terminal-area mitigation strategies (such as derated-thrust takeoffs [102] and CDAs) in addition to system-wide (fleet-level) policies such as ULS or NO_x stringency. The dependency of aviation impacts on background emissions therefore necessitates that policies designed to reduce aviation impacts be developed (and analyzed) alongside those of other sectors.

Finally, future-year anthropogenic emissions projections are updated/modified over time (as evidenced by Table 14) with the addition and implementation of new emissions control policies as well due to inherent variations in projection methodologies such as socioeconomic and activity forecasts. The sensitivity of aviation impacts to background emissions suggests that the uncertainties in background emissions projections need to be incorporated into the aviation air quality analysis in order to quantify the potential range of outcomes that might occur. A sensitivity study (much like the one performed in this thesis) may capture the uncertainty bounds through a low, mid and high estimate of future-year background emissions. Alternative methods including surrogate adjoint models that could be used to obtain the sensitivity of aviation emissions amid a range of varying background scenarios.

6.3 Implications for Future-year Aviation Policy Analysis

This aim of this section is to assess the performance of the current aviation policy analysis methodology in APMT-Impacts (codified in the RSMv2) in predicting future-year aviation $PM_{2.5}$. As described in Section 2.6, the RSMv2 regression coefficients are derived based on CMAQ simulations that used a fixed background emissions scenario (for the year 2001), and as such the RSMv2 estimates future-year impacts in isolation to changes in emissions from other sectors. The performance of the RSMv2 is compared with the CMAQ simulations performed in this thesis, to illustrate the differences that exist if changes in background emissions are taken into account.

The PM outputs from both models are normalized with their respective base year concentrations; this is done to narrow the focus of the analysis to changes relative to the base year predicted concentrations of each model, given that there are a large number of differences between the two modeling platforms (tabulated in Table 20) that make a one-to-one comparison of concentrations challenging.

The base and future-year aviation emissions that are used in the CMAQ simulations are aggregated into annual airport-level totals (similar to the numbers presented in Appendix H) and input to the RSM, noting that only the four inputs of fuel-burn, NO_x, SO_2 and BC are used. A mid-range lens is selected, along with default distributions on emissions and regression parameter uncertainties. Pre-SMAT results from the RSM and CMAQ are used in the comparison.

Table 20: Differences between thesis and RSMv2 CMAQ modeling platforms

	Thesis CMAQ configuration	RSM-Build CMAQ configuration
Model	CMAQ v4.7.1	CMAQ v4.5
Aviation Emissions	2006, 2020 and 2030 LTO	Design space sampling
Background Emissions	Base year 2005 NEI and future year 2025 NEI	2001 NEI
Meteorology	2005	2001
Simulation time period	One year	Four representative months
Grid	36km x 36km CONUS	36km x 36km CONUS

Figure 6-1 shows the domain-averaged $PM_{2.5}$ concentration outputs for the three aviation emissions scenarios of 2006, 2020 and 2030. Total $PM_{2.5}$ domain averaged concentrations are predicted to increase in the future years by the RSM, though not at the same rate as the CMAQ outputs. Examining the growth in individual PM species it is observed that, while the EC growth rate is similar, there are differences in the growth rates for other PM species. The larger growth rate of OC in the RSMv2 is attributed to high regression error in the response surface for OC (an R^2 of 0.750 for OC) which is documented in Brunelle-Yeung's thesis [11]. The increments in sulfates and large growth in nitrate and ammonium PM in the CMAQ results are explained by increased oxidation and higher amounts of free ammonia due to the future-year background scenario, as illustrated by the analysis in Section 5.2. The RSMv2, having been developed based on a static 2001 background scenario, is not able to capture the changes in sulfate, nitrate and ammonium $PM_{2.5}$ concentrations (and therefore, changes in total $PM_{2.5}$) that are induced by the changing future-year background.

The RSMv2, therefore, has to be upgraded to (a) reflect the advancements in the science of modeling air quality, overcoming the differences listed in Table 20 and (b) incorporate the effects of changing background scenario on aviation $PM_{2.5}$ to effectively estimate future-year aviation air quality impacts and, subsequently, aviation policy efficacies. The characteristics of speed, accuracy and functionality still need to be preserved, however, in order for the upgraded module to be successfully incorporated into the APMT-Impacts framework.

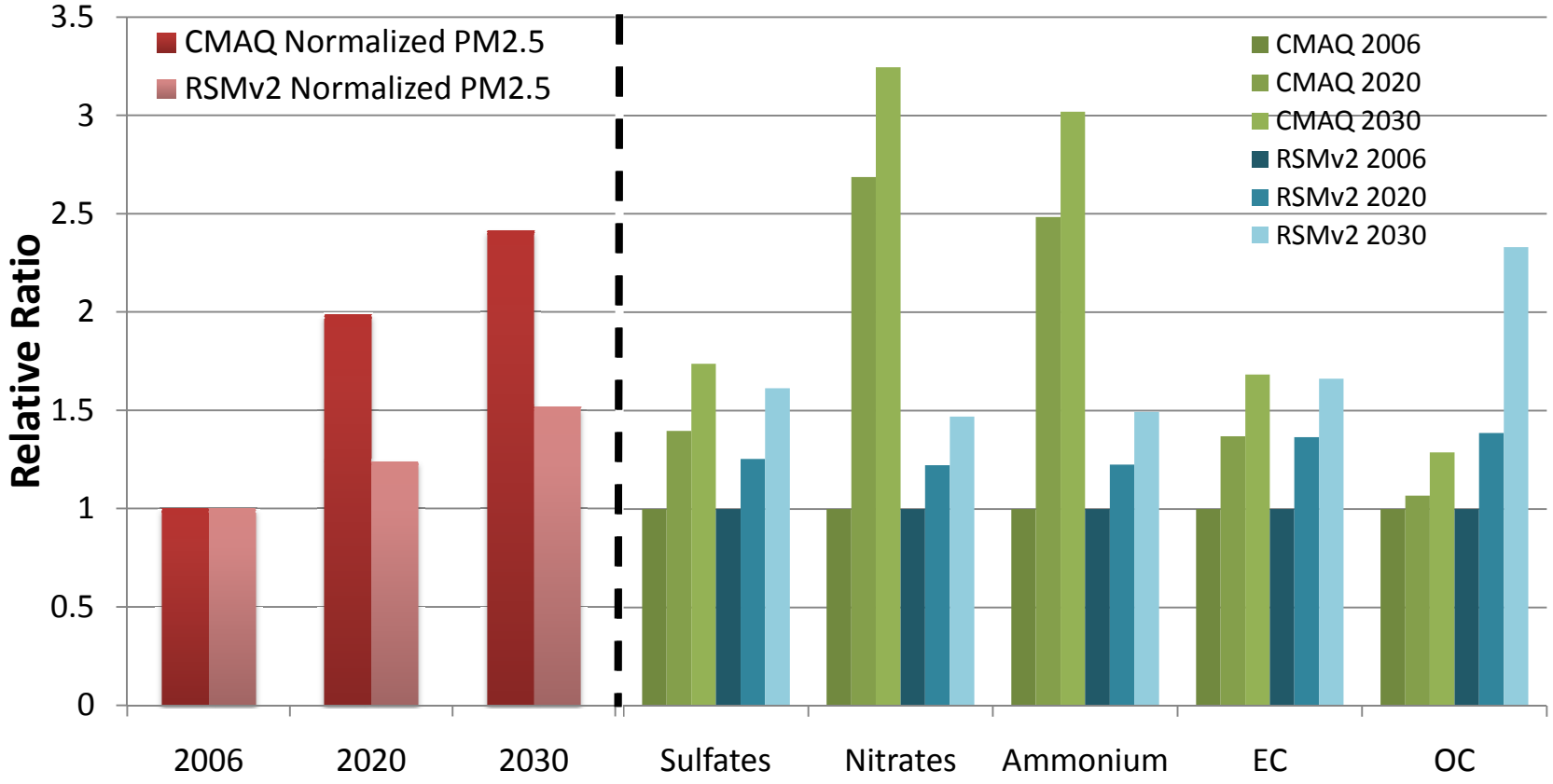

Figure 6-1: $PM_{2.5}$ relative growth rates comparison between RSMv2 and CMAQ simulations

Chapter 7 Conclusion

7.1 Summary

In summary, the CMAQ model was validated against measurements to establish model biases before being employed to estimate current and future-year aviation air quality impacts on surface-level annual $PM_{2.5}$ and 8-hour daily maximum ozone and the sensitivity of future-year impacts to variations in background emissions forecasts. Aviation activity and emissions were computed for the base year as well as future years, and annual aviation fuel burn was forecast to grow by 26% and 57% by 2020 and 2030 respectively. Uncertainties in the current and future aviation emissions were also characterized. Background (non-aviation anthropogenic) emissions were forecast to decline in the future, and background emissions scenarios were developed to assess the sensitivity of aviation air quality impacts to changes in background emissions forecasts.

The three aims of the thesis that were presented in Section 1.3 were achieved via the analyses presented in the Chapters 5 and 6. Specifically, the air quality impacts of aviation were shown to grow in the future years. Domain-averaged surface-level annual aviation $PM_{2.5}$ concentrations were shown to grow by approximately 100% in 2020 and 140% by 2030 relative to the base year 2006 levels, and reasons for this growth (driven by ammonium nitrate PM) were found in the enhanced oxidative capacity of the future-year atmosphere as well as increased free ammonia. Domain-averaged 8-hour daily maximum seasonal ozone impacts were demonstrated to grow by approximately 90% in 2020 and 120% in 2030 relative to 2006 concentrations, noting the inhomogeneous spatial impacts that occur within the domain, and the behavior of ozone was explained by NO_x-VOC-O_3 chemistry.

Aviation $PM_{2.5}$ varied by approximately ±25% with a greater-than-predicted and less-than-predicted change in background emissions between 2005 and 2025 respectively, while ozone response was similar in direction but asymmetric in magnitude at +34%/-21% change in concentrations. Spatial variability was seen in the way aviation impacts were affected by the perturbations in background emissions, with a larger spread of grid cell changes in $PM_{2.5}$ than ozone.

Finally, the effect of the future-year background scenario on the aviation policy analysis tool, the RSMv2, was shown by comparing growth in future-year aviation-attributable $PM_{2.5}$ concentrations predicted by the RSMv2 and CMAQ for all three years of aviation emissions. A much larger growth rate in nitrate and ammonium $PM_{2.5}$ is observed in the CMAQ outputs compared with the RSMv2 outputs, due to the changing background emissions scenario from 2005 to 2025 in the CMAQ simulations. The need for the development of an updated RSM, which accounts for the changing future-year background scenario, was underscored.

A discussion of the results highlighted the need for aviation air quality impacts mitigation efforts, with increased emphasis on NO_x Stringency policies given that the growth in future-year aviation PM is driven by increases in nitrate PM. The sensitivity of aviation air quality impacts to changes in background emissions implies that aviation policies should be constructed and evaluated together with plans and proposals from the other anthropogenic sectors, using well-accepted modeling methodologies and an integrated environmental impacts assessment framework, failing which aviation policy impacts could be overestimated or underrepresented. Finally, the need to account for the various uncertainties in background and aviation emissions in the modeling methodologies was emphasized.

7.2 Limitations and Future Work

One limitation of this study is that it does not consider aviation cruise emissions (i.e. emissions above the LTO cutoff of 3000ft). LTO emissions were selected in accordance with regulatory impacts analyses methodologies that currently exist, but as shown by Barrett et al. [52], cruise emissions could result in up to 5 times as many premature adult mortalities. The global nature of aviation and its air quality impacts also suggests that a global simulation (one that includes future-year forecasts of aviation and anthropogenic emissions worldwide) may be required to fully capture the air quality impacts felt within the US.

Aviation primary PM emissions methodologies need to be updated to reflect data from new measurement campaigns. Stettler et al. [61] propose a new method of estimating BC from regressions of measured data against engine pressure ratio, smoke number and CO and NO_x EIs; they also suggest a modified method of estimating primary OC emissions based on incomplete combustion and lubrication oil.

Aviation emissions forecasts could be further refined to include the advancements in aircraft and engine technology, and the improvements in airspace and airport management that are expected to be achieved in the future years. In addition to modeling expected changes in technology, further studies could attempt to quantify the level of technological change that would be required to meet certain goals, such as the FAA's plan to achieve a 50% reduction in aviation-attributable health impacts by 2018 compared to 2005 [103]. Future-year aviation air quality and health impacts of multiple aviation emissions reduction strategies could be efficiently analyzed through a future-year RSM (described below).

The work performed in this thesis can be furthered by considering the health impacts that arise as a result of future-year air quality impacts of aviation. Computing health impacts would necessitate calculating population exposure to aviation $PM_{2.5}$ and ozone concentrations, an exercise that would yield further information about the present and future-year spatial impacts of aviation. Future-year population forecasts, along with updated CRFs for $PM_{2.5}$ and ozone would be required to adequately characterize health impact incidences in the future years.

Finally, as mentioned in Section 6.3, the current air quality tool used in APMT policy analyses, the RSMv2, needs to be upgraded to account for the scientific advances in modeling methods as well as the change in aviation impacts due to future-year background emissions scenarios and their uncertainties. Potential developmental methodologies might include:

- Building two RSMs using the current CMAQ modeling platform, one with the base year 2005 background emissions and another using a future year background emissions and interpolating between the two depending on the analysis year.
- Relating the change in aviation impacts as a function of the background scenario, for instance, through a parameter known as Adjusted Gas Ratio (presented in Pinder et al. [104]) which characterizes the sensitivity of nitrate PM to total ammonia and total nitrate concentrations.

Further investigation needs to be conducted to determine which of these methods is the most applicable and practical to implement.

Bibliography

[1] ICAO Secretariat. (2010). *ICAO Environmental Report 2010: Aviation Outlook.* ICAO.

[2] JPDO. (2006). *Making the NextGen Vision a Reality: 2006 Progress Report.* JPDO.

[3] ICAO. (n.d.). *Economic Contribution of Civil Aviation.* Retrieved August 5, 2011, from http://www.icao.int/icao/en/atb/fep/EconContribution.pdf

[4] FAA ATO. (2009). *The Economic Impact of Civil Aviation on the US Economy.* Washington, D.C.: FAA.

[5] FAA. (2011). *Next Generation Air Transportation System (NextGen) Implementation Plan.* Washington, D. C.: FAA.

[6] US EPA. (2004). *Benefits of the Proposed Inter-State Air Quality Rule.* Reseach Triangle Park, NC: US EPA OAQPS.

[7] Ratliff, G., Sequeira, C., Waitz, I., Ohsfeldt, M., Thrasher, T., Graham, M., & Thompson, T. (2009). *Aircraft Impacts on Local and Regional Air Quality in the United States.* Cambridge, MA: Partnership for AiR Transportation Noise and Emissions Reductions.

[8] Woody, M., Baek, B. H., Adelman, Z., Omary, M., Lam, Y. F., West, J. J., & Arunachalam, S. (2011). An assessment of Aviation's contribution to current and future fine particulate matter in the United States. *Atmospheric Environment 45(20)* , 3424-3433.

[9] Kuhn, S. R. (2010). *Cost-benefit Analysis of Ultra-Low Sulfur Jet Fuel.* Cambridge, MA: Master's Thesis, Massachusetts Institute of Technology, Department of Aeronautics and Astronautics.

[10] Masek, T. (2008). *A Response Surface Model of the Air Quality Impacts of Aviation.* Cambridge, MA: Master's Thesis, Massachusetts Institute of Technology Department of Aeronautics and Astronautics.

[11] Brunelle-Yeung, E. (2009). *The Impacts of Aviation Emissions on Human Health Through Changes in Air Quality and UV Irradiance.* Cambridge, MA: Master's Thesis, Massachusetts Institute of Technology Department of Aeronautics and Astronautics.

[12] Mahashabde, A., Wolfe, P., Ashok, A., Dorbian, C., He, Q., Fan, A., Lukachko, S., Mozdzanowska, A., Wollersheim, C., Barrett, S. R., Locke, M., & Waitz, I. A. (2011). Assessing the environmental impacts of aircraft noise and emissions. *Progress in Aerospace Sciences 47(1)* , 15-52.

[13] ICAO. (2nd ed. (1993)). *ICAO Annex 16 "International standards and recommended practices, Environmental protection", Volume II "Aircraft engine emissions" plus amendments (1997, 1999, 2005).* ICAO.

[14] Wayson, R., & Fleming, G. (2000). *Consideration of Air Quality Impacts by Airplane Operations at or above 3000 feet AGL.* Washington, D.C.: FAA Office of Environment and Energy.

[15] CAEP. (2010). *CAEP/8 NOx Stringency Cost-Benefit Analysis Demonstration Using APMT-Impacts.* CAEP, available online at http://web.mit.edu/aeroastro/partner/reports/caep8/caep8-nox-using-apmt.pdf.

[16] Jacob, D. J. (1999). Chapter 4. Atmospheric Transport. In D. J. Jacob, *Introduction to Atmospheric Chemistry.* Princeton University Press.

[17] US EPA. (2006). *Response Surface Modeling. Technical Support Document for the Proposed PMNAAQS Rule.* Research Triangle Park, NC: US EPA OAQPS.

[18] State of Florida. (2010). *Regional Haze Plan for Florida Class I Areas, Appendix C: Modeling Analysis Protocol and Quality Assurance Project Plan.* FL: Department of Environmental Protection, State of Florida.

[19] Appel, K. W., Foley, K. M., Bash, J. O., Pinder, R. W., Dennis, R. L., Allen, D. J., & Pickering, K. (2011). A multi-resolution assessment of the Community Multiscale Air Quality (CMAQ) model v4.7 wet deposition estimates for 2002–2006. *Geoscientific Model Development 4* , 357-371.

[20] US EPA. (1999). *Regulatory Impact Analysis - Control of Air Pollution from New Motor Vehicles: Tier 2 Motor Vehicle Emissions Standards and Gasoline Sulfur Control Requirements, Appendix A. Summary of Emission Inventories for 47 States and for Four Urban Areas.* US EPA Office of Mobile Sources.

[21] US EPA. (2006). *2006 National Ambient Air Quality Standards for Particle Pollution, Appendix O -- Model Evaluation.* Research Triangle Park, NC: US EPA.

[22] US EPA. (2010). *Air Quality Modeling Technical Support Document: Light-Duty Vehicle Greenhouse Gas Emission Standards Final Rule.* Research Triangle Park, NC: US EPA OAQPS.

[23] CMAS. (2010). *Operational Guidance for the Community Multiscale Air Quality (CMAQ) Modeling System version 4.7.1 (June 2010 release).* Chapel Hill, NC: Community Modeling and Analysis System, Institute for the Environment, University of North Carolina at Chapel Hill.

[24] Byun, D., & Schere, K. (2006). Review of the Governing Equations, Computational Algorithms, and Other Components of the Models-3 Community Multiscale Air Quality (CMAQ) Modeling System. *Applied Mechanics Reviews 59(2)* , 51-77.

[25] Yarwood, G., Rao, S., Yocke, M., & Whitten, G. (2005). *Updates to the Carbon Bond Mechanism: CB05.* US EPA.

[26] Byun, D., Pleim, J. E., Tang, R. T., & Bourgeois, A. (1999). *Meteorology-Chemistry Interface Processor (MCIP) For Models-3 Community Multiscale Air Quality (CMAQ) Modeling System.* Research Triangle Park, NC: US EPA.

[27] Grell, G. A., Dudhia, J., & Stauffer, D. R. (1994). *A Description of the Fifth-Generation Penn State/NCAR Mesoscale Model (MM5).* Boulder CO.: National Center for Atmospheric Research.

[28] Denman, K.L., G. Brasseur, A. Chidthaisong, P. Ciais, P.M. Cox, R.E. Dickinson, D. Hauglustaine, C. Heinze, E. Holland, D. Jacob, U. Lohmann, S Ramachandran, P.L. da Silva Dias, S.C. Wofsy & X. Zhang. (2007). *Couplings Between Changes in the Climate System and Biogeochemistry. In: Climate Change 2007: The Physical Science Basis. Contribution of Working Group I to the Fourth Assessment Report of the Intergovernmental Panel on Climate Change.* Cambridge University Press, Cambridge, UK: Climate Change 2007: The Physical Science Basis. Contribution of Working Group I to the Fourth Assessment Report of the Intergovernmental Panel on Climate Change.

[29] Bey, I., Jacob, D. J., Yantosca, R. M., Logan, J. A., Field, B. D., Fiore, A. M., Li, Q., Liu, H. Y., Mickley, L. J., & Schultz, M. G. (2001). Global modeling of tropospheric chemistry with assimilated meteorology: Model description and evaluation. *Journal of Geophysical Research 106(D19)* , 23073-23095.

[30] Lam, Y. F. and Fu, J. S. (2010). Corrigendum to "A novel downscaling technique for the linkage of global and regional air quality modeling" published in Atmos. Chem. Phys., 9, 9169–9185, 2009. *Atmospheric Chemistry and Physics 10* , 4013-4031.

[31] Lam, Y. F., Fu, J. S., & Mickley, L. J. (2011). Impacts of future climate change and effects of biogenic emissions on surface ozone and particulate matter concentrations in US. *Atmospheric Chemistry and Physics 11* , 2183-2231.

[32] Wang, Y., Jacob, D. J., & Logan, J. A. (1998). Global simulation of tropospheric O3-NOx-hydrocarbon chemistry, 1. Model formulation. *Journal of Geophysical Research 103(D9)* , 10,713-10,726.

[33] Park, R. J., Jacob, D. J., Field, B. D., & Yantosca, R. M. (2004). Natural and transboundary pollution influences on sulfate-nitrate-ammonium aerosols in the United States: implications for policy. *Journal of Geophysical Research 109* .

[34] Whitten, G. Z., Hogo, H., & Killus, J. P. (1980). The Carbon-Bond Mechanism: A Condensed Kinetic Mechanism for Photochemical Smog. *Environmental Science and Technology 14(6)* , 690-700.

[35] Isukapalli, S. S. (1999). *Uncertainty Analysis of Transport-Transformation Models.* Piscataway, NJ: Ph.D. Thesis, Rutgers The State University of New Jersey.

[36] Roselle, S., Schere, K., Pleim, J., & Hanna, A. (1999). *Photolysis Rates for CMAQ.* US EPA.

[37] Appel, K. W., Gilliam, R. C., Davis, N., Zubrow, A., & Howard, S. C. (2011). Overview of the atmospheric model evaluation tool (AMET) v1.1 for evaluating meteorological and air quality models. *Environmental Modeling and Software 26(4)* , 434-443.

[38] US EPA. (2007). *Guidance on the Use of Models and Other Analyses for Demonstrating Attainment of Air Quality Goals for Ozone, PM2.5, and Regional Haze.* Research Triangle Park, NC: US EPA OAQPS.

[39] IMPROVE. (n.d.). *Interagency Monitoring of Protected Visual Environments (IMPROVE).* Retrieved July 16, 2011, from http://vista.cira.colostate.edu/improve/Default.htm

[40] Sisler, J. F., & Malm, W. C. (1994). The relative importance of soluble aerosols to spatial and seasonal trends of impaired visibility in the United States. *Atmospheric Environment 28(5)* , 851-862.

[41] Chu, S.-H. (2004). PM2.5 episodes as observed in the speciation trends network. *Atmospheric Environment 38(31)* , 5237-5246.

[42] NIOSH. (1998). *Method 5040 Issue 3 (Interim): Elemental Carbon (Diesel Exhaust). In: NIOSH Manual of Analytical Methods. National Institute of Occupational Safety and Health, Cincinnati, OH;.* Cincinnati, OH: CDC.

[43] Federal Register. (1999). *Ambient Air Monitoring Reference and Equivalent Methods: Designation of a New Reference Method.* 40 CRF Part 50.

[44] Frank, N. H. (2006). Retained Nitrate, Hydrated Sulfates, and Carbonaceous Mass in Federal Reference Method Fine Particulate Matter for Six Eastern U.S. Cities. *Journal of Air and Waste Management 56(4)* , 500-511.

[45] US EPA CASTNet. (1991). *Clean Air Status and Trends Network (CASTNET).* Retrieved July 16, 2011, from http://java.epa.gov/castnet/

[46] Eder, B., & Yu, S. (2006). A performance evaluation of the 2004 release of Models-3 CMAQ. *Atmospheric Environment 40(26)* , 4811-4824.

[47] US EPA AQS. (2011, June 24). *About the AQS Database*. Retrieved July 16, 2011, from US EPA AirData: http://www.epa.gov/air/data/aqsdb.html

[48] US EPA. (2010). *Light-Duty Vehicle Greenhouse Gas Emissions Inventory for Air Quality Modeling Technical Support Document.* Research Triangle Park, NC: US EPA OAQPS.

[49] Foley, K. M., Roselle, S. J., Appel, K. W., Bhave, P. V., Pleim, J. E., Otte, T. L., & Mathur, R. (2010). Incremental testing of the Community Multiscale Air Quality(CMAQ) modeling system version 4.7. *Geoscientific Model Development 40(26)* , 4811-4824.

[50] Mahashabde, A. (2009). *Assessing Environmental Benefits and Economic Costs of Aviation Environmental Policy Measures.* Cambridge, MA: Ph.D. Thesis, Massachusetts Institute of Technology Department of Aeronautics and Astronautics.

[51] ICAO Air Transport Bureau. (2010). *Local Air Quality*. Retrieved July 16, 2011, from http://www.icao.int/icao/en/env2010/LocalAirQuality.htm

[52] Barrett, S. R., Britter, R., & Waitz, I. A. (2010). Global mortality attributable to aircraft cruise emissions. *Environmental Science and Technology 44(19)* , 7736–7742.

[53] EDMS. (2010). *Emissions and Dispersion Modeling System (EDMS)*. Retrieved July 16, 2011, from http://www.faa.gov/about/office_org/headquarters_offices/apl/research/models/edms_model/

[54] Volpe. (2003). *Volpe National Transportation Systems Center/US DOT: Enhanced Traffic Management System (ETMS), Functional Description, Version 7.6.*

[55] Wilkerson, J. T., Jacobson, M. Z., Malwitz, A., Balasubramanian, S., Wayson, R., Fleming, G. G., & Naiman, A. D. (2010). Analysis of emission data from global commercial aviation: 2004 and 2006. *Atmospheric Chemistry and Physics 10* , 6391-6408.

[56] FAA. (2005). *Official Airline Guide.* FAA Office of Aviation Policy and Plans (APO).

[57] Kim, B., Fleming, G. G., Balasubramanian, S., Malwitz, A., Waitz, I. A., Kima, K., Stouffer, V., Long, D., Kostiuk, P., Locke, M., Holsclaw, C., Morales, A., McQueen, E., & Gillette, W. (2005). *System for assessing Aviation's Global Emissions (SAGE) Version 1.5 Technical Manual.* Washington DC: FAA.

[58] Baughcum, S. L., Tritz, T. G., Henderson, S. C., & Pickett, D. C. (1996). *Scheduled Civil Aircraft Emissions Inventories for 1992: Database Development and Analysis.* Hampton, VA: NASA Langley Research Center.

[59] Wayson, R. L., Fleming, G. G., & Iovinelli, R. (2009). Methodology to estimate particulate matter emissions from certified commercial aircraft engines. *Journal of Air and Waste Management 59* , 91-100.

[60] ICAO. (2010). ICAO Air Transport Bureau: ICAO Engine Emissions Databank. ICAO. Retrieved from http://www.caa.co.uk/default.aspx?catid=702

[61] Stettler, M. E., Eastham, S., & Barrett, S. R. (2011). Air Quality and Public Health Impacts of UK Airports. Part I: Emissions. *Atmospheric Environment 45(31)* , 5415-5424.

[62] Jun, M. (2011). *Microphysical Modeling of Ultrafine Hydrocarbon-Containing Aerosols in Aircraft Emissions.* Cambridge, MA: Ph. D. Thesis, Masachusetts Institute of Technology Department of Aeronautics and Astronautics.

[63] Wey, C. C., Anderson, B. E., Hudgins, C., Wey, C., Li-Jones, X., Winstead, E., Thornhill, L. K., Lobo, P., Hagen, D., Whitefield, P., Yelvington, P. E., Herndon, S. C., Onasch, T. B., Maike-Lye, R. C., Wormhoudt, J., Knighton, W. B., Howard, R., Bryant, D., Corporan, E., Moses, C., Holve, D., & Dodds, W. (2006). *Aircraft particle emissions experiment (APEX).* Cleveland, OH: National Aeronautics and Space Administration John H. Glenn Research Center at Lewis Field.

[64] CAEP. (2008). *Report of Airport Local Air Quality Task Group (LAQTG).* ICAO.

[65] Hileman, J. I., Ortiz, D. S., Bartis, J. T., Wong, H. M., Donohoo, P. E., Weiss, M. A., & Waitz, I. A. (2009). *Near-Term Feasibility of Alternative Jet Fuels.* Arlington, VA: RAND Corporation.

[66] Schumann, U., Arnold, F., Busen, R., Curtius, J., Karcher, B., Petzold, A., Schlager, H., Schroder, F., & Wohlfrom, K.-H. (2002). Influence of fuel sulfur on the composition of aircraft exhaust plumes: The experiments SULFUR 1-7. *Journal of Geophysical Research 107(D15)* , 4247-4247.

[67] Wood, E. C., Herndon, S. C., Timko, M. T., Yelvington, P. E., & Maike-Lye, R. C. (2008). Speciation and chemical evolution of nitrogen oxides in aircraft exhausts near airports. *Environmental Science and Technology 42(6)* , 1884-1891.

[68] Barrett, S. R., Prather, M., Penner, J., Selkirk, H., Balasubramanian, S., Dopelheuer, A., Fleming, G. G., Gupta, M., & Halthore, R. (2010). *Guidance on the use of AEDT Gridded Aircraft Emissions in Atmospheric Models.* Washington D.C.: FAA.

[69] Wormhoudt, J., Herndon, S., Yelvington, P., & Maike-Lye, R. (2007). Nitrogen Oxide (NO/NO2/HONO) Emissions Measurements in Aircraft Exhaust. *Journal of Propulsion and Power 23* , 906-911.

[70] FAA. (2010). *Terminal Area Forecast Summary.* FAA.

[71] FAA. (2000). *Field Formulation of the National Plan of Integrated Airport Systems (NPIAS).* Department of Transportation, FAA.

[72] GRA, Incorporated. (2001). *Forecasting Aviation Activity by Airport.* FAA.

[73] ICAO CAEP. (2010). *Amendments to ICAO Annex 16 Volume II: Aircraft Engine Emissions.* reported in ICAO Working Paper A37-WP/21.

[74] SH&E, Inc. (2004). *San Diego International Airport Aviation Activity Forecasts.* San Diego, CA: San Diego County Regional Airport Authority.

[75] Jacobs Consultancy. (2008). *Master Plan Update: Portland International Airport.* Portland, OR: Port of Portland.

[76] FAA. (2011). *FAA Aerospace Forecast: Fiscal years 2011-2031.* US DOT FAA Aviation Policy and Plans.

[77] Gawdiak, Y., Carr, G., & Hasan, S. (2009). JPDO Case Study of NextGen High Density Operations. *AIAA Aviation Technology, Integration and Operations Conference (ATIO).* Hilton Head, South Carolina: AIAA.

[78] US EPA. (2008). *Documentation for the 2005 Point Source, National Emissions Inventory.* Research Triangle Park, NC: US EPA OAQPS.

[79] US EPA CAA. (n.d.). *"Clean Air Act", Title 42 Chapter 85 United States Code, 2008 ed.* Retrieved from http://www.epa.gov/air/caa/

[80] US EPA. (2011). *Integrated Planning Model (IPM).* Retrieved July 16, 2011, from http://www.epa.gov/airmarkt/progsregs/epa-ipm/index.html

[81] US EPA. (2007). *Documentation for the Final 2002 Mobile National Emissions Inventory, Version 3.* Research Triangle Park, NC: US EPA OAQPS.

[82] US EPA. (2006). *2006 National Ambient Air Quality Standards for Particle Pollution, Appendix D -- Inventory, Attachment 1: Improving EPA Emissions Forecasting For Regulatory Impact Analyses.* Research Triangle Park, NC: US EPA.

[83] US EPA. (2008). *Technical Support Document: Preparation of Emissions Inventories For the 2002-based Platform, Version 3, Criteria Air Pollutants.* Research Triangle Park, NC: US EPA OAQPS.

[84] US EPA. (2010). *IPM Analysis of the Proposed Transport Rule*. Retrieved July 16, 2011, from http://www.epa.gov/airmarkets/progsregs/epa-ipm/transport.html

[85] US EPA. (2008). *The 2002-Based Multi-Pollutant Modeling Platform Report, Volume III: Air Toxics Appendix A: HAPS in the 2002 NEI.* US EPA OAQPS.

[86] Frey, H. C. (2007). Quantification of Uncertainty in Emission Factors and Inventories. *16th Annual International Emission Inventory Conference Emission Inventories: "Integration, Analysis, and Communications".* Raleigh, NC: US EPA.

[87] NARSTO. (n.d.). *Methods for Assessment of Uncertainty and Sensitivity in Inventories.* Retrieved July 16, 2011, from ftp://narsto.esd.ornl.gov/pub/EI_Assessment/12EIAssess.Chapter8.pdf

[88] Abdel-Aziz, A., & Frey, H. C. (2003). Development of hourly probabilistic utility NOx emission inventories using time series techniques: Part II—multivariate approach. *Atmospheric Environment 37(38)* , 5391-5401.

[89] Frey, H. C., & Zheng, J. (2002). Probabilistic Analysis of Driving Cycle-Based Highway Vehicle Emission Factors. *Environmental Science and Technology 36(23)* , 5184-5191.

[90] Wisner, E., Mobley, D., Pouliot, G., & Hunt, B. (2010). Emissions Uncertainty: Focusing on NOx Emissions from Electric Generating Units. *19th Annual International Emission Inventory Conference "Emissions Inventories - Informing Emerging Issues".* San Antonio, TX: US EPA.

[91] Bollman, A. D., Wilson, J. H., & Jansses, M. (2007). Using Historical Information to Improve Emission Projections (or How to Avoid Being Doomed to Repeat History). *16th Annual International Emission Inventory Conference, Emission Inventories: "Integration, Analysis, and Communications".* Raleigh, NC: US EPA.

[92] US EPA. (2004). *Draft Regulatory Impact Analysis: Final Regulatory Analysis: Control of Emissions from Nonroad Diesel Engines.* US EPA OAQPS.

[93] US EPA. (2005). *Clean Air Interstate Rule Emissions Inventory Technical Support Document.* US EPA.

[94] McCluney, L. O. (2007). Calculating 8-Hour Ozone Design Values. *AQS Conference.* Pittsburgh, PA: US EPA OAQPS.

[95] Jacob, D. J. (1999). Chapter 11. Oxidizing Power of the Troposphere. In D. J. Jacob, *Introduction to Atmospheric Chemistry.* Princeton University Press.

[96] Sienfeld, J. H., & Pandis, S. N. (2006). *Atmospheric Chemistry and Physics - From Air Pollution to Climate Change (2nd Edition).* John Wiley & Sons.

[97] Barrett, S. R., Yim, S. H., Gilmore, C. K., Murray, L. T., Tai, A. P., Kuhn, S. R., Yantosca, R. M., Byun, D., Ngan, F., Li, X., Ashok, A., Koo, J., Levy, J., Dessens, O., Balasubramanian, S., Fleming, G. G., Wollersheim, C., Malina, R., Pearlson, M. N., Stratton, R. W., Arunachalam, S., Binkowski, F. S., Jacob, D. J., Hileman, J. I., & Waitz, I. A. (forthcoming). Public Health, Climate and Economic Impacts of Desulfurizing Aviation Fuel. *Environmental Science and Technology* .

[98] Abt Associates. (2010). *Modeled Attainment Test Software v2.3.1.* Research Triangle Park, NC: US EPA OAQPS.

[99] Timin, B. (2009, December 21). *Air Quality Modeling.* Retrieved July 30, 2011, from US EPA OAQPS: www.epa.gov/apti/video/pdfs/BrianTimin_pts_1&2.pdf

[100] Clarke, John-Paul et. al. (2006). *Development, design, and flight test evaluation of a continuous descent approach procedure for nighttime operation at Louisville International Airport.* Cambridge, MA: Partnership for AiR Transportation Noise and Emissions Reductions.

[101] Simaiakis, I., & Balakrishnan, H. (2010). Analysis and control of airport departure processes to mitigate congestion impacts. *Transportation Research Record: Journal of the Transportation Research Board* , 22-30.

[102] King, D., & Waitz, I. A. (2005). *Assessment of the effects of operational procedures and derated thrust on American Airlines B777 emissions from London's Heathrow and Gatwick airports.* Cambridge, MA: Partnership for AiR Transportation Noise and Emissions Reductions.

[103] FAA. (2011). *Destination 2025: the FAA Strategic Plan.* FAA, IdeaScale: http://d2025.ideascale.com/a/panel.do.

[104] Pinder, R. W., Dennis, R. L., & Bhave, P. V. (2008). Observable indicators of the sensitivity of PM2.5 nitrate to emission reductions—Part I: Derivation of the adjusted gas ratio and applicability at regulatory-relevant time scales. *Atmospheric Environment 42(6)* , 1275-1286.

Appendices

Appendix A CMAQ Vertical Layer Structure

Layer	Sigma Coordinate	Pressure(mb)	Height(m)
34	0.000	100	15668.0
33	0.05	145.6	13664.8
32	0.10	191.3	12080.6
31	0.15	237	10759.7
30	0.20	282.6	9621.2
29	0.25	328.3	8617.3
28	0.30	374	7717.4
27	0.35	419.6	6900.4
26	0.40	465.3	6151.2
25	0.45	511.0	5458.5
24	0.50	556.6	4813.9
23	0.55	602.3	4210.5
22	0.60	647.9	3643.1
21	0.65	693.6	3107.2
20	0.70	739.3	2599.3
19	0.74	775.8	2211.1
18	0.77	803.2	1929.7
17	0.80	830.6	1656.0
16	0.82	848.9	1477.6
15	0.84	867.1	1302.3
14	0.86	885.4	1130.1
13	0.88	903.7	960.7
12	0.90	921.9	794.2
11	0.91	931.0	711.9
10	0.92	940.2	630.3
9	0.93	949.3	549.3
8	0.94	958.4	469.0
7	0.95	967.6	389.3
6	0.96	676.7	310.3
5	0.97	985.8	231.8
4	0.98	995.0	154.0
3	0.985	999.5	115.3
2	0.990	1004.1	76.7
1	0.995	1008.7	38.3
0	1.000	1013.24	0

Appendix B CMAQ Model Build Parameters and Computational Architecture

Model Build Parameters

Module	***Option***
Mechanism	cb05cltx_ae5_aq
ModAdepv	module aero_depv2
ModAdjc	// yamo option does not need denrate
ModAero	module aero5_txhg
ModChem	module ebi_cb05cltx_ae5
ModCloud	module cloud_acm_ae5_tx
ModCpl	module gencoor
ModDriver	module ctm_yamo
ModHadv	module hyamo
ModHdiff	module multiscale
ModInit	module init_yamo
ModPa	module pa
ModPhot	module phot_table
ModUtil	module util
ModVadv	module vyamo
ModVdiff	module acm2_txhg
PAOpt	pa_noop
Tracer	trac0

Computational Architecture

Fortran Compiler	Portland Group Fortran (pgf90) v10.9
Fortran Compiler flags	-Mfixed -Mextend -02 -module ${MODLOC} -I.
MPICH	mpich2-1.1
C Compiler Flags	-v -g -I${MPICH}/include
OS	RHEL 5.5 x86_64

Appendix C CMAQ Configuration Summary

The table below summarizes the CMAQ inputs and run configuration for the individual CMAQ runs that are performed in this study:

	Simulation				
	1	2	3	4	5
Aviation Emissions	None	2006 (FOA3a)	None	2020 (Scaled 2006 (FOA3a))	2030 (Scaled 2006 (FOA3a))
Background Emissions	2005 NEI		2025 NEI		
Initial Conditions	2005 GEOS-Chem IC		2025 GEOS-Chem IC		
Boundary Conditions	2005 GEOS-Chem BC		2025 GEOS-Chem BC		
Photolysis lookup tables	JPROC program using default parameters				
Meteorology	2005 Meteorology				
Sea salt mask	Sea salt (OCEAN) data processed by UNC				
Simulation time period	376 Days (Jan 1-Dec 31, plus 11 day spin-up period)				
Grid	36km x 36km CONUS; Origin (-2664km, 2016km) from grid center (40 Lat, -97 Lon), 34 Vertical Layers				

Appendix D Excluded Military and Piston-engine Aircraft

TAF Bin	AEDT Code
Military	AN12
Military	AN26
Military	CNA552
Military	HS125-1000
Military	MIL-C12
Military	MIL-HUNTER
Military	MIL-JCOM
Military	MIL-JCOM-A
Military	MIL-JCOM-B
Military	MIL-KC135
Military	NORD-C160
Piston	AEROSTAR
Piston	BEECH55
Piston	DC3
Piston	IAI1123
Piston	MOONEY-M20K
Piston	SR20
Piston	SR22

Appendix E Excluded Airports in Alaska and Hawaii

EPACT ID	AIRPORT NAME	CITY NAME	STATE
ELW	ELLAMAR	ELLAMAR	ALASKA
FAK	FALSE ISLAND	FALSE ISLAND	ALASKA
FLT	FLAT	FLAT	ALASKA
KCC	COFFMAN COVE	COFFMAN COVE	ALASKA
MKP	MCKINLEY PARK	MCKINLEY PARK	ALASKA
MOS	MOSES POINT	ELIM	ALASKA
PABE	BETHEL	BETHEL	ALASKA
PABI	ALLEN ARMY AIRFIELD	DELTA JUNCTION/FT GREELEY	ALASKA
PACD	COLD BAY	COLD BAY	ALASKA
PACV	MERLE K (MUDHOLE) SMITH	CORDOVA	ALASKA
PADK	ADAK AIRPORT	ADAK ISLAND	ALASKA
PADL	DILLINGHAM	DILLINGHAM	ALASKA
PADQ	KODIAK	KODIAK	ALASKA
PADU	UNALASKA	UNALASKA	ALASKA
PAED	ELMENDORF AFB	ANCHORAGE	ALASKA
PAEI	EIELSON AFB	FAIRBANKS	ALASKA
PAEN	KENAI MUNI	KENAI	ALASKA
PAFA	FAIRBANKS INTL	FAIRBANKS	ALASKA
PAFB	LADD AAF	FAIRBANKS/FT WAINWRIGHT	ALASKA
PAGS	GUSTAVUS	GUSTAVUS	ALASKA
PAHN	HAINES	HAINES	ALASKA
PAHO	HOMER	HOMER	ALASKA
PAIL	ILIAMNA	ILIAMNA	ALASKA
PAJN	JUNEAU INTL	JUNEAU	ALASKA
PAKN	KING SALMON	KING SALMON	ALASKA
PAKT	KETCHIKAN INTL	KETCHIKAN	ALASKA
PAKW	KLAWOCK	KLAWOCK	ALASKA
PAMM	METLAKATLA SEAPLANE BASE	METLAKATLA	ALASKA
PAMO	MOUNTAIN VILLAGE AIRPORT	MOUNTAIN VILLAGE	ALASKA
PAMR	MERRILL FIELD	ANCHORAGE	ALASKA
PANC	TED STEVENS ANCHORAGE INTL	ANCHORAGE	ALASKA
PAOM	NOME	NOME	ALASKA
PAPG	PETERSBURG JAMES A JOHNSON	PETERSBURG	ALASKA
PAPO	MOUNTAIN VILLAGE AIRPORT	MOUNTAIN VILLAGE	ALASKA
PASC	DEADHORSE	DEADHORSE	ALASKA
PASI	SITKA ROCKY GUTIERREZ	SITKA	ALASKA
PASY	EARECKSON AIR STATION	SHEMYA	ALASKA
PATL	TATALINA LRRS	TAKOTNA	ALASKA

EPACT ID	AIRPORT NAME	CITY NAME	STATE
PAVD	VALDEZ PIONEER FIELD	VALDEZ	ALASKA
PAWD	SEWARD AIRPORT	SEWARD	ALASKA
PAWG	WRANGELL	WRANGELL	ALASKA
PAYA	YAKUTAT	YAKUTAT	ALASKA
RDB	RED DOG AIRPORT	RED DOG	ALASKA
TKE	TENAKEE	TENAKEE SPRINGS	ALASKA
PHBK	BARKING SANDS PMRF	KEKAHA,KAUAI	HAWAII
PHKO	KONA INTL AT KEAHOLE	KAILUA/KONA	HAWAII
PHLI	LIHUE	LIHUE	HAWAII
PHNG	KANEOHE BAY MCAF	KANEOHE	HAWAII
PHNL	HONOLULU INTL	HONOLULU	HAWAII
PHNY	LANAI	LANAI CITY	HAWAII
PHOG	KAHULUI	KAHULUI	HAWAII
PHTO	HILO INTL	HILO	HAWAII

Appendix F FAA-EPA May 2009 Total Organic Gas (TOG) Speciation Profile

Real Organic Species	***Mass Fraction***		***Real Organic Species***	***Mass Fraction***
Ethylene	0.154590		n-Decane	0.003202
Acetylene	0.039386		1,2,3-Trimethylbenzene	0.001062
Ethane	0.005215		n-Undecane	0.004442
Propylene	0.045336		n-Dodecane	0.004616
Propane	0.000781		n-Tridecane	0.005354
Isobutene/1-Butene	0.017538		C14-alkane	0.001860
1,3-Butadiene	0.016870		C15-alkane	0.001771
cis-2-Butene	0.002105		n-tetradecane	0.004164
3-Methyl-1-butene	0.001123		C16-alkane	0.001460
1-Pentene	0.007761		n-pentadecane	0.001726
2-Methyl-1-butene	0.001396		n-hexadecane	0.000487
n-Pentane	0.001984		C18-alkane	1.77×10^{-5}
trans-2-Pentene	0.003594		n-heptadecane	8.84×10^{-5}
cis-2-Pentene	0.002757		phenol	0.007262
2-Methyl-2-butene	0.001846		naphthalene	0.005412
4-Methyl-1-pentene	0.000687		2-methyl naphthalene	0.002062
2-Methylpentane	0.004085		1-methyl naphthalene	0.002466
2-Methyl-1-pentene	0.000342		dimethylnapthalenes	0.000898
1-Hexene	0.00736		C4-Benzene + C3-aroald	0.006564
trans-2-Hexene	0.000297		C5-Benzene+C4-aroald	0.003241
Benzene	0.016815		Methanol	0.018052
1-Heptene	0.004385		Formaldehyde (FAD)	0.123081
n-Heptane	0.000639		Acetaldehyde (AAD)	0.042718
Toluene	0.006421		Acetone	0.003693
1-Octene	0.002757		Propionaldehyde	0.007266
n-Octane	0.000625		Crotonaldehyde	0.010328
Ethylbenzene	0.001743		Butyraldehyde	0.001185
m-Xylene/p-Xylene	0.002822		Benzaldehyde	0.004695
Styrene	0.003094		Isovaleraldehyde	0.000325
o-Xylene	0.00166		Valeraldehyde	0.002452
1-Nonene	0.002455		o-Tolualdehyde	0.002298
n-Nonane	0.000624		m-Tolualdehyde	0.002778
Isopropylbenzene	3.17×10^{-5}		p-Tolualdehyde	0.000482
n-Propylbenzene	0.000533		Methacrolein	0.00429
m-Ethyltoluene	0.001541		Glyoxal	0.018165
p-Ethyltoluene	0.000642		Methylglyoxal	0.015033
1,3,5-Trimethylbenzene	0.000541		acrolein	0.024493
o-Ethyltoluene	0.000654		C-10 paraffins*	0.14608
1,2,4-Trimethylbenzene	0.003502		C-10 olefins*	0.05843
1-Decene	0.001846		decanal*	0.05843
			dodecenal*	0.02922

Appendix G Split Fractions of CB05 Lumped Species

AEDT Total Hydrocarbon (THC) emissions are mapped into CMAQ CB05 species as shown by the split factors below. The split factors specify the number of moles of CB05 lumped species that is contained in 1 g of Total Organic Gas (TOG) emissions. The factors are derived from the FAA-EPA aviation TOG speciation profile, and the CB05 real organic species to model species assignment table listed in Appendix A of [25]. AEDT THC emissions were first converted into TOG emissions by multiplying by a factor of 1.16, before being split into the various lumped species.

The split factor is calculated as follows:

$$SF_i = \sum_{j=1}^{81} \left(\frac{MF_j}{MW_j} * A_{j,i} \right)$$

where

i: index of CMAQ lumped species (PAR, OLE …)

j: index of Real Organic Species, given in the FAA-EPA profile (total of 81 species)

SF_i: Split Factor for lumped species I [mol CMAQ lumped species/g TOG]

MF_j: Mass fraction of Real Organic Species j [g Real Organic Species / g TOG]

MW_j: Molecular weight of Real Organic Species j [g Real Organic Species /mol Real Organic Species]

$A_{j,i}$: Assignment (from Yarwood et al.) of Real Organic Species j to CMAQ lumped species I [mol CMAQ lumped species/mol Real Organic Species]

CMAQ CB05 lumped Species	***Split Factor***		***CMAQ CB05 lumped Species***	***Split Factor***
PAR	0.026533799998		BENZALD_T	0.000044242194
OLE	0.002857357262		BENZENE	0.000215265955
TOL	0.000230510527		BUTADIENE	0.000311878161
XYL	0.000222004500		CUMENE	0.000000263657
FORM	0.004705928693		CUMENE_T	0.000000263657
ALD2	0.000996034898		ETHYLBENZ	0.000016416577
ETH	0.005510604161		ETHYLBENZ_T	0.000016416577

CMAQ CB05 lumped Species	***Split Factor***		***CMAQ CB05 lumped Species***	***Split Factor***
ISOP	0.000000000000		ETHYLENE	0.005510604161
MEOH	0.000563325600		FORMPRIM	0.004099153430
ETOH	0.000000000000		MTHYLNAP2_C	0.000000000000
CH4	0.000000000000		MTHYLNAP2_F	0.000014500197
ETHA	0.000173417727		MXYL	0.000013289691
IOLE	0.000409306043		NAPHTHALENE	0.000042223517
ALDX	0.001560273901		OXYL	0.000015634836
TERP	0.000000000000		PROPIONAL	0.000125102683
UNR	0.003367383095		PROPIONAL_T	0.000125102683
NVOL	0.000000000000		PXYL	0.000013289691
ACROLEIN	0.000436883954		STYRENE	0.000029709829
ACROLEIN_PRIMARY	0.000436883954		STYRENE_T	0.000029709829
ALD2PRIM	0.000969710356		TOLU	0.000069690317
BENZALD	0.000044242194			

Appendix H Aviation Emissions and Scale Factors on an Airport Basis

The entire inventory contains roughly 3550 airports in the modeling domain; for the top 60 busiest airports (ranked by total fuel burn in 2006), the data presented below includes airport-level emission totals and the TAF scaling factors and NO_x stringency reduction ratios for each airport. The airports below represent approximately 80% of the baseline 2006 national aviation fuel burn shown in Table 10. Note that, while TAF scaling factors are applied to both arrival and departure flight legs, separate NO_x stringency reductions are applied to the TAF-scaled 2020/2030 inventories depending on flight leg, since the CAEP/8 NO_x stringency emissions inventory contains data on a flight-leg basis.

	Baseline 2006 LTO (short tons/year)									2020 Scale (Relative to Baseline)					2030 Scale (Relative to Baseline)				
Airport	*Fuel-Burn*	*CO*	*NOx*	*HC*	*SO2*	*POA*	*PEC*	*PSO4*	*Operations*	*TAF-GA*	*TAF-AC*	*TAF-AT*	*NO_x Str Arr*	*NO_x Str Dep*	*TAF-GA*	*TAF-AC*	*TAF-AT*	*NO_x Str Arr*	*NO_x Str Dep*
KATL	394,921	5,733	3,880	759	450	59	19	36	967,118	-12%	53%	7%	-3%	-4%	8%	99%	33%	-5%	-7%
KORD	386,249	5,078	4,256	689	440	54	19	35	930,277	-73%	17%	-5%	-3%	-4%	-72%	56%	5%	-5%	-7%
KJFK	296,385	4,506	3,473	676	338	55	13	27	366,738	-14%	62%	69%	-4%	-4%	-14%	132%	110%	-6%	-8%
KDFW	291,319	3,269	3,169	526	332	40	18	27	690,925	-55%	21%	-7%	-2%	-3%	-55%	47%	9%	-4%	-6%
KLAX	287,332	3,627	3,601	500	328	39	11	26	599,178	12%	23%	-37%	-3%	-4%	26%	53%	-35%	-6%	-7%
KEWR	230,225	3,547	2,445	447	262	37	7	21	434,483	-20%	17%	10%	-3%	-4%	-20%	39%	33%	-6%	-8%
KIAH	210,861	3,479	2,015	341	240	27	5	19	593,215	-30%	38%	10%	-2%	-4%	-15%	91%	36%	-5%	-7%
KLAS	183,672	2,335	2,107	301	209	24	11	17	493,947	-20%	22%	4%	-2%	-3%	3%	63%	30%	-4%	-6%
KMIA	182,012	2,424	2,119	419	207	33	6	17	358,967	-25%	33%	-13%	-3%	-4%	-25%	72%	8%	-6%	-8%
KPHL	175,177	2,864	1,797	357	200	29	6	16	492,581	-10%	28%	8%	-2%	-3%	-1%	70%	41%	-4%	-6%
KDEN	174,028	2,617	1,893	335	198	26	8	16	579,030	-68%	37%	10%	-2%	-3%	-64%	79%	30%	-4%	-6%
KPHX	171,059	2,115	1,980	218	195	17	10	16	497,299	-48%	5%	4%	-2%	-2%	-40%	23%	31%	-4%	-5%
KDTW	168,410	2,635	1,725	489	192	38	12	15	465,255	-43%	-14%	39%	-3%	-4%	-37%	9%	61%	-5%	-7%
KLGA	160,673	2,333	1,498	327	183	27	7	15	396,508	-37%	9%	-23%	-2%	-3%	-37%	17%	-26%	-4%	-5%
KMSP	157,414	2,187	1,757	381	179	30	10	14	455,777	-62%	23%	24%	-2%	-3%	-59%	58%	59%	-5%	-6%
KMEM	156,906	2,820	1,846	699	179	55	8	14	362,923	-44%	7%	-6%	-4%	-4%	-38%	36%	3%	-6%	-6%
KSFO	148,178	1,830	1,917	256	169	20	7	14	337,194	-18%	47%	-5%	-3%	-4%	-7%	88%	1%	-6%	-7%
KBOS	139,243	1,860	1,611	282	159	22	6	13	366,338	-18%	9%	-5%	-3%	-3%	-7%	27%	-4%	-5%	-7%
KMCO	129,999	1,548	1,440	192	148	15	6	12	342,258	-19%	34%	-9%	-3%	-4%	-6%	77%	38%	-5%	-7%
KCLT	126,631	2,151	1,253	272	144	22	3	12	486,116	-24%	67%	-4%	-2%	-3%	-16%	127%	18%	-5%	-6%
KIAD	117,731	1,752	1,384	307	134	24	6	11	390,412	-26%	76%	-7%	-3%	-4%	-17%	156%	19%	-5%	-7%
KSEA	114,417	1,361	1,349	157	130	12	5	11	332,984	-13%	48%	-75%	-2%	-3%	5%	82%	-75%	-4%	-6%
KSLC	89,187	1,582	876	198	102	16	4	8	353,093	-2%	23%	-8%	-2%	-3%	4%	54%	11%	-4%	-6%

	Baseline 2006 LTO (short tons/year)									2020 Scale (Relative to Baseline)					2030 Scale (Relative to Baseline)				
Airport	Fuel-Burn	CO	NOx	HC	SO2	POA	PEC	PSO4	Operations	TAF-GA	TAF-AC	TAF-AT	NO_x Str Arr	NO_x Str Dep	TAF-GA	TAF-AC	TAF-AT	NO_x Str Arr	NO_x Str Dep
KBWI	85,685	1,086	972	141	98	11	3	8	271,243	-40%	27%	-12%	-2%	-2%	-35%	59%	-5%	-3%	-5%
KDCA	84,919	1,104	884	132	97	11	4	8	274,785	153%	6%	-12%	-2%	-2%	253%	11%	-14%	-3%	-4%
KFLL	84,461	1,104	902	175	96	14	4	8	254,913	-14%	37%	-15%	-2%	-3%	4%	79%	-10%	-5%	-6%
KMDW	76,012	1,062	834	161	87	13	3	7	264,764	-28%	30%	-50%	-1%	-2%	-28%	73%	-38%	-3%	-4%
KOAK	71,513	926	874	142	82	11	3	7	206,870	-13%	-13%	-8%	-2%	-3%	9%	11%	6%	-4%	-5%
KSAN	70,268	861	784	106	80	9	3	6	215,288	-35%	28%	-10%	-2%	-3%	-23%	74%	7%	-4%	-5%
KTPA	68,706	909	753	152	78	12	3	6	220,168	-21%	22%	-49%	-2%	-3%	-8%	55%	-36%	-4%	-6%
KIND	68,629	1,108	816	249	78	19	3	6	192,757	-36%	28%	-36%	-3%	-4%	-26%	39%	-25%	-6%	-6%
KCVG	68,074	1,099	656	132	78	11	3	6	339,000	-26%	-29%	-36%	-3%	-4%	-14%	-12%	-26%	-5%	-7%
KSDF	65,953	957	761	153	75	12	2	6	157,318	-29%	3%	-16%	-2%	-3%	-15%	17%	1%	-5%	-6%
KSTL	65,492	785	736	129	75	10	3	6	262,371	-45%	2%	-40%	-2%	-3%	-37%	20%	-31%	-4%	-5%
KCLE	55,473	958	557	140	63	11	1	5	242,078	-29%	1%	-2%	-2%	-3%	-20%	29%	13%	-4%	-6%
KPDX	51,823	655	618	84	59	7	2	5	226,823	-17%	42%	-8%	-2%	-3%	0%	85%	14%	-4%	-6%
KMCI	48,444	690	509	116	55	9	2	4	169,321	-59%	7%	28%	-2%	-3%	-58%	34%	68%	-4%	-5%
KPIT	47,281	801	472	127	54	10	2	4	220,560	-10%	11%	-65%	-2%	-2%	6%	35%	-60%	-4%	-5%
KSJC	46,613	581	546	93	53	7	2	4	164,327	-15%	-7%	-4%	-2%	-2%	-1%	23%	31%	-3%	-5%
KRDU	46,410	655	506	130	53	10	2	4	190,530	-18%	31%	-18%	-2%	-3%	-5%	75%	4%	-4%	-5%
KBNA	45,127	688	466	121	51	9	2	4	178,581	-29%	-3%	20%	-1%	-2%	-11%	12%	55%	-3%	-4%
KMKE	41,093	691	404	139	47	11	2	4	182,653	-23%	23%	2%	-2%	-3%	-3%	57%	15%	-4%	-6%
KSNA	40,303	544	447	96	46	7	2	4	136,652	-15%	26%	-56%	-2%	-2%	-4%	59%	-43%	-3%	-5%
KHOU	39,521	632	378	102	45	8	1	4	171,491	-10%	9%	-40%	-1%	-2%	4%	20%	-32%	-3%	-4%
KILN	37,467	704	340	243	43	19	3	3	63,253	-9%	21%	-7%	-4%	-6%	3%	52%	8%	-7%	-9%
KSMF	36,674	449	434	52	42	4	2	3	123,384	-43%	3%	4%	-2%	-2%	-34%	34%	31%	-4%	-5%
KONT	36,231	489	443	77	41	6	2	3	106,369	-16%	-28%	5%	-2%	-3%	-3%	-22%	18%	-5%	-6%
KSAT	36,158	537	378	103	41	8	2	3	143,032	-11%	21%	43%	-2%	-3%	2%	51%	90%	-4%	-5%
KAUS	35,865	527	368	96	41	7	2	3	134,841	-23%	14%	-9%	-2%	-3%	-14%	31%	14%	-4%	-5%
KDAL	35,782	610	345	108	41	8	1	3	169,364	-41%	68%	-35%	-2%	-2%	-28%	94%	-24%	-3%	-5%
KBDL	33,716	426	390	69	38	5	1	3	115,315	-28%	-11%	-18%	-2%	-3%	-12%	6%	-3%	-4%	-6%
KCMH	31,493	470	338	99	36	8	1	3	147,760	-42%	40%	-18%	-2%	-2%	-31%	86%	-11%	-3%	-5%
KPBI	31,035	524	305	132	35	10	2	3	127,742	-27%	14%	-23%	-3%	-3%	-15%	36%	-2%	-5%	-7%
KRSW	27,169	318	291	45	31	4	1	2	78,560	-17%	34%	-23%	-2%	-3%	-12%	85%	-1%	-5%	-6%
KABQ	26,727	350	299	47	30	4	1	2	102,774	-16%	7%	-7%	-2%	-2%	4%	26%	12%	-3%	-4%
KJAX	25,560	408	263	79	29	6	1	2	100,400	-21%	19%	-34%	-2%	-3%	0%	47%	-19%	-5%	-6%
KMSY	25,190	330	267	62	29	5	1	2	93,323	-35%	92%	-27%	-2%	-3%	-26%	126%	-17%	-4%	-6%
KBUR	23,388	325	249	44	27	4	1	2	93,459	-65%	8%	-30%	-2%	-2%	-61%	30%	-20%	-3%	-5%

Appendix I $PM_{2.5}$ and Ozone Species

The following table lists the components that are aggregated to form $PM_{2.5}$, its constituents and ozone. The 'I' and 'J' suffixes to the species names refer to aerosol Aitken and Accumulation modes of formation. All PM species are reported in concentration units of ug/m3, while ozone is reported in concentration units of ppbv.

Description	**Variable**	**Equation (In terms of CMAQ chemical species)**
Sulfate PM	ASO4T	ASO4I + ASO4J
Nitrate PM	ANO3T	ANO3I + ANO3J
Ammonium PM	ANH4T	ANH4I + ANH4J
Elemental Carbon PM	AECT	AECI + AECJ
Organic PM	PM_ORG_TOT	AORGAT + AORGBT + AORGCT + 1.167*AORGPAT
Crustal PM	A25J	A25J
$PM_{2.5}$ Total	PM25	ASO4T+ANO3T+ANH4T+AECT+PM_ORG_TOT+A25J
Ozone	O3	O3
	where the following species are defined as	
Anthropogenic Secondary Organic Aerosol (SOA)	AORGAT	AXYL1J+AXYL2J+AXYL3J +ATOL1J+ATOL2J+ATOL3J +ABNZ1J+ABNZ2J+ABNZ3J +AALKJ+AOLGAJ
Biogenic SOA	AORGBT	AISO1J+AISO2J+AISO3J +ATRP1J+ATRP2J+ASQTJ +AOLGBJ
Cloud SOA	AORGCT	AORGCJ
Anthropogenic POA	AORGPAT	AORGPAI+AORGPAJ

Appendix J MATS Options and Settings

The following tables describe the settings and program options used in MATS. Note that there are separate tables for $PM_{2.5}$ and Ozone-Benefits.

MATS Option Page – Annual $PM_{2.5}$ Calculation	***Choice***
MATS Version	**2.3.1**
Analysis Type	Annual PM Analysis
Choose Desired Output	**Standard Analysis**
	– Interpolate monitor data to FRM sites. Temporally-adjust
	Quarterly Model Data
	– Output used quarterly average model data file
Output Choice-Advanced	**Spatial Field Estimates**
	– *Forecast*: Interpolate FRM and speciation monitor data to spatial field. Temporally adjust
	– *Forecast*: Interpolate gradient-adjusted FRM and speciation monitor data to spatial field. Temporally adjust
	Miscellaneous Outputs
	– *Quarterly average files*: Spatial Field
	– *Quarterly average files*: Spatial Field - gradient-adjusted
	– *Species fractions spatial field*: Spatial Field
	– *Species fractions spatial field*: Spatial Field - gradient-adjusted
	– *Quarterly average speciated monitors*: File "E"
Data Input	**Species Data**
	– *Species Monitor Data File:* Species-for-fractions-0206-v2.csv
	PM2.5 Monitor Data
	– *Unofficial Daily Average PM2.5 Data File*: PM25-for-fractions-0206-v3.csv
	– *Official Quarterly Average FRM Data file*: Annual-official-FRM-99-08-v2.csv
	Model Data
	– Quarterly model data input
Species Fraction Calculation Options	**IMPROVE-STN Monitor Data**

MATS Option Page – Annual $PM_{2.5}$ Calculation	***Choice***
	– *Monitor Data Years*: 2004-2006
	– *Delete Specified Data values:* EPA-specified deletions from monitor data
	– *Minimum Data Requirements*: Minimum number of valid days per quarter = 11
	– *Minimum Data Requirements*: Minimum number of valid years required for valid season = 1
	– *Minimum Data Requirements*: Minimum number of valid seasons for valid monitor = 1
	PM2.5 Monitor Data
	– *Monitor Data Years*: 2004-2006
	– *Delete Specified Data values:* EPA-specified deletions from monitor data
	– *Minimum Data Requirements*: Minimum number of valid days per quarter = 11
	– *Minimum Data Requirements*: Minimum number of valid years required for valid season = 1
	– *Minimum Data Requirements*: Minimum number of valid seasons for valid monitor (point calculations) = 4
	– *Minimum Data Requirements*: Minimum number of valid seasons for valid monitor (spatial fields calculation) = 1
Species Fractions Calculation Options - Advanced	**Interpolation Options**
	– *PM2.5*: Inverse Distance Squared Weights (90000)
	– *SO4*: Inverse Distance Squared Weights (90000)
	– *NO3*: Inverse Distance Squared Weights (90000)
	– *EC:* Inverse Distance Squared Weights (90000)
	– *Salt*: Inverse Distance Squared Weights (90000)
	– *Crustal*: Inverse Distance Squared Weights (90000)
	– *DON*: Inverse Distance Squared Weights (90000)
	– *OC*: Inverse Distance Squared Weights (90000)
	– *NH4*: Inverse Distance Squared Weights (90000)
	Miscellaneous Options
	– *Ammonium*: Use DON values
	– *Default Blank Mass*: Default Blank Mass = 0.5
	– *Organic Carbon:* Organic carbon mass balance floor = 1

MATS Option Page – Annual $PM_{2.5}$ Calculation	***Choice***
	– *Organic Carbon:* Organic carbon mass balance ceiling = 0.8
PM2.5 Calculation Options	**PM2.5 Monitor Years**
	– Start year=2005, End year=2005
	– Official Design Values
	– *Valid FRM Monitors*: Minimum number of Design Values = 1
	– *Valid FRM Monitors*: Required Design Values = [None selected]
	– *NH4 Future calculation:* Calculate future year NH4 using base year NH4 and the NH4 RRF
Model Data Options	**Temporal adjustment at monitor**
	– *Grid for Point Forecast* = 3x3
	– *Grid for Spatial Forecast* = 1x1

MATS Option Page – Ozone Benefits calculations	***Choice***
MATS Version	**2.3.1**
Analysis Type	Ozone Analysis
Choose Desired Output	**Point Estimates**
	– Temporally-adjust ozone levels at monitor
	Spatial Field
	– *Baseline*: Interpolate monitor data to spatial field.
	– *Baseline*: Interpolate gradient-adjusted monitor data to spatial field.
	– *Forecast*: Interpolate monitor data to spatial field. Temporally adjust ozone levels
	– *Forecast*: Interpolate gradient-adjusted monitor data to spatial field. Temporally adjust
Data Input	**Monitor Data**
	– *Ozone Data:* ozone_2000-2007_dailymax_season_avg.csv
	Model Data
	– Yearly model data input

MATS Option Page – Ozone Benefits calculations	***Choice***
	Using Model Data
	– *Temporal adjustment at monitor*: 1x1, Maximum
Filtering and Interpolation	**Choose Ozone Design Values**
	– *Start Year*: 2002-2004
	– *End Year*: 2004-2006
	Valid Ozone Monitors
	– *Minimum Number of design values*: 1
	– *Required Design Values*: None selected
	Default Interpolation Method
	– *Inverse Distance weights*
RRF and Spatial Gradient	**RRF Setup**
	– *Initial threshold value (ppb)*:0
	– *Minimum number of days in baseline at or above threshold*: 0
	– *Minimum allowable threshold value (ppb)*: 0
	– *Min number of days at or above minimum allowable threshold:* 0
	– *Subrange first day of ozone season used in RRF*: 1
	– *Subrange last day of ozone season used in RRF*: 153
	Spatial Gradient Setup
	– *Start Value*: 1
	– *End Value*: 153